The Treatment of High Hardness Waters by Electrocoagulation: Factors Affecting Contaminant Removal, Electrode Fouling, and Precipitate Separation

by

Héline Chow

A thesis

presented to the University of Waterloo

in fulfillment of the

thesis requirement for the degree of

Doctor of Philosophy

in

Civil Engineering - Water

Waterloo, Ontario, Canada, 2021

Examining Committee Membership

The following served on the Examining Committee for this thesis. The decision of the Examining Committee is by a majority vote.

External Examiner	Dr. Madjid Mohseni Professor Department of Chemical and Biological Engineering University of British Columbia
Supervisor	Dr. Anh Pham Assistant Professor Department of Civil and Environmental Engineering University of Waterloo
Internal Member	Dr. Monica Emelko Associate Professor Department of Civil and Environmental Engineering University of Waterloo
Internal Member	Dr. Hyung-Sool Lee Associate Professor Department of Civil and Environmental Engineering University of Waterloo
Internal-External Member	Dr. Jeffrey Gostick Associate Professor Department of Chemical Engineering University of Waterloo

Author's Declaration

This thesis consists of material all of which I authored or co-authored: see Statement of Contributions included in the thesis.

This is a true copy of the thesis, including any required final revisions, as accepted by my examiners.

I understand that my thesis may be made electronically available to the public.

Statement of Contributions

Important contributions towards this thesis were made by my supervisor Dr. Anh Pham. His input and guidance aided towards the overall study design, and analysis and interpretation of the results.

Chapter 3 and 4 of this thesis are published papers co-authored by myself and Dr. Pham. For these chapters, I developed the methodology and experimental design, carried out the experiments, analyzed the experimental data, and wrote the papers with guidance and support from Dr. Pham.

Chapter 5 of this thesis contains unpublished materials as well as some figures that were published in a paper co-authored by myself, Dr. Pham, Markus Ingelsson (University of Calgary), and Dr. Edward Roberts (University of Calgary). For the published data (i.e. Figure 5-1, Figure 5-3, Figure 5-4), I developed the methodology and experimental design, carried out the lab experiments, and collected and analyzed the experimental data. The text that describes these figures (sections 5.2 and 5.3.1) was altered from the published material for this thesis. The writing of this text was based on my own interpretation of the data and was also informed by the discussion with Dr. Pham, as well as with Markus Ingelsson and Dr. Roberts. For the unpublished data, which is expected to be submitted for a journal publication, I developed the methodology and experimental design, carried out the lab experiments, and collected and analyzed the experimental data.

I certify, with the above qualifications, that this thesis and the research to which it refers is the product of my own work.

Abstract

Electrocoagulation (EC) is an emerging electrochemical technology for the treatment of contaminated waters and wastewaters. EC involves the application of electric current to metal electrodes to release metal ions into the surrounding contaminated water. These metal ions form precipitates, which subsequently adsorb contaminants. Compared with chemical coagulation, EC offers several distinct benefits, including lower sludge production, adjustable/controllable treatment rates, low material costs, and reduced energy consumption. EC is especially appealing for the treatment of high-salinity wastewater streams (e.g., oil and gas produced water, hydraulic fracturing flowback) as the addition of more salts to such types of wastewaters is usually not desirable. Despite growing interests in EC, the optimization and implementation of this technology in the water and wastewater treatment sector has been laggard, partly because factors that affect EC performance are still not thoroughly understood. The overall goal of this PhD research is to gain further insights into the potential utility of EC, focusing particularly on answering the following two questions: (1) Can EC effectively treat heavily contaminated wastewater streams consisting of different types of contaminants? (2) How can electrode fouling in EC be mitigated without disrupting the treatment process?

In the first research chapter (Chapter 3), the treatment of oil sands thermal in-situ produced water by iron EC (Fe-EC) and aluminum EC (Al-EC) was investigated. Oil sands thermal in-situ produced water is a heavily contaminated wastewater streams consisting of silica, sulfide, and hardness. Effective removal of silica, sulfide and hardness from produced water can reduce corrosion and scaling of steam generators, enhancing water recycling and reuse in the oil sands industry. In Fe-EC, the precipitation of FeS minerals resulted in a rapid removal of sulfide and adsorption of silica onto FeS. In Al-EC, silica was removed via adsorption onto aluminum

hydroxides, while sulfide was removed by stripping and electrochemical oxidation. The removal of sulfide was less efficient with Al-EC than with Fe-EC. In Fe-EC, Ca^{2+} and Mg^{2+} were removed from the organic-free synthetic produced water but not from the authentic water, likely due to the influence of organic species. Also, contaminant removals in Fe-EC were controlled by charge density but not current density. Overall, the research reported in this chapter suggests that EC can be a promising technology for the treatment of thermal in-situ produced water.

In the second research chapter (Chapter 4), the treatment of a synthetic groundwater containing high hardness was investigated, in order to gain insights into how electrode fouling by hardness can be mitigated. Electrode fouling is considered as a major problem in EC because it can cause decreased coagulant production, increased ohmic resistance and energy consumption, and reduced contaminant removal efficiency. Therefore, researchers have put significant efforts into finding techniques to prevent/mitigate fouling. One technique that has gained great deal of interest is polarity reversal (PR), which involves periodically switching the direction of the current such that the anode becomes the cathode and *vice versa*. Compared with other fouling removal techniques (e.g., mechanical/chemical cleaning, pre-treatment by ion exchange to remove Ca^{2+} and Mg^{2+}), PR is especially appealing because it allows for the removal of fouling to occur concurrently with the production of coagulant. PR also does not require chemical addition, reactor shutdown, or additional infrastructure other than a current switch. While it has been suggested that PR can help mitigate electrode fouling, conflicting results about the utility of this approach have been reported in the literature. In this research, it was found that operating Fe-EC under the PR mode reduced neither electrode fouling nor energy consumption. Notably, the faradaic efficiency (ϕ) in Fe-EC decreased with increasing PR frequency; ϕ was as low as 10% when a PR frequency of 0.5 minutes was employed. Unlike Fe-EC, operating Al-EC under the PR mode resulted in high

coagulant production efficiencies, reduced energy consumption, and diminished electrode fouling. In addition to comparing PR-EC and DC-EC, a novel strategy to minimize electrode fouling was investigated. This strategy involved operating Fe DC-EC and Al DC-EC with a Ti-IrO_2 cathode, whose fouling by Ca- and Mg-containing minerals could be readily avoided by periodically switching the current direction.

Building upon the investigation with synthetic groundwater in Chapter 4, the effect of PR on coagulant production under other water chemistry conditions was examined in Chapter 5. As in the synthetic groundwater experiments, ϕ in Fe-EC also decreased with increasing PR frequency in the experiments with NaCl, Na_2SO_4, and synthetic produced water solutions. Notably, ϕ was < 20% in all PR Fe-EC experiments with synthetic produced water. This result suggests that the mitigation of electrode fouling in the Fe-EC/synthetic produced water system by PR does not appear to be a promising strategy, because a low ϕ would be detrimental to contaminant removal. In comparison, ϕ was above 100% (i.e., super faradaic efficiency) in most Al-EC experiments. Given that maintaining a high coagulant production is paramount to the removal of silica (i.e., the main target contaminant in the oil sands thermal in-situ produced water), Al-EC was deemed more promising for the treatment oil sands thermal in-situ produced water. While operating Al-EC under PR can mitigate electrode fouling, the use of high PR frequency should be avoided, as this would result in decreased coagulant production (hence, decreased silica removal), decreased calcium and magnesium removal, and smaller precipitates that would be more challenging to separate post EC treatment.

Acknowledgements

Funding for this research was provided by the Natural Sciences and Engineering Research Council of Canada (NSERC-STPGP #506951-217). I was supported in part by the Ontario Graduate Scholarship, the Queen Elizabeth II Graduate Scholarship in Science and Technology, and the Flora T.T. Ng and Garry L. Rempel Doctoral Scholarship in Sustainable Development.

First, I would like to thank my supervisor Dr. Anh Pham who took the time over the last 5 years to help make this thesis the best it could be. This thesis would not be possible without his guidance and support.

I would also like to thank everyone in the community at the University of Waterloo and Carleton University who provided me with the resources and support I needed to complete this thesis. I would like to thank all the lab technicians who helped me run samples, set up experiments, and fix all the problems that arose throughout my lab work. Thank you, Marie Tudoret, Jianqun Wang, Charles Del Castel, Mark Merlau, Mark Sobon, and Nina Neinig.

I would also like to thank all the students in my research group, past and present, for always being available to answer questions and brainstorm with. Thank you, Nick Zrinyi, Blessing Medon, Alannah Taylor, Seyfollah Gilak, and My Dinh. I already miss spending time in the lab with you all.

Last but not least, I would like to thank my friends and family who supported me over the last 5 years. Randi-lee Caines-Luffman, Elyse Batista, Celine Vandenberg, Khusro Mir, Grant Jensen, Elli Papangelakis, Melissa Mark, Geoffrey Scott, the “Ottawa Gals,” everyone in the “fun office,” and the “Dream Team.” I couldn’t have made it here without you, and I can’t wait to see where we go together in future.

Table of Contents

List of Figures

List of Tables

List of Equations

List of Abbreviations

Alternating current electrocoagulation	AC-EC
Alternating pulsed current	APC
Aluminum based electrocoagulation	Al-EC
Brunauer–Emmett–Teller	BET
Canada's oil sands innovation alliance	COSIA
Chemical coagulation	CC
Chemical oxygen demand	COD
Direct current	DC
Direct current electrocoagulation	DC-EC
Dissolved oxygen	DO
Electrocoagulation	EC
Energy dispersive X-ray spectrometer	EDX
Energy dispersive X-Ray spectroscopy	EDS
Environmental scanning electron microscope	ESEM
Hybrid aluminum Ti-IrO_2 and based electrocoagulation	Al/Ti-IrO_2 EC
Hybrid iron Ti-IrO_2 and based electrocoagulation	Fe/Ti-IrO_2 EC
Inductively coupled plasma - optical emission spectroscopy	ICP-OES
Iron based electrocoagulation	Fe-EC
Natural organic matter	NOM
Oxidation-reduction potential	ORP
Polarity reversal	PR
Polarity reversal electrocoagulation	PR-EC
Selected-area electron diffraction	SAED
Synthetic ground water	SGW
Synthetic produced water	SPW
Total organic carbon	TOC
Transmission electron microscopy	TEM
X-ray diffraction	XRD

List of Symbols

Anode Area	A
Anodic Potential (V)	E_{anode}
Cell Voltage (V)	U
Charge Density (C/L)	q
Concentration (mg/L or M)	C
Current (mA)	I
Current Density (mA/cm^2)	i
Diameter (mm)	d
Degrees of Freedom	df
Electrolysis Time (s)	t
Faradaic Efficiency (%)	ϕ
Faraday's Constant (C/mol)	F
Mass of Coagulant Produced (g)	m
Mean Value	μ
Molecular Weight (g/mol)	M
Number of Samples	n
Number of Electrons Transferred	z
Polarity Reversal Frequency (min)	f
Standard Potential (V)	E^0
Value of One Observation	x_i
Variance	σ^2
Volume of Solution (L)	V

Chapter 1

Introduction

1.1 Motivation

The focus of this PhD research is the treatment of water and wastewater by electrocoagulation (EC). EC involves the application of electric current to submerged iron (Fe) and aluminum (Al) electrodes to release iron and aluminum ions into the surrounding solution. These ions are then polymerized, forming oxyhydroxide precipitates that can adsorb contaminants [1–5]. Subsequently, the precipitates laden with contaminants are separated from the treated water by various methods, such as flotation, filtration, or gravitational settling. Compared with chemical coagulation (CC, in which iron and aluminum ions are introduced to the solution via the addition of salts such as $FeCl_3$, $Fe_2(SO_4)_3$, and $Al_2(SO_4)_3$), EC offers several distinct benefits, including lower sludge production, adjustable/controllable treatment rates, low material costs, and reduced energy consumption [6–10]. EC is especially appealing for the treatment of high-salinity wastewater streams (e.g., oil and gas produced water, hydraulic fracturing flowback) as the addition of more salts to such types of wastewaters is not desirable. While previous studies have shown that EC is suitable for the treatment of not only groundwater and surface water but also heavily contaminated industrial wastewater streams [8,11–13], the optimization and implementation of EC has been impeded by several knowledge gaps surrounding factors affecting EC performance. Therefore, the overall goal of this PhD research is to address some of these knowledge gaps, focusing specifically on preventing electrode fouling and enhancing the removal of multiple contaminants in complex wastewater matrices.

A major operational problem in EC is the build-up of materials on the surface of the electrodes, a phenomenon often referred to as fouling. Electrode fouling occurs mainly due to the accumulation on the electrode surface of metal oxyhydroxides and Ca-/Mg-containing minerals, with the latter being particularly problematic for the treatment of high hardness waters, such as groundwater, oil and gas produced water, and boiler blowdown [14–18]. Electrode fouling is a concern because it can lead to various operational issues, including increased energy consumption, lower migration of coagulant to the bulk solution, and clogging of the reactor[6,19–23]. To decrease fouling, it has been recently proposed that the electric current in EC should be switched constantly or intermittently. This mode of EC operation, also known as polarity reversal (PR), is hypothesized to initiate chemical/electrochemical reactions that can displace the accumulated materials. However, the effectiveness of PR at removing/preventing electrode fouling has not been studied in detail. In addition, it is currently unclear how PR affects coagulant production, contaminant removal, and energy consumption in EC. **Therefore, one of the objectives of this PhD research is to compare and contrast Fe-EC and Al-EC systems that are operated in the direct current (DC) and the PR mode.**

As mentioned earlier, EC is an attractive technology for the treatment of high-salinity wastewaters. One example of such waters is oil sands thermal in-situ produced water (PW), which is a waste product of oil sands extraction. Thermal in-situ PW typically consists of bitumen residue, organic compounds, suspended solids, and inorganic salts. Of these constituents, dissolved silica, present at concentrations as high as 350 mg/L, is particularly problematic because its precipitation can lead to scaling of steam generators and clogging of disposal wells. Currently, dissolved silica is removed from the PW by lime softening or evaporative treatment [24]. However, these treatment technologies have high capital cost, are energy intensive and difficult to operate [25]. Lime softening

is also chemical intensive and generates large volume of sludge. Therefore, novel cost-effective technologies that can effectively remove silica are needed to help the oil sands industry increase water recycling, reduce energy consumption and production cost, and reduce environmental impact. To this end, Canada's Oil Sands Innovation Alliance (COSIA) has identified the development of innovative silica removal technologies as one of the industry's priorities [24]. In addition to silica, removing calcium, magnesium, and sulfide from in-situ PW is also desirable because these solutes can cause scaling and corrosion of pipelines and steam generators [26,27].

Several studies have shown that EC can remove silica, sulfide, Ca^{2+}, and Mg^{2+} [14,28–31], raising the potential of this technology to treat thermal in-situ PW typically that contains these contaminants. However, these previous studies dealt with wastewater streams (e.g., municipal wastewater, hydraulic fracturing PW, brackish water, or cooling tower blowdown water) that were less complex than thermal in-situ PW typically. These studies also often focused on the removal of only one specific contaminant (e.g., sulfide in wastewater, or silica from brackish water [28,31]. Whether EC can remove silica, sulfide, calcium or magnesium when these species coexist in a complex water matrix like in-situ PW has not yet been investigated. **Thus, the other objective of this PhD research is to explore the treatment of in-situ PW by EC,** focusing on investigating 1) the ability of EC to remove multiple contaminants in a single treatment step, 2) whether PR can be employed as an effective means of preventing electrode fouling by silica, Ca^{2+}, and Mg^{2+} in in-situ PW, and 3) how PR affects the precipitate separation post EC treatment.

1.2 Thesis Organization

This PhD thesis reports the results of the research designed to address the knowledge gaps described in section 1.1. Chapter 2 describes the relevant background information on coagulation, EC, current challenges associated with the technology, and the specific objectives of this research. Chapter 3, written as a stand-alone published manuscript [32], investigates the ability of EC to simultaneous remove of silica, sulfide, and hardness from in-situ PW. Chapter 4, also written as a stand-alone published manuscript [33], focuses on determining how PR affects electrode fouling and coagulant production efficiency. Chapter 5, containing some published materials [34], investigates the effect of solution chemistry and PR on coagulant production efficiency, precipitate characteristics, and contaminant removal. The last chapter, Chapter 6, summarizes the key conclusions of this research and provides direction for future work.

Chapter 2

Background

2.1 Water Treatment by Coagulation

One of the most common water treatment techniques is chemical coagulation (CC). Coagulation involves the addition of chemical coagulants to create the conditions necessary for the removal of particulate and dissolved matter. While this process is broken down into two distinct steps, namely coagulation (i.e., the addition of chemicals) and flocculation (i.e., the aggregation and growth of particles), for simplicity the two processes will be referred to as coagulation in this thesis.

2.1.1 Coagulation Principles

The stability of particles in water is dependent on the balance between two forces, namely the repulsive electrostatic force and the attractive van der Waals force. Under normal conditions the repulsive force dominates, resulting in stable particles that will not aggregate or settle. In contrast, coagulation allows attractive forces to dominate, resulting in the destabilizing of particles and the formation of flocs. The three main mechanisms by which coagulation promotes the aggregation of particles are 1) the compression of the electrical double layer, 2) adsorption and charge neutralization, and 3) enmeshment or "sweep floc". These processes describe the attachment portion of coagulation; however, for attachment to occur the transport of coagulant to the contaminants must also be promoted. To promote contact between the coagulant and contaminants, the solution is often mixed mechanically or in line.

2.1.2 Coagulation with Iron and Aluminum Salts

The most common iron coagulants are ferric chloride ($FeCl_3$) and sulfate ($Fe_2(SO_4)_3$), while the most common aluminum coagulant is "alum" ($Al_2(SO_4)_3*14H_2O$). When added to water, these coagulants will dissociate to yield trivalent ions (reactions 1-3).

$$FeCl_3 \rightarrow Fe^{3+} + 3Cl^- \quad (1)$$

$$Fe_2(SO_4)_3 \rightarrow 2Fe^{3+} + 3SO_4^{2-} \quad (2)$$

$$Al_2(SO_4)_3 \rightarrow 2Al^{3+} + 3SO_4^{2-} \quad (3)$$

The metal ions will then undergo hydrolysis to form various iron and aluminum oxyhydroxides, depending on the pH and oxygen availability within the solution. The addition of metal salts, and their subsequent hydrolysis, will also result in the production of H^+ ions, causing the pH to drop. The amorphous solids that are produced from this process are sensitive to pH changes and may re-dissolve. The re-dissolution of the metal precipitates will result in non-ideal coagulation conditions and reduced treatment efficiency. Therefore, pH adjustments are often necessary in CC to maintain optimal coagulation conditions.

CC using iron and aluminum salts is a well-established technique for the removal of suspended particles as well as a wide variety of contaminants in both drinking water and wastewaters. Some contaminants that can be removed by CC include natural organic matter [35,36], algae [37,38], pathogens [39], phosphorus [40,41], dissolved organic nitrogen [42,43], arsenic [44,45], copper [46], fluoride [47], manganese [48,49], and silica [50,51].

2.1.3 Drawbacks of Chemical Coagulation

While CC is a well-studied and proven technology, its use for water treatment still has drawbacks, which generally fall into two categories, namely cost and treatment complexity. On the cost side, the transport and storage of chemical coagulants requires additional expense. CC also has large mixing requirements, which leads to high energy demands and operational costs. On the treatment complexity side, the addition of metal ions via metal salts also results in the addition of counter ions to the water, which are undesirable for water recycling since they can damage pipes and equipment. Therefore, additional treatment may be needed to remove these counter ions, increasing both cost and treatment complexity. As mentioned previously, the addition of metal salts also decreases the pH of the water, which can impact treatment efficiency and later treatment processes that often function optimally at neutral pH values. Often, this decrease in pH is mitigated by increasing the alkalinity of the water through the addition of a base, which not only further increases treatment costs but also creates additional sludge that must be treated and disposed of.

2.2 Electrocoagulation

Electrocoagulation (EC) involves the application of current to metal electrodes to release metal ions into the surrounding water. Generally, water treatment by EC occurs via the steps listed below and summarized in Figure 2-1.

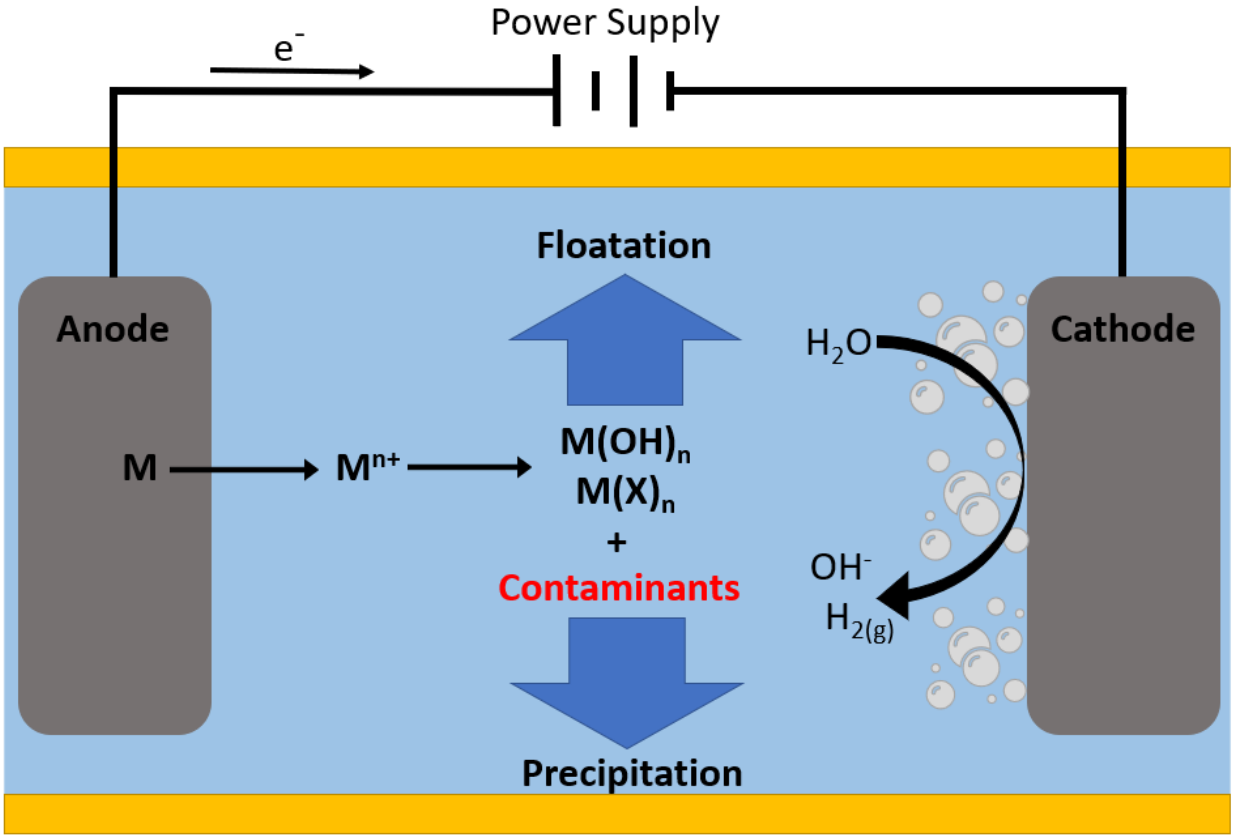

Figure 2-1. The electrocoagulation process

1. On the anode, the electrochemical corrosion driven by the electric current produces metal ions:

$$M \rightarrow M^{n+} + ne^- \qquad (4)$$

2. On the cathode, the reduction of water produces OH^- and H_2 gas:

$$2H_2O + 2e^- \rightarrow H_2 + 2OH^- \qquad (5)$$

3. The metal ions released via reaction 4 destabilize the suspended particles in the solution. The metal ions also react with H_2O (i.e., hydrolysis) and/or other dissolved species in the solution to form precipitates:

$$M^{n+} + nH_2O \rightarrow M(OH)_{n(s)} + nH^+ \quad (6)$$

$$M^{n+} + nX \rightarrow M(X)_{n(s)} \quad (7)$$

4. Contaminants are adsorbed onto the surface of the precipitates.
5. The precipitates aggregate and form flocs, which subsequently are separated by sedimentation, floatation, or filtration.

Compared to CC, EC offers several distinct advantages, including no chemical addition, little change in pH due to the simultaneous production of OH^- and H^+, smaller space requirements, no addition of unnecessary counter ions, less mixing requirements due to uniform corrosion of the electrodes directly into the surrounding solution, and reduced sludge generation [6,8–11]. EC is especially appealing for the treatment of high-salinity waste streams as the addition of salts and other chemicals to such types of waste is not desirable. Additionally, EC can also be more easily implemented as a small-scale point of use treatment since it does not require the storage and transport of chemicals and is relatively easy to operate.

Given the aforementioned potential benefits of EC, there have been extensive efforts put towards investigating the treatment of various water streams by EC over the last couple of decades, including, surface water [10], groundwater [52–54], municipal wastewater [55], landfill leachate [56,57], boiler blowdown [14,15], and industrial wastewaters [5,58,59]. Of these waters, the treatment of groundwater by EC to remove arsenic (As) is one of the most studied [60–64], and researchers have successfully demonstrated the removal of As by EC in the laboratory as well as in the field [65]. In addition to As, other types of contaminants and solutes have also been shown to be removed by EC, including

chromium (VI) [3,66–68], heavy metals [69–73], dyes [13,74–80], perfluoroalkyl acids [81–84], dissolved silica [15,85], hardness [15,29,86,87], fluoride [52,88–90], natural organic matter (NOM) [91,92], and chemical oxygen demand (COD) [29,58,70,93–95].

To further describe the details of the processes that occur in EC, the following sections of this chapter are organized to provide background on EC theory. First, a description of common EC parameters and their associated equations are presented. This is followed by a description of the processes that occur in EC reactors with iron and aluminum electrodes. Finally, this section ends with a discussion of electrode fouling and the current proposed fouling control strategies.

2.2.1 Key Electrocoagulation Parameters

As mentioned earlier, the release of coagulants in EC occurs when a current is applied to the submerge metal electrodes. There are three main parameters that are used in EC literature to describe this process, namely current density j (A/cm^2), charge density q (C/L), and faradaic efficiency (ϕ).Whereas j is the current I (A) applied to the system normalized by the surface area of the anode A (cm^2), q is a measure of the amount of charge that passes through the system of given volume V in a given time t:

$$j = \frac{I}{A}$$

Equation 1 Current density

$$q = \frac{(I \times t)}{V}$$

Equation 2 Charge density

Current density *i*, controls the rate at which coagulant is released into the solution, which can impact the nature of the precipitates produced, their ability to coagulate, and the pH conditions within the reactor (see sections 2.4.2 - 2.4.4). The varying concentration gradients, which is the result of lower or higher current density, can also influence the migration of coagulant from the electrode surface into the bulk solution. Higher current densities can also lead to higher electrode potentials, which control what electrochemical reactions can occur. Meanwhile, charge density q controls the total coagulant dose within the reactor. Similar to CC, coagulant dose can directly affect contaminant removal, particularly for contaminants that react directly with the metal ions or adsorb to the metal precipitates. The total amount of metal ions in solution can also impact the type of precipitates that can form [96].

The other parameter that is important in EC is the faradaic efficiency (ϕ), which is the ratio between the actual mass of coagulant produced (m) over the theoretical amount predicted by Faraday's law:

$$m_{theoretical} = \frac{ItM}{zF}$$

Equation 3 Faraday's law

$$\phi = \frac{m_{measured}}{m_{theoretical}}$$

Equation 4 Faradaic efficiency

where z is the number of electrons transferred in the anodic reaction (reaction 4) (e.g., z = 2 for Fe, 3 for Al), F is Faraday's constant (96,485 Coulombs/eq), M is the molecular weight (56 for Fe, 27 for Al) and t is the electrolysis time (s). Ideally, the only anodic reaction should be the production of metal ions (ϕ = 1). If other reactions were to occur, ϕ would decrease. Consequently, higher

current densities, which can trigger side reactions, may result in low ϕ. Thus, j is an important parameter to optimize in conjunction with ϕ.

2.2.2 Iron-based Electrocoagulation

One of the most frequently used electrode materials used in EC is zero-valent iron (Fe^0) as it is relatively inexpensive and readily available, although more expensive materials such as aluminum (Al^0) [11,13], magnesium (Mg^0) [97,98], and zinc (Zn^0) [99,100] are used in certain applications. In iron-based electrocoagulation (Fe-EC), Fe(II) ions are released via anodic oxidation (reaction 8).

$$Fe \rightarrow Fe(II) + 2e^- \qquad (8)$$

The ions are then diffused into the bulk solution where they are oxidized by dissolved oxygen into Fe(III) ions. Subsequently, the Fe(III) ions rapidly precipitate out to form solids that have high surface area and adsorption capability (e.g., reaction 9) [2].

$$4Fe(II) + O_2 + 10H_2O \rightarrow 4Fe(OH)_{3(s)} + 8H^+ \qquad (9)$$

Over the past two decades, researchers have put significant effort into characterizing the physio-chemical properties of the precipitates generated in Fe-EC, and elucidating factors affecting the adsorption of contaminants onto the precipitates. It has been shown that both the solution chemistry and EC operation parameters control the nature of the precipitates. For example, in oxygenated solutions the precipitates are lepidocrocite (γ-FeOOH) or a mixture of lepidocrocite and ferrihydrite (i.e., a poorly crystalline iron hydroxide), whereas magnetite (Fe_3O_4) is produced in anoxic solutions [96,101]. However, if the anoxic solution contains carbonate and sulfate, the predominant product would be carbonate green rust or sulfate green rust [96]. Dissolved silica, a solute commonly present in groundwater, can also influence the formation of iron precipitates by

slowing the oxidation of iron (reaction 8) [102] and the crystallization of iron hydroxide [103]. The precipitates produced by Fe-EC in the presence of silica have been shown to be ferrihydrite [96,103].

Current and charge density can also affect the solution chemistry and mass transport characteristic in Fe-EC. For example, the rapid release of Fe(II) from the anode when EC is operated at a high *j* will result in a quick consumption of dissolved oxygen via reaction 9. Oxygen can also be consumed via reduction at the cathode (reaction 10).

$$O_2 + 4e^- + 4H^+ \rightarrow 2H_2O \qquad (10)$$

If the rate of oxygen consumption is faster than the rate of replenishment from the surrounding air, an initially oxygenated solution can quickly become anoxic. Thus, the nature of the precipitate produced in Fe-EC would continuously change during the treatment. Also, as bulk and cathodic reactions involve H^+ and OH^- (reactions 5, 9, 10), the solution pH, as well as the local pH in the boundary layer of the electrodes, change during EC operation. It is well known that the solution pH has a tremendous effect on the chemistry of dissolved iron and iron minerals, including controlling the rate of Fe(II) oxidation (reaction 9) [104], the dissolution and precipitation of iron minerals [105], and the mineral surface charge surface[106]. Therefore, a change in pH during Fe-EC treatment will influence the physio-chemical properties (e.g., crystallinity, surface area and charge, surface adsorption density) of the precipitates and the efficiency of contaminant adsorption.

As well as controlling the formation of the precipitates, the solutes present in the to-be-treated water can affect the removal of contaminants either by directly competing with the contaminants for surface adsorptive sites or by inhibiting the growth and aggregation of precipitates into larger flocs that can be easily separated from the treated water. For example, it has been shown that the removal of As by Fe-EC was significantly reduced in the presence of phosphate because the latter

binds strongly to iron precipitates, reducing the number of surface sites available for As adsorption [60]. Although dissolved silica did not significantly impact the adsorption of As, its presence led to the formation of ferrihydrite colloids that would settle out at a slower rate [96]. NOM could also influence the removal of contaminants in Fe-EC as NOM can compete with the contaminants for surface adsorptive sites, as well as prevent the coagulation and flocculation of the precipitates.

2.2.3 Aluminum-based Electrocoagulation

In aluminum-based electrocoagulation (Al-EC), Al(III) ions are released from the anode and react with water to form aluminum oxyhydroxides (reactions 11, 12, 13) [12,107,108].

$$Al \rightarrow Al(III) + 3e^- \quad (11)$$

$$Al(III) + 3H_2O \rightarrow Al(OH)_3 + 3H^+ \quad (12)$$

$$nAl(OH)_3 \rightarrow Al_n(OH)_{3n} \quad (13)$$

The aluminum species formed during EC are dependent on the pH of the bulk solution as well as the pH near the electrodes. At low pH, cationic monomeric species such as Al^{3+} and $Al(OH)_2^+$ are formed, while at higher pH values $Al(OH)^{2+}$, $Al_2(OH)_2^{4+}$ and $Al(OH)^{4-}$ are also present [11,107]. The most common precipitate formed in Al-EC is amorphous $Al(OH)_3$ polymorphs, particularly bayerite, though studies also reported the presence of boehmite (AlOOH) [109–111]. However, pH and co-existing ions can determine the nature of the precipitates formed, leading to the formation of other aluminum species. For example, in the presence of phosphate the precipitates become a mixture of $Al(OH)_3$ and $AlPO_4$ [41]. In the presence of fluoride, various intermediate species of aluminum fluoride complexes can be formed including Al(OH)F, $AlFO_2H$ and AlF_2 [5]. The solution chemistry also plays a role in the production of coagulant and/or the prevention of corrosion at the surface of the aluminum electrodes. For example, the presence of phosphate can impede the corrosion of aluminum electrodes by forming a passive layer of $AlPO_4$, while the presence of

chloride ions can facilitate corrosion [41,108]. Of particular concern is sulfate, which has been shown to lower faradaic efficiency and reduce contaminant removal [90,112].

While Al-EC follows principles similar to those of Fe-EC (as described above), there is an important difference between Fe-EC and Al-EC, that is aluminum is soluble at high pH. Therefore, chemical corrosion of the aluminum cathode is possible due to the high pH region generated via reaction 5. This additional chemical corrosion increases the amount of coagulant being produced, such that ϕ would be above what would have been predicted by Faraday's law. This phenomenon is often referred to as super-faradaic efficiency [108,113–115]. While this phenomenon can be beneficial as more coagulant is produced with less energy provided to the system, it will also increase electrode consumption, requiring the electrodes to be replaced more frequently.

2.2.4 Floc Formation in EC

Sections 1.4.2 and 1.4.3 above describe the processes that result in the formation of precipitates and the removal of contaminants from the solution. Following these processes, the precipitates aggregate and are removed from the treated solution. As discussed in section 1.2, coagulation not only consists of attachment but also the growth and aggregation of the precipitates into flocs [116]. The growth and aggregation of aluminum and iron flocs in CC and EC can be quite different, due to 1) the dosing of the coagulant 2) the pH conditions, and 3) the production of gas bubbles [117].

In EC, coagulants are gradually introduced to the solution across the electrode surface. In contrast, coagulant dosing in CC happens all at once, resulting in vastly different solution conditions. As discussed previously, the main change to solution chemistry in CC is a pH drop due to metal hydrolysis [116]. The low pH impacts what metal species can form and can keep the metal

ions dissolved, resulting in non-ideal coagulation conditions. For aluminum, both low and high pH values promote the formation of soluble aluminum species (Al^{3+} and $Al(OH)_2^+$ and low pH and $Al(OH)^{2+}$, $Al_2(OH)_2^{4+}$ and $Al(OH)^{4-}$ at high pH). When these soluble aluminum species transition to insoluble forms, such as bayerite or boehmite, the flocs tend to be much smaller in size [118]. Conversely, if the Al^{3+} ions are introduced directly within the pH range of 5-8, amorphous boehmite is formed. Amorphous boehmite more readily forms large flocs that can enmesh other precipitates and contaminants. To achieve this "ideal" pH for coagulation in CC, the addition of a base is often necessary. In contrast, the pH change in EC is buffered by the production of OH^- at the cathode, resulting in a more neutral to alkaline environment that is more conducive to the formation of the large boehmite flocs [21,118–120].While the effect of pH is similar for iron species, it is only readily soluble at low pH values and therefore has a much larger optimal pH range (5-10) for coagulation [2,121,122]. While pH adjustment will remain necessary in CC to bring the solution pH to 5, Fe-EC unlikely requires any chemical addition to adjust the solution pH.

The gradual dosing of coagulant in EC also results in a more "diffusion limited aggregation process" in which floc formation is limited by the contact between the metal precipitates [118]. Flocs formed under gradual dosing conditions are described as having looser, larger structures, which can impact settling, flotation, and contaminant removal. These looser, larger structures also tend to be more fragile. In contrast, CC flocs are produced under the "reaction limited aggregation" regime, resulting in more compact flocs [118]. In EC, current density can also affect floc formation by controlling the dosage rate of coagulant. Higher current densities will result in higher concentrations of coagulant being produced over a shorter period of time. This will push the conditions within the boundary layer of the anode to more "reaction limited aggregation", similar to that in CC [118]. Current density will also change the migration of particles within the reactor by

controlling the strength of the electric field. Higher current densities result in stronger electric fields, which promote the faster migration of particles in the reactor and more collisions between particles, thereby enhancing coagulation [118,123,124]. However, these positive effects must be balanced with the charge density, which dictates total coagulant dose. Higher current density means higher charge density for the same current processing time and volume. If the dose surpasses the optimal value, there will be wasted electrode and energy and larger flocs that may be less likely to float [21,124]. Additionally, high current densities can result in side-reactions, diverting energy away from the production of coagulant.

Another difference between EC and CC is the production of hydrogen gas at the cathode in EC. These small gas bubbles can become a part of the floc structure and promote flotation [20,125]. Current density will affect the rate of hydrogen production and, therefore, affect the introduction of gas bubbles to the floc structure. Gas generation can also impact electrode fouling, which will be discussed in future sections (section 2.2.5.3).

In addition to the factors discussed above, hydrodynamics within the EC reactor will also play a large role in floc formation. The hydrodynamics within the reactor will be determined by reactor shape, electrode distance, and mixing patterns. In general, high mixing and turbulence in the reactor is necessary for the migration of coagulant from the electrodes to the bulk solution [9]. High mixing will also be beneficial to coagulation to ensure a high degree of particle collisions. However, excessive shear can also lead to floc breakage [126]. To balance these two factors, it may be beneficial to separate the coagulant dosing and high mixing zones from the floc formation zones to ensure optimal conditions for each.

As discussed, the pH of the solution preceding and during coagulation can greatly impact the floc growth in EC. Other solution chemistry parameters, such as the types of pollutants present

will also impact floc growth [117,119]. For example, the presence of oils can coat the precipitates produced and can cause them to float, reducing their ability to collide and grow. Furthermore, the presence of silica can influence the crystallinity of iron oxides and affect their ability to coagulate [127,128]. Therefore, much like CC, EC must be optimized for specific water chemistry conditions.

2.2.5 Fouling in Electrocoagulation

One of the major long-term operational challenges associated with EC is the build-up of materials on the surface of the electrodes over time, which is often referred to as **fouling,** although other terms such as scaling and electrode passivation have also been used in the literature. The types of fouling materials present on the electrodes differ depending on if the electrode is an anode or cathode, owing to the different reactions and pH conditions in the vicinity of each electrode (i.e., low pH at the anode, high pH at the cathode). The anode fouling layer consists of primarily metal oxyhydroxides, which build up over time as the metal ions produced at the electrode-electrolyte boundary undergo hydrolysis and/or react with species in the boundary layer [2,114]. Meanwhile, in the high pH region at the cathode, calcium and magnesium ions can react with OH^- or carbonate in the surrounding water to form minerals (reactions 14-17) [72,129–131].

$$HCO_3^- + OH^- \rightarrow CO_3^{2-} + H_2O \quad (14)$$

$$Ca^{2+} + CO_3^{2-} \rightarrow CaCO_{3(s)} \quad (15)$$

$$(1-x)Ca^{2+} + xMg^{2+} + CO_3^{2-} \rightarrow Ca_{1-x}Mg_xCO_{3(s)} \quad (16)$$

$$Mg^{2+} + 2OH^- \rightarrow Mg(OH)_{2(s)} \quad (17)$$

Fouling can cause different side effects, depending on the electrode and fouling materials present. For example, if the build-up of materials on the surface becomes severe, fouling can decrease the inter-electrode gap and clog the EC reactor [132]. Faradaic efficiency in the bulk solution can also decrease if the migration of metal ions into the bulk solution is impeded by the formation

of metal oxyhydroxides directly onto the electrode surface, enmeshing metal ions in the fouling layers[17,19,22,133]. Additionally, the presence of Ca- and Mg- containing minerals can impede the chemical corrosion of the electrode's surface and decrease coagulant production. The presence of fouling layers also increases electrode overpotential and, therefore, energy consumption over time [20,21,23,114,133,134]. If overpotential continues to increase, side reactions that direct energy away from the production of metal ions become possible, potentially reducing coagulant production and contaminant removal [96,112]. Anodic fouling, in particular, can decrease the number of active sites available for corrosion on the electrode surface. This decrease can result in a localized area of high current density, which can also trigger side reactions and can lead to non-uniform corrosion of the electrode. Some possible side reactions include the oxidation of water and chloride ions into $O_{2(g)}$ and $Cl_{2(g)}$ (reactions 18 and 19) [96].

$$2H_2O \leftrightarrow O_2 + 4H^+ + 4e^- \quad E^0 = 1.23 \text{ V vs. SHE} \qquad (18)$$

$$2Cl^- \leftrightarrow Cl_2 + 2e^- \quad E^0 = 1.36 \text{ V vs. SHE} \qquad (19)$$

Due to the negative side effects associated with fouling researchers have suggested several types of fouling mitigations strategies that seek to remove the fouling layers present or to pre-emptively prevent their formation.

2.2.5.1 Fouling Prevention Strategies

One of the main mitigation strategies to prevent the formation of fouling layers is aggressive ion addition, which is often suggested in cases where passivating oxyanions such as SO_4^{2-}, phosphate, NO_3^- are present in the solution [17,108,112,134–136]. Aggressive ion addition works by allowing ions to directly react with the electrode surface to form soluble metal complexes [17,108]. The main aggressive ion suggested by the current research is Cl^-, which promotes pitting corrosion on both iron and aluminum electrodes [17,109,134,137,138]. Some studies have even suggested specific

ratios of Cl^- ions with respect to passivating oxyanions to ensure corrosion of the electrode surfaces [17,107,114,139]. Despite the effectiveness of this technique, there are drawbacks to aggressive ion addition. Firstly, the addition of salts adds significant cost to the treatment, particularly considering that the main advantage of EC is its ability to treat water without the addition of salts. Secondly, aggressive ion addition may also require further treatment downstream of the EC reactor to remove the salts before discharge to the environment. Finally, it has also been suggested that high Cl^- ion concentrations could result in the generation of toxic by-products if organics are present [66,140–142].

Another option to prevent the formation of fouling in EC is pre-treatment to remove the ions that can precipitate within the boundary layers, particularly Ca^{2+} and Mg^{2+}, via ion exchange or lime softening. However, this would increase the treatment complexity of the system and add significant cost.

2.2.5.2 Fouling Removal Techniques

To overcome the drawbacks of fouling mitigation, several fouling removal strategies have also been proposed, including mechanical and chemical cleaning, increasing the flow rate, and ultrasonication. Mechanical cleaning involves physically removing the fouling layers by brushing or scraping the surface of the electrodes[2,19,64,133]. Amrose et al. (2013) showed that periodically removing these layers with a steel brush reduced energy consumption and enhanced contaminant removal, demonstrating the importance of removing fouling in EC. While this technique is highly effective and is recommended by several researchers[2,19,22], it requires shutting down the EC reactor for a period of time and physically removing the electrodes to clean them. This increases the labour required for the treatment process and is not suitable for continuous EC operations. Alternatively, the fouling layers can be removed by washing the electrodes with acid. However, this technique has the same drawbacks as the mechanical cleaning (i.e., operation disruption), and also requires

the purchase and disposal of concentrated acids [22]. Another fouling removal method that has been proposed is hydrodynamic scouring, which involves the application of increased flow through the reactor to dislodge the fouling layers [9]. To maximize the effectiveness of this technique, it was suggested that the EC reactor should also be designed to increase the shear across the surface of the electrodes [9]. However, increasing the flow rate or optimizing the reactor design may not always be possible since the flow rate may affect other processes within the EC reactor. For example, increased flow rate would result in large space requirements if a certain residence time must be attained for proper contaminant removal. Additionally, higher flow rates will result in more turbulence within the reactor, which is detrimental to the formation of large flocs. Ultrasonication-assisted EC, also referred to as sono-EC, combines the EC process with sonication to enhance pollutant removal and dislodge any fouling layers on the electrodes' surface [143,144]. Sonication induces cavitation, which is the formation, growth and collapse of bubbles within solution. These bubbles can dislodge the fouling layers and create cracks and defects on the surface of the electrodes, thus increasing the rate of corrosion by increasing the surface area [143,145]. Several studies have reported increased contaminant removal using sono-EC with minimal additional operating costs [143,146–151] . However, other studies have indicated large cost increases [152], and increased passivation under high-power sonication conditions [147]. Furthermore, it has also been suggested that sonication may break apart the flocs formed in EC, leading to lower contaminant and solids removal [147]. Therefore, while sono-EC is a promising technology for fouling removal and enhanced EC performance, more research is needed to optimize its use. Given that the use of sono-EC requires complicated infrastructure and additional energy consumption, it is not ready for widespread adoption.

2.2.5.3 Polarity Reversal

Due to the drawbacks of the other fouling mitigation and removal strategies, researchers have begun focussing on alternating current (AC) and polarity reversal (PR) as a cost-effective, easily applicable fouling mitigation strategy [17,23,155–158,59,68,74,82,84,97,153,154]. These techniques involve switching the direction of the current applied to the reactor, such that the anode becomes the cathode and vice versa. While in AC the current changes gradually over time (sinusoidal function), the current direction in PR is switched intermittently (square function) (Figure 2-2).

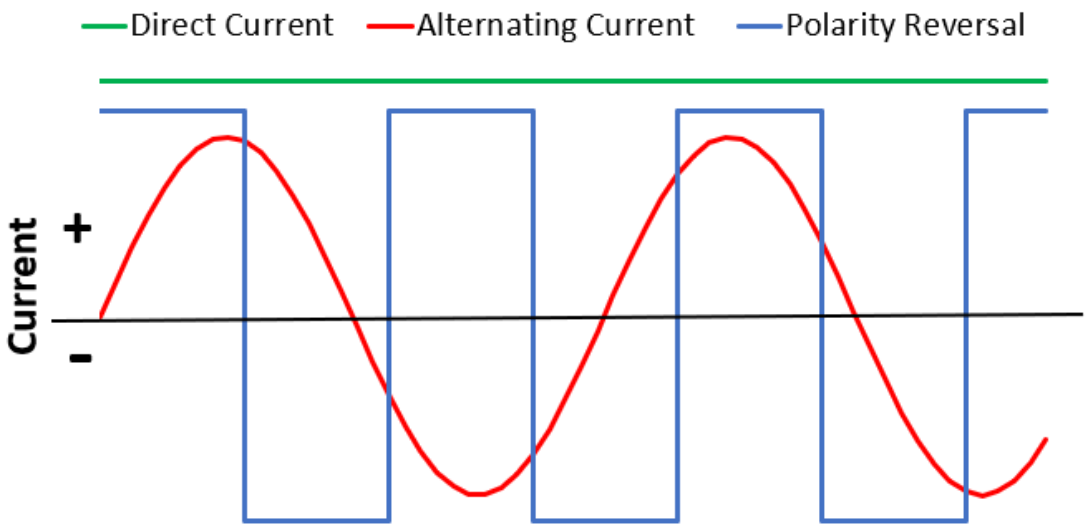

Figure 2-2. The mode of application of current in EC

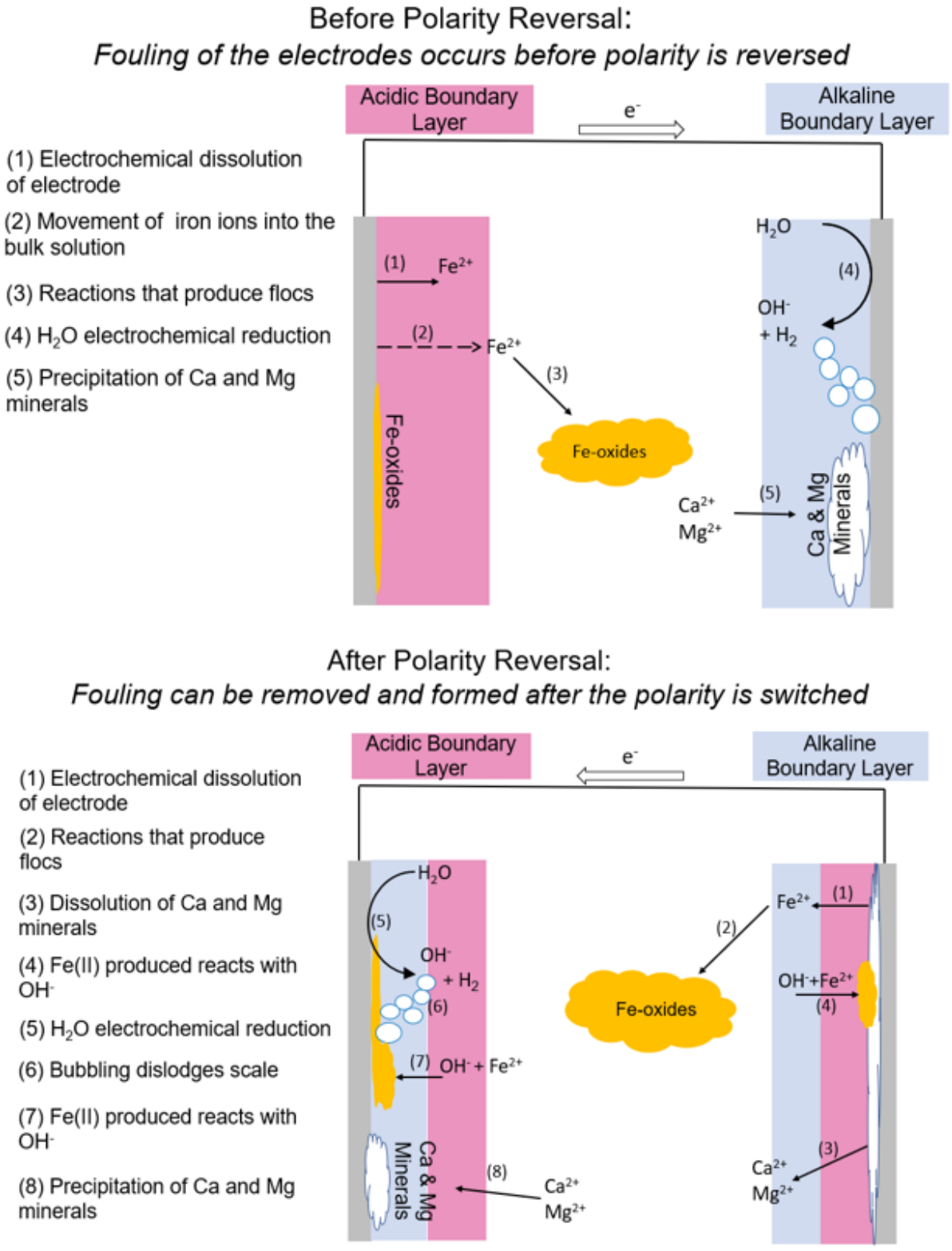

Figure 2-3. Processes that may occur in the vicinity of the electrodes before and after polarity reversal in EC

To date, the ability of these techniques to mitigate electrode fouling remains poorly understood, with conflicting results being reported in the literature. Studies have shown that PR-EC consumed less energy yet were more effective at removing contaminants than DC-EC [59,153,159–161]. This enhanced performance was often claimed to be the direct result of the diminished electrode fouling. However, few studies analyzed the electrode surface to support this claim. Based on Scanning Electron Microscopy (SEM) images, Mao et al [153] Karamati-Niaragh et al [157], and Vasudevan et al[158,162] reported that iron and aluminum electrodes were dissolved more uniformly in PR-EC than in DC-EC. In contrast, two recent studies observed the formation of thick fouling layers in PR-EC [22,163], raising significant questions about whether alternating currents can effectively mitigate electrode fouling. The removal of electrode fouling layers by PR was also invoked in a few studies to explain the higher Faradaic efficiency (i.e., the coagulant production efficiency per unit of electric charge passed through the system) [23,164]. Contrary to these observations, however, several studies have reported a lower Faradaic efficiency in PR-EC than in DC-EC, with an efficiency that decreased as the current reversal frequency (*f*) increased [9,163,165–167]. The PR *f* optimal for contaminant removal appeared to be dependent on the electrode type (e.g., Fe *versus* Al) and the contaminant to be removed [68,74,77,168–170]. It is difficult to directly compare these past results, since the experimental conditions (e.g., solution composition, electrode type, PR *f*, current density, and reactor design) vary greatly between studies. For example, since Cl^- ions can inhibit electrode passivation by inducing pitting corrosion[17,134,137,13817,134,137,138], it is not possible to compare the results of the systems that treated concentrated brine and seawater [9] with those that treated groundwater[19]. As another example, Muller et al [22] air-dried the iron electrodes between each current cycle. As such, the build-up of thick surface layers observed in this study may be due to the oxidation of the electrode surface by air. Whether such a build-up of

surface layers will occur in a continuously operated system is not certain. In the same study, it was speculated that the $CaCO_3$ formed on the cathode trapped or dissolved the iron and diminished the coagulant production when the current direction was switched [22]. Although the formation and removal of Ca- and Mg-containing precipitates in PR-EC systems has not been investigated, the potentially detrimental effect of $CaCO_3$ on coagulant production as seen by Muller et al should be considered if PR-EC is used to treat hard water (e.g., groundwater). Overall, given the complexity of the chemical/electrochemical processes that control the fouling of the electrodes in EC, and the varying nature of the fouling layer with different operating conditions, more research is needed to elucidate the factors that affect fouling mitigation by means of current reversal.

2.3 The Treatment of Oil Sands Thermal In-Situ Produced Water

As mentioned earlier, EC is a promising technology for the treatment of high-salinity wastewaters, since the addition of salts and other chemicals to such types of waters is not desirable. An example of one of high-salinity waste streams is PW, which is wastewater generated from the thermal in-situ extraction of oil sands. Thermal in-situ extraction involves the injection of steam into the subsurface to liquify bitumen deposits. The oil-water mixture is then pumped to the surface where oil is separated, leaving behind the PW. As a result of oil extraction, PW is comprised of a complex mixture of bitumen residue, dissolved organic compounds, inorganic salts, and suspended solids (SS). The characteristics of PW collected at the Peace River, Leming Cold Lake and Getty's Kern River facilities are presented in Table 1.

Table 2-1. Composition of Produced Water.

Parameter	Peace River (average values)[1]	Leming Cold Lake[2]	Getty's Kern River (average values)[2]
pH	7-9	8-9	7.2
Na^+ (mg/L)	1850	1000-4000	190
K^+ (mg/L)	50	1000-4000	n/a
Ca^{2+} (mg/L)	65	40-60	n/a
Mg^{2+} (mg/L)	18	4-8	n/a
Cl^- (mg/L)	1950	2000-6000	185
HCO_3^- (mg/L)	1660	100-400	292
SO_4^{2-} (mg/L)	40	40-200	82
CO_3^{2-} (mg/L)	2.0	n/a	n/a
H_2S (mg/L)	110	10-40	0
SiO_2 (mg/L)	80	150-300	125
Oil and grease (mg/L)	75	5000-10000	50
TDS (mg/L)	4750	4000-10000	622

1. *Royal Dutch Shell. (2014). Peace River Produced Water Quality . Shared data file*
2. *Butler, R. M. (1991). Thermal Recovery of Oil and Bitumen. New Jersey: Prentice-Hall Inc.*

Traditionally, PW is reused to produce steam for further oil extraction. The main operational challenge concerning the reuse of PW is the formation of scales in boilers and pipes due to the high concentrations of silica, calcium, and magnesium in PW. Additionally, corrosive agents, such as sulfide, are also a concern since they can corrode pipes and boilers. Thus, these solutes must be removed from PW prior to its reuse. In the following sections, the treatment of PW by various methods along with the drawback associated with each method are described. As will become obvious, the drawbacks of each method highlight the need for an alternative process for the treatment of PW.

2.3.1 Lime Softening

One of the most common ways to remove hardness from PW is lime softening [26,171]. The purpose of lime softening is to reduce hardness and silica. This is accomplished through the addition of lime and soda ash, along with coagulants and flocculants to promote the precipitation of calcium, magnesium, and silica [172–174]. Calcium and magnesium are removed through the formation of sparingly soluble minerals, most commonly calcium carbonate and magnesium hydroxide. Silica removal occurs by the adsorption and/or coprecipitation of silica with magnesium hydroxide precipitates. In lime softening, the temperature is kept at above 49 °C (49 to 60 °C and 108 to 116 °C for warm and hot lime softening, respectively) to further reduce the solubility of calcium, magnesium, and silica. If magnesium is not present in sufficient quantities to remove silica, magnesium oxide is added [172]. While effective, warm/hot lime softening treatment requires further polishing by weak or strong acid cation exchange to remove residual calcium and magnesium. Due to the complexity of lime softening, the treatment of PW by this technology is costly, complex, and produces large volumes of precipitates (i.e., sludge) that require treatment and disposal [174,175].

2.3.2 Evaporation

Another method that is used to treat PW is evaporation by falling film vertical tube (FFVTE), wherein the PW is evaporated into vapour that then condenses into clean water [175]. The waste generated from this process is a highly concentrated brine, which is disposed of by deep injection. The treatment by FFVTE begins by pumping the PW to a heat exchanger, which raises the PW's temperature to its boiling point. The heated PW is then pumped to the bottom of the evaporation chamber where it combines with the already processed brine slurry. This mixture is then pumped to the top of the chamber where it flows down into heat transfer tubes where a portion will evaporate. The vapour created is then collected through mist eliminators and is condensed in a compressor chamber. Any remaining fluid that did not evaporate in the tubes is recycled to the top, with a portion of it being taken out at the bottom for disposal. The treatment by FFVTE has several advantages over the traditional lime softening systems, including reduced operational complexity (since FFTE treatment is a one stage process), reduced maintenance, smaller footprint, and lower chemical demand. Despite these advantages, the treatment by evaporation has several drawbacks, including the generation of a highly concentrated brine, which must be disposed of, high capital and operational costs, scaling of the evaporator over time, and high energy demand [25,175].

2.3.3 Electrocoagulation for the Treatment of Oil Sands Thermal In-Situ Produced Water

Due to the drawbacks of lime softening and evaporation, novel cost-effective technologies that can effectively remove silica are needed to help the oil sands industry increase water recycling, reduce energy consumption and production cost, and reduce environmental impact. To this end, Canada's Oil Sands Innovation Alliance (COSIA) has identified the development of innovative silica removal technologies as one of the industry's priorities [24]. In addition to silica, removing

calcium, magnesium, and sulfide from in-situ PW is also desirable because these solutes can cause scaling and corrosion of pipelines and steam generators [26,27].

As a part of this PhD research, the treatment of thermal in-situ produced water by electrocoagulation (EC) will be explored. It is hypothesized that EC can remove the contaminants of concern in PW, since studies have demonstrated that EC can remove silica [14,28], sulfide [30], calcium, and magnesium [15,29] in various water chemistry conditions. It is noted that these previous studies often dealt with wastewater streams that were less complex than PW and focused on the removal of only one specific contaminant (e.g., sulfide in wastewater, or silica in brackish water). Therefore, the ability of EC to remove these contaminants simultaneously in a complex water matrix such as PW warrants further investigation, especially because the removal of contaminants from in-situ PW by EC can occur via principles and mechanisms that can be fundamentally different from those in other EC applications. In particular, unlike the other water streams that have been treated by EC, in-situ PW contains a significant amount of sulfide (as much as 300 mg/L, measured as H_2S) whose presence can lead to the formation of sparingly soluble iron sulfide minerals such as mackinawite or greigite, as well as elemental sulfur via the following reactions:

Anodic reactions:	$HS^- \rightarrow S^0 + H^+ + 2e^-$	*(20)*
Bulk reactions:	$Fe(II) + HS^- \rightarrow FeS + H^+$	*(21)*
	$Fe(II) + 3HS^- + S^0 \rightarrow Fe_3S_4 + 3H^+$	*(22)*

It has been shown that mackinawite (FeS) is produced when Fe(II) reacts with HS^- in solutions free of dissolved oxygen [30]. However, FeS can also be formed in an initially oxygenated solution, because reaction 21 occurs much more rapidly than the formation of iron oxyhydroxides, and also because during the EC process dissolved oxygen can be quickly depleted [30]. The ratio of FeS to iron hydroxide produced in Fe-EC depends on the solution chemistry (e.g., pH or the concentration

of dissolved oxygen), the EC operational parameters (e.g., the rate at which Fe(II) ions are released into the solution, and the total amount of Fe(II) released), and the solution mass transport characteristics (e.g., the concentration of dissolved oxygen in the vicinity of anode, the rate at which oxygen is replenished from the surrounding air). For the in-situ PW/Fe-EC system, it is hypothesized that the precipitates will consist primarily of iron sulfides. If this is the case, a significant reduction of the concentration of sulfide can be expected from the Fe-EC treatment. Also, the removal of dissolved silica could be affected by the affinity of silica to the surface of iron sulfide minerals if they are the dominant precipitates. Contrary to Fe-EC, the precipitates formed when PW is treated by Al-EC will likely be $Al(OH)_3$, since sulfide does not react with aluminum ions. Thus, while silica can be removed by Al-EC by adsorbing onto silica [14], it can be expected that sulfide will not be removed by adsorption or precipitation.

A better understanding of the mechanisms that control contaminant removal is also vital for the proper function of EC systems. For example, since PW contains high concentrations of calcium and magnesium, if these solutes are removed by precipitating on the cathode (due to the alkaline environment around this electrode), electrode fouling likely would occur. Since electrode fouling can be detrimental to the performance of EC it should be minimized. Therefore, an understanding of not only the amount of removal but the mechanism which control removal is crucial for the operation of EC.

2.4 Objectives

The overarching goal of the research reported in this thesis is to investigate the fundamental factors that control contaminant removal, electrode fouling, and precipitate characteristics in EC. The research focuses specifically on 1) the ability of EC to simultaneously remove multiple contaminants in the complex water matrix of PW, 2) the use of PR to reduce electrode fouling, 3) the effect of PR in conjunction with water chemistry on coagulant production, and 4) the effect of PR on contaminant removal and precipitate characteristics. Overall, this research will help address some the key knowledge gaps that hamper the use of EC and will aid industry in the development of this technology into a more robust and effective method for the treatment contaminated waters.

Objective I: To investigate the mechanisms through which silica, sulfide, and hardness are removed from PW by EC. This objective focuses on developing a mechanistic understanding of how EC operating parameters affect the removal of each contaminant within the bulk of the solution where active precipitation/adsorption reactions occur during EC. The physio-chemical properties of the precipitates formed when PW is treated by EC will be investigated to gain insights into the mechanisms of sulfide removal.

The experiments conducted in this portion of research employed a SPW formulation that simulated the water chemistry of authentic thermal in-situ PW. A few experiments were also conducted with authentic in-situ produced water collected from a heavy oil thermal in-situ facility. A batch reactor setup was used for all experiments. It is recognized that the flow conditions in batch reactor setups do not represent those of full-scale continuous flow EC treatment systems. However, batch reactor setups are advantageous for studying the mechanisms that control contaminant removal, since the mass balance of coagulant and contaminant within the reactor can

be more readily tracked. Understanding the fundamental factors that control contaminant removal is vital to the design and proper operation of larger, more complex systems.

Objective II: To determine the effect of PR and solution chemistry on electrode fouling and coagulant production. The electrodes are where electrochemical reactions in EC take place, including the reactions that release coagulants into the solution. During EC, electrode fouling can retard the electrochemical processes and increase energy consumption. This objective will explore if the use of PR in EC can help prevent electrode fouling. The effect of PR on coagulant production will also be investigated in varying water chemistry conditions, which can impact the processes occurring at the electrodes.

In this portion of research, a flow-through reactor setup was used wherein a fresh experimental solution was flown through the reactor. Thus, there was a constant supply of contaminants and fouling ions into the reactor, allowing for the accumulation of fouling layers on the electrodes as well as their effects on the performance of EC to be observed. To examine the effect of solution chemistry, four working solutions were used, namely NaCl, Na_2SO_4, high hardness synthetic groundwater, and the SPW used in Objective I. These solutions were chosen for their increasing complexity and varying effects on EC performance. For example, the SGW and SPW solutions contained buffers (e.g., HCO_3^-), which have previously been reported to affect EC performance by creating a passive layer at the electrode surfaces and thereby preventing the release of Fe(II/III) [17]. In the NaCl solution, the coagulant production is expected to be high because Cl^- can help dissolve the electrode surface layers and facilitate pitting [137]. In contrast, SO_4^{2-} has been shown to promote iron and aluminum passivation [17]. In the SGW and SPW solutions, Ca^{2+} and Mg^{2+} are expected to contribute to the fouling of the cathode in DC-EC [72], and on both electrodes in PR-EC. Lastly, the SPW contains HS^-, which can be electrochemically

oxidized into elemental sulfur (S^0), and/or can react with Fe^{2+} to generate sparingly soluble iron sulfide minerals (FeS).

Objective III: To investigate the effect of PR on contaminant removal, and precipitate characteristics. This objective seeks to determine if PR affects the precipitates produced in a synthetic produced water (SPW). If there is a change in the nature of the precipitates, it can impact their ability to adsorb contaminants and their separation from the liquid stream post-EC. Therefore, the effect of PR on contaminant removal and solids separation will also be investigated.

The experiments conducted in this portion of research employed batch reactors to enable closing mass balance of coagulant and contaminants, as well as quantifying the rate at which precipitates settle.

Chapter 3

Effective Removal of Silica and Sulfide from Oil Sands Thermal in-situ Produced Water by Electrocoagulation

This chapter was published in the Journal of Hazardous Materials, Volume 380, Chow H., Pham ALT., Effective removal of silica and sulfide from oil sands thermal in-situ produced water by electrocoagulation, 120880, Copyright Elsevier (2019)

3.1 Chapter Introduction

In-situ thermal recovery technologies such as Steam-Assisted Gravity Drainage (SAGD) and Cyclic Steam Stimulation (CSS) are being increasingly used for the extraction of bitumen in oil sands deposits [176]. These technologies involve the injection of steam into the subsurface to reduce the viscosity of dense bitumen. The oil and steam mixture migrates to the production well and is extracted to the surface. Subsequently, the thermal in-situ produced water (i.e., the water produced as a result of steam condensation) is separated from oil, treated and either recycled for steam production or disposed via deep ground injection.

In-situ produced water is comprised of a complex mixture of bitumen residue, dissolved organic compounds, inorganic salts, and suspended solids [24]. Among these constituents, dissolved silica, present at concentrations as high as 350 mg/L, is particularly problematic because its precipitation can lead to scaling of steam generators and clogging of disposal wells. Currently, dissolved silica is removed from the produced water by lime softening or evaporative treatment [24]. However, these treatment technologies have high capital cost, are energy intensive and difficult to operate [25]. Lime softening is also chemical intensive and generates large volume of sludge.

Therefore, novel cost-effective technologies that can effectively remove silica are needed to help the oil sands industry increase water recycling, reduce energy consumption and production cost, and reduce environmental impact. To this end, Canada's Oil Sands Innovation Alliance (COSIA) has identified the development of innovative silica removal technologies as one of the industry's priorities [24]. In addition to silica, removing calcium, magnesium, and sulfide from in-situ produced water is also desirable because these solutes can cause scaling and corrosion of pipelines and steam generators [26,27].

In this study, the treatment of in-situ produced water by electrocoagulation (EC) was explored for the first time. EC typically employs electric current to corrode iron or aluminum anodes to release Fe(II) (or Al(III)) ions into the solution[7,94]. These ions then react with solutes in the solution to form Fe-containing (or Al-containing) precipitates that can adsorb a wide variety of contaminants. such as arsenic, chromium, heavy metals, natural organic matter, and viruses [1,3,61,109]. Compared with other chemical and biological water treatment technologies, EC offers distinct advantages including no/minimal chemical addition, adjustable/controllable treatment rate, and reduced sludge generation[6–8,177].

Several studies have shown that EC can remove silica, sulfide, calcium, and magnesium [14,28–31], raising the potential of this technology to treat in-situ produced water that contains these contaminants. However, these previous studies dealt with wastewater streams (e.g., municipal wastewater, hydraulic fracturing produced water, brackish water, or cooling tower blowdown water) that were less complex than in-situ produced water. These studies also often focused on the removal of only one specific contaminant (e.g., sulfide in wastewater, or silica from brackish water [28,31]. Whether EC can remove silica, sulfide, calcium or magnesium when these species coexist in a complex water matrix like in-situ produced water has not yet been investigated.

It is hypothesized that the complex composition of the in-situ produced water will greatly influence the performance of EC because the nature of the precipitates generated in EC and the adsorption of contaminants are controlled by the solution chemistry. For example, it has been shown that in oxygenated solutions the precipitates produced by Fe-EC were lepidocrocite or a mixture of lepidocrocite and ferrihydrite, whereas magnetite was produced in anoxic [91,96]. In contrast, iron sulfide minerals (FeS) were produced when EC was applied to sulfide-containing waste streams [30,31]. Because in-situ produced water contains up to a few hundred mg/L of sulfide, it is likely that the precipitates generated by Fe-EC treatment would be FeS. However, silica in the in-situ produced water may influence the formation of FeS because silica is known to inhibit the precipitation and crystallization of Fe-(hydr)oxides [103,128]. Therefore, the nature of the precipitates formed during the treatment of in-situ produced water by EC, and whether these precipitates can effectively adsorb contaminants remain to be investigated.

The objective of this study was to determine if EC can be used to remove silica and sulfide, as well as calcium and magnesium, from in-situ produced water. Understanding the complex chemical processes that take place in the EC/in-situ produced water system may lead to the development of a more efficient water treatment process for the oil sands industry. To gain insights into the contaminant removal mechanisms, solutions with increasing water chemistry complexity were employed, including 1) synthetic solutions containing only inorganic species (i.e., silica, calcium, magnesium, sulfide, and other inorganic ions); 2) synthetic solutions containing the inorganic species and model organic molecules with functional groups representing those of the organics in the in-situ produced water; and 3) authentic in-situ produced water that was collected from a heavy oil thermal in-situ facility. These solutions were treated by Fe-EC and Al-EC, employing different current and charge density values. The concentrations of the contaminants,

the potentials of the anode and cathode, and the consumption of power were monitored throughout the experiments. Additionally, to identify the nature of the precipitates, a series of characterization techniques such as X-ray Diffraction (XRD), Transmission Electron Microscopy (TEM), Energy Dispersive X-Ray Spectroscopy (EDS), and Selected-Area Electron Diffraction (SAED) were employed.

3.2 Methods and Materials

3.2.1 Materials

All chemicals were of reagent grade and were used without further purification. All solutions were prepared using 18.2 MΩ·cm water (Millipore System). The electrodes used in the EC experiments were iron rods (d = 4.8 mm, 98%+ purity) and aluminum rods (d = 6 mm, 95.8% purity) obtained from Goodfellow and Metal Supermarkets. Testing solutions included synthetic produced water prepared in the laboratory, and authentic in situ produced water that was collected from a heavy oil thermal in situ facility in Alberta, Canada. The synthetic produced water was prepared daily by dissolving $Na_2SiO_3.9H_2O$, $NaHS.H_2O$, $MgCl_2.6H_2O$, $CaCl_2$, Na_2SO_4, $NaHCO_3$, and NaCl into water to achieve a working solution consisting of approximately 58 mg/L (as Si) dissolved silica, 110 mg/L (as H_2S) sulfide, 65 mg/L Ca^{2+}, 20 mg/L Mg^{2+}, 1700 mg/L HCO_3^-, 1900 mg/L Na^+, 1945 mg/L Cl^-, and 40 mg/L SO_4^{2-}. The pH of the solution was adjusted to 7.6 – 7.8, which is a typical pH of in situ produced water. In some experiments, the solution also contained 5 mM of either 1,3-propanedithiol, cysteine, or glutathione. These model organic compounds were chosen to represent the thiol, carboxylic acid, and amine functional groups of the dissolved organic compounds in the produced water. The pH of the solution was adjusted to 7.6 – 7.8. The composition of the authentic in-situ produced water sample is provided in the first column of **Error! Reference source not found.** of Chapter 2.

3.2.2 Electrocoagulation Experiments

Experiments were carried out at 22 ± 1 °C in a three-electrode batch cell consisting of 500 mL of reaction solution that was constantly stirred by a magnetic stir bar. The cell was covered with a lid which has three openings that held three electrodes (i.e., working, counter, and reference

electrodes), and two more openings for sample subsampling and ORP/pH measurements. The working and counter electrodes (i.e., anode and cathode, respectively) were iron rods (in the Fe-EC experiment) or aluminum rods (in the Al-EC experiment), and were placed 1 cm apart. The electrodes were submerged to a depth of 4.8 cm, and therefore the surface area that was exposed to the solution was 6.15 cm2 ± 0.1 cm (Fe^0 electrodes) and 9.3 cm2 ± 0.1 cm (Al^0 electrodes). To measure the potential of the anode, a reference electrode (3 M NaCl Ag/AgCl, 0.209 V vs. SHE) was placed 0.25 cm apart from the anode. The cell was controlled by a VSP potentiostat (Bio-logic Science Instruments). A picture of the experimental setup is provided in the. A picture of the experimental setup is shown in Figure 3-1.

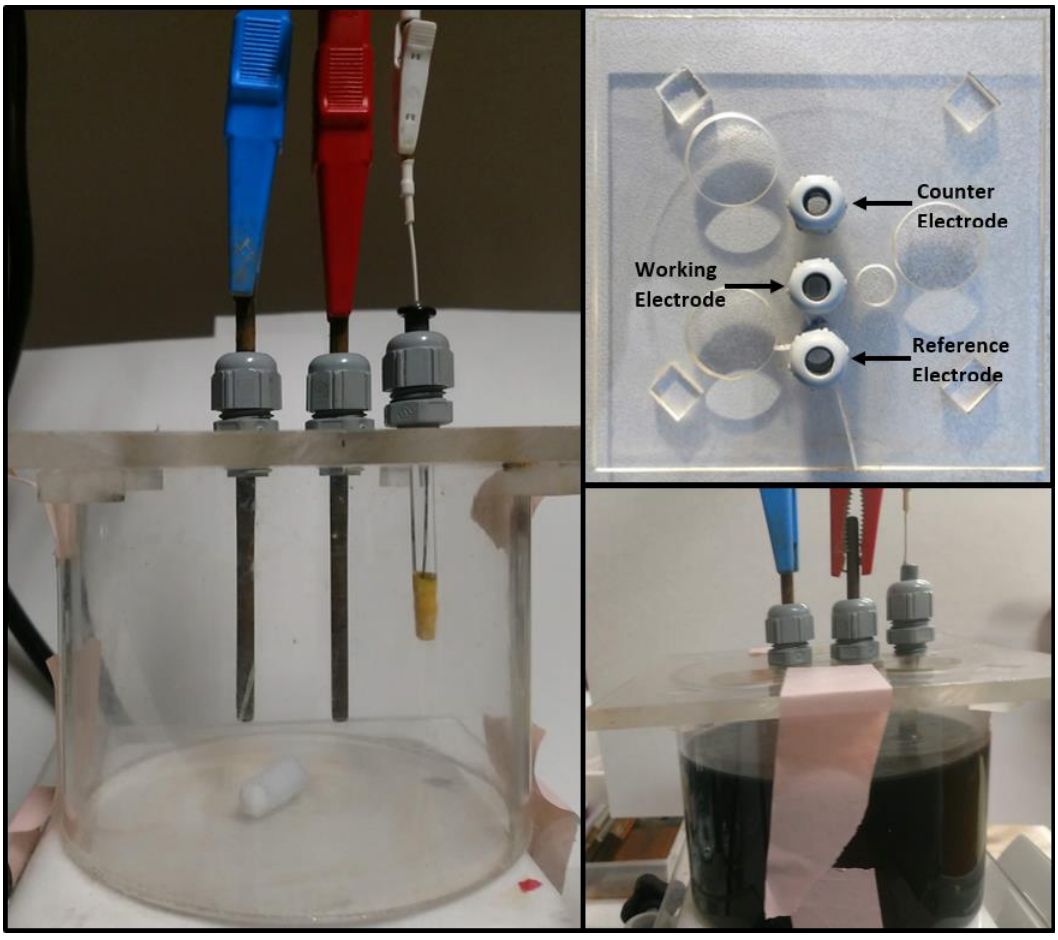

Figure 3-1. Three-electrode electrochemical cell used for 500 mL batch EC experiments

Before each experiment Fe^0 and Al^0 electrodes were sonicated in water, polished using a sandpaper, and rinsed again with deionized water. Electrocoagulation experiments were conducted under galvanostatic mode (i.e., constant current), employing a current range of 0.05 – 0.8 A. At predetermined time intervals, 10 mL of solution was withdrawn from the reactor and was divided into two aliquots. The first aliquot was filtered through a 0.2-μm syringe filter, and dissolved silica, sulfide, Ca^{2+} and Mg^{2+} were analyzed in the filtrate. The second aliquot was digested with 37 wt. % HCl until all precipitates were dissolved. Subsequently, the digested sample was analyzed for total iron and iron(II). The anode potential and cell voltage, together with the solution pH and ORP, were monitored throughout the course of the experiment. The experiments with synthetic produced water were conducted in triplicate, whereas due to the limited amount of sample available the experiments with authentic produced water were conducted in duplicate. Contaminant concentration profiles were plotted against charge density q (C/L), which represents the electrical charge passed per liter of solution. Charge density is related to current (I) and electrolysis time (t) according to Equation 2. Therefore, q is proportional to the amount m of iron released into the solution $m = \frac{I \times t \times M}{z \times F} \times \phi$, where M is the molecular weight of Fe, z is the number of electron involved in the anodic reaction, F is Faraday's constant (96,485 Coulombs/eq), and ϕ is current efficiency (i.e., the fraction of the charge applied that leads to the oxidation of Fe).The performance of EC across the 0.05 – 0.8 A current range was evaluated by comparing the contaminant removal at similar q values (i.e., at similar amount m of iron released). Since longer electrolysis times t are required with lower I values in order to achieve a similar q, the electrolysis time spanned from 19.5 min (for experiments with $I = 0.8$ A) to 312 min (for experiments with $I = 0.05$ A). The continuous change in solution volume due to sample sub-sampling (i.e., 10 mL at each time point) was accounted for in all calculations.

3.2.3 Analytical Methods

A Thermo Scientific Orion Ag/AgCl pH electrode and an Ag/AgCl VWR sympHony ORP/Redox probe were used to measure pH and ORP. Total dissolved iron and dissolved Fe(II) were measured using the 1,10-phenanthroline method [178]. Dissolved silica was measured using the molybdosilicate method [179]. Because the presence of sulfide affects the analysis, samples were acidified by HCl and sparged with N_2 to remove all sulfide prior to addition of the $(NH_4)_6MO_7O_{24}$ reagent. Sulfide was measured colormetrically using the Cline method[180]. Calcium and magnesium were analyzed on a Thermo Dionex Aquion Ion Chromatograph. An Inductively Coupled Plasma Optical Emission Spectrometer (ICP-OES) was employed to analyze for Si, Ca, Mg and Fe in a subset of samples. Prior to the ICP-OES analysis, samples were acidified and stored in a 3 wt. % HNO_3 solution.

Collection of precipitates for X-ray Diffraction (XRD) characterization involved filtering samples through a 0.22-µm pore size membrane. The materials deposited on the filter were scrapped out, smeared on a zero-background sample holder, and analyzed for crystal structure on a Rigaku Ultima IV X-ray diffractometer with Cu Kα radiation. The morphology, surface composition, and crystal structure of the precipitates were analyzed using a FEI Tecnai G2 F20 transmission electron microscope (TEM) coupled with an Aztec energy dispersive X-ray spectrometer (EDS). Liquid samples containing precipitates were deposited on a TEM grid, blotted with a kimwipes paper, and allowed to dry at room temperature. Sample preparation for XRD and TEM characterizations was conducted under N_2 atmosphere to minimize oxidation.

3.3 Results and Discussion

3.3.1 Synthetic In-situ Produced Water (organic free)

Both Fe-EC and Al-EC were able to remove dissolved silica, sulfide, calcium and magnesium from the synthetic in-situ produced water (Figure 3-2). The contaminant removal efficiency was dependent on the nature of the contaminant, the amount of charge passed through the reaction cell, and the type of anode employed (i.e., Fe vs. Al). At the end of the experiment (i.e., $q = 2090$ C/L), over 95% of silica and over 99% of sulfide were removed by Fe-EC, while only silica was effectively removed (~99%) by Al-EC. The removal efficiencies of Ca^{2+} (80–85%) and Mg^{2+} (20–25%) were comparable in both EC systems. The following discussion will focus on elucidating the electrochemical (i.e., anodic reactions) and chemical (i.e., precipitation and adsorption) processes taking place in the Fe-EC system. Subsequently, Al-EC will be briefly discussed and compared with Fe-EC.

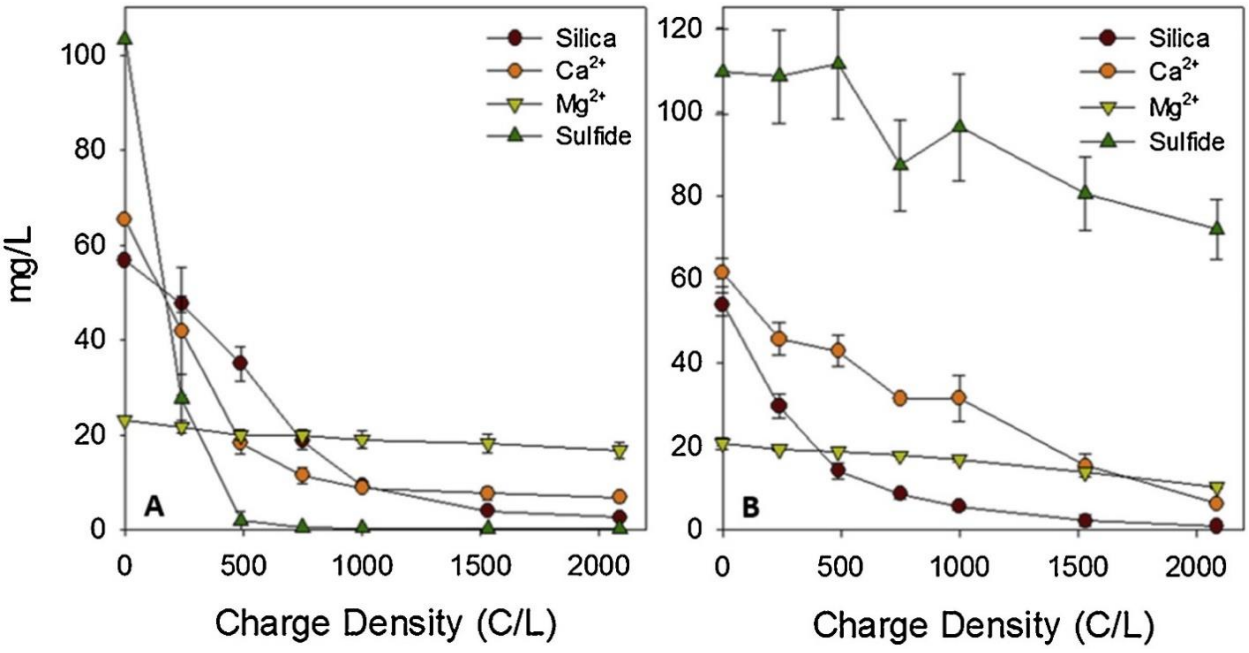

Figure 3-2. Removal of contaminants from synthetic produced water by Fe-EC (A) and Al-EC (B). I = 0.2 A (j =32.5 mA/cm^2).

3.3.2 Anodic Reactions in Fe-EC

When a current of $I = 0.2$ A (which corresponds to current density of j = 32.5 mA/cm^2) was applied, the ohmic drop-compensated anodic potential varied between -0.45 and - 0.35 V vs. SHE (Figure 3-3).

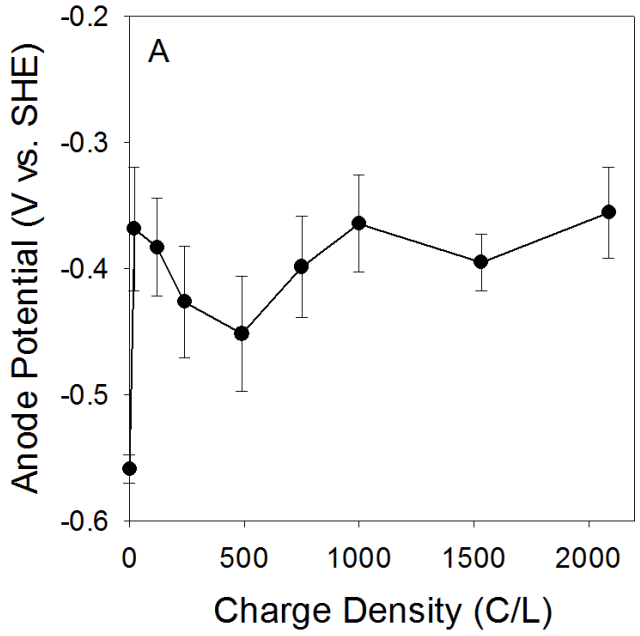

Figure 3-3. The potential of the Fe anode of the experiment presented in Figure 3-2 A.

This potential range indicates that the predominant anodic reaction in the Fe-EC system was the oxidation of iron to Fe(II) (E_h = −0.44 V) [181] . Consistent with this hypothesis, the amount of Fe(II) released from the anode were 90–95% of the theoretical amount (which was calculated by assuming that $z = 2$ in the Faradaic equation (Figure 3-4). Approximately 3% of the iron released from the anode was Fe(III). As such, the anodic reactions in our system could also include the oxidation of Fe^0 and Fe(II) to Fe(III). However, the actual amount of Fe(III) formed from the anodic reactions could not be determined as some of the Fe(III) could have been reduced by HS^- to Fe(II) [4]:

$$Fe(III) + 2HS^- = FeS + S^0 + 2H^+ \qquad (1)$$

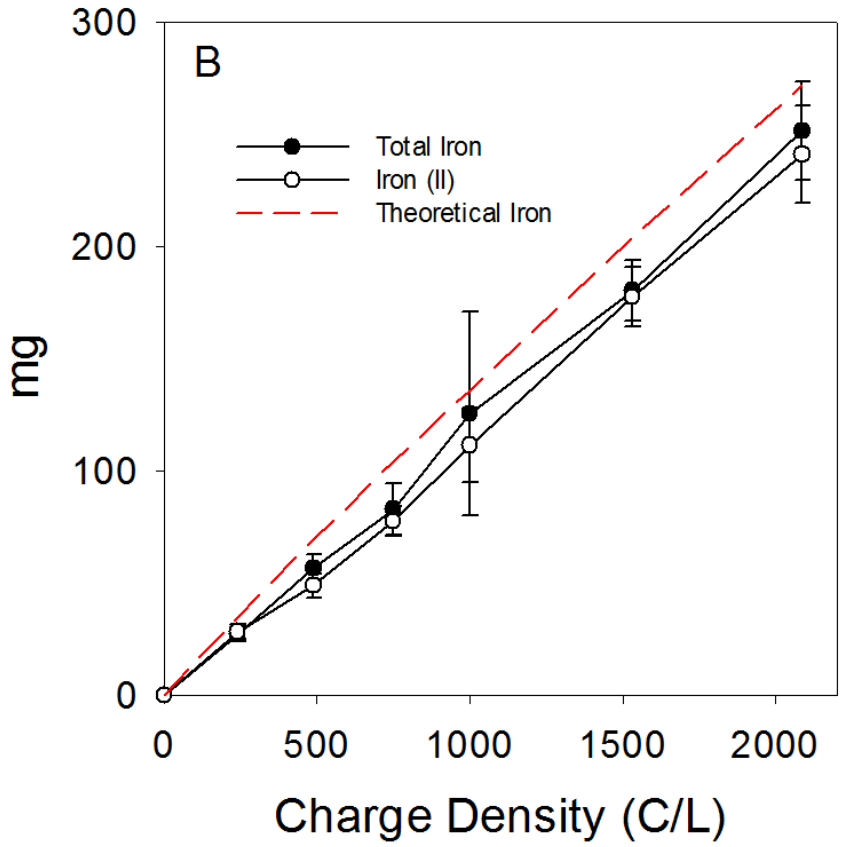

Figure 3-4. Measured amounts of total Fe and Fe(II), and the theoretical amount of total Fe predicted from Faraday's law ($z = 2$, $\phi = 1$) of the experiment presented in Figure 3-2 A.

3.3.3 Removal of Sulfide and Formation of FeS

Fe-EC was very effective at removing sulfide; at q = 750 C/L (corresponding to an iron dose of $Fe/S_{initial}$ = 1.17/1 mol/mol), over 99.9% of the initial sulfide was removed from the synthetic solution (Figure 3-2 A). Concurrent with sulfide removal was the formation of black-color precipitates whose morphology and SAED pattern suggest that they are poorly crystalline mackinawite (Figure 3-5 A and B). Therefore, the removal of sulfide was attributable to the reaction between Fe(II) and HS^-, which produced FeS mineral [4].

$$Fe(II) + HS^- \rightarrow FeS + H^+ \qquad (2)$$

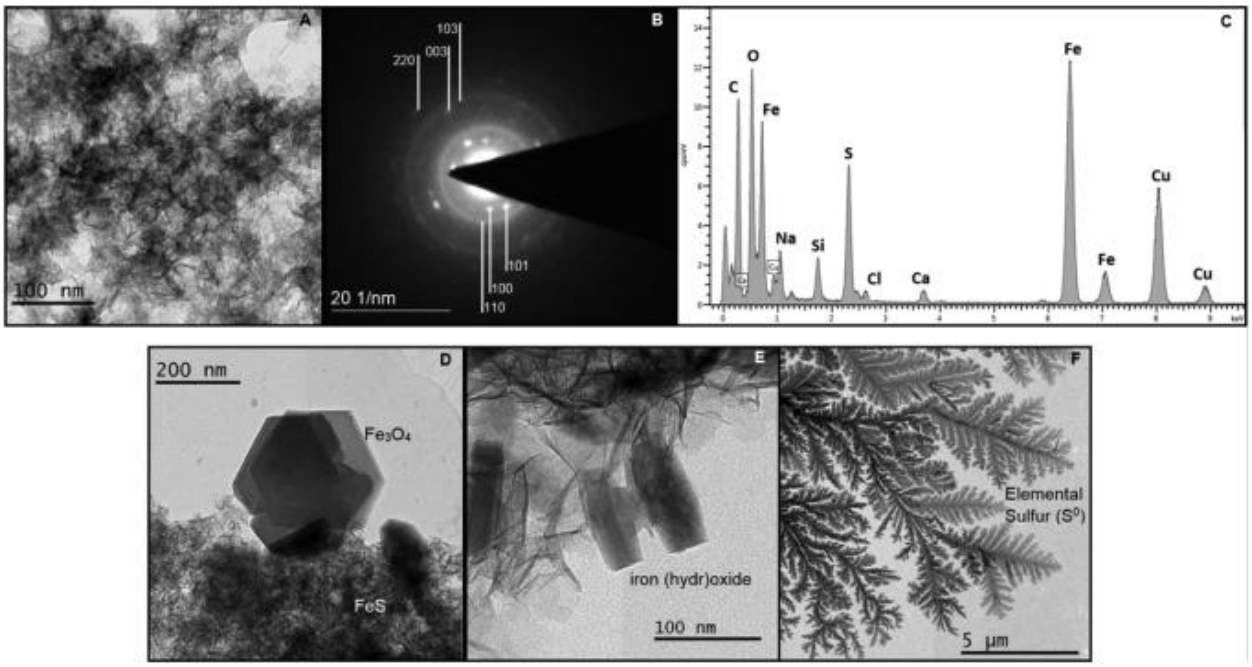

Figure 3-5. (A–C): TEM image and associated EDS spectrum and SAED pattern of the FeS precipitates formed in the Fe-EC experiments with synthetic produced water. (D–E): TEM images showing the formation of Fe-(hydr)oxides after all sulfide was removed. The hexagonal -shape precipitate in panel D was identified to be magnetite (Fe_3O_4). The precipitate in panel E did not have a well-defined SAED pattern. (F) TEM image showing the presence of elemental sulfur (S^0) in the precipitate mixture.

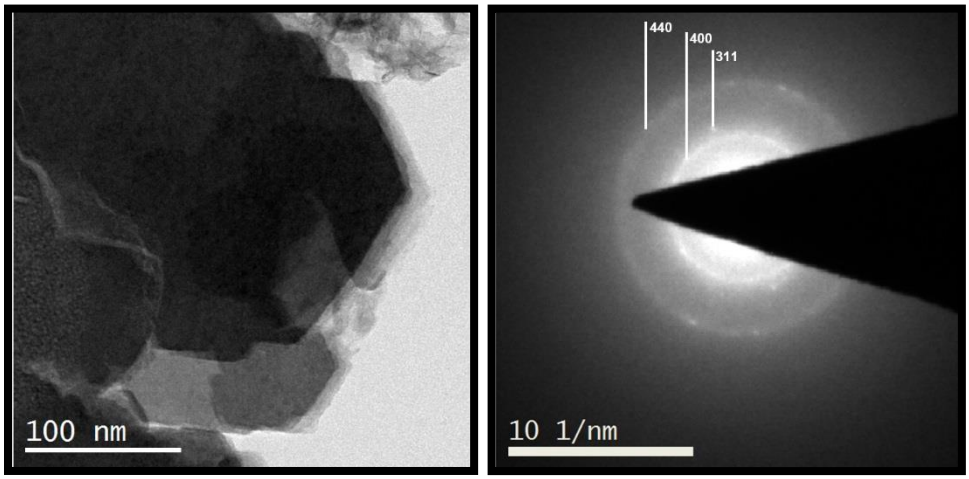

Figure 3-6. TEM image and SAED pattern of magnetite.

The nearly complete removal of sulfide at $Fe/S_{initial}$ = 1.17/1 is consistent with the stoichiometry of the above reaction. TEM analyses revealed that FeS was the only type of iron precipitate produced when $q \leq 750$ C/L. At $q > 750$ C/L (*i.e.*, once all sulfide had been removed), the presence of different phases of Fe-(hydr)oxide were observed, one of which was magnetite (Figure 3-5 D and Figure 3-6). However, most Fe-(hydr)oxide precipitates lacked a well-defined diffraction pattern (Figure 3-5 E and Figure 3-7). It is also noted that, unlike the nanocrystalline mackinawite generated in other studies when Fe(II) reacted with HS^- [182–185], the FeS produced in our experiments also lacked well-defined XRD (Figure 3-8) and Debye-ring patterns (Figure 3-5 B).

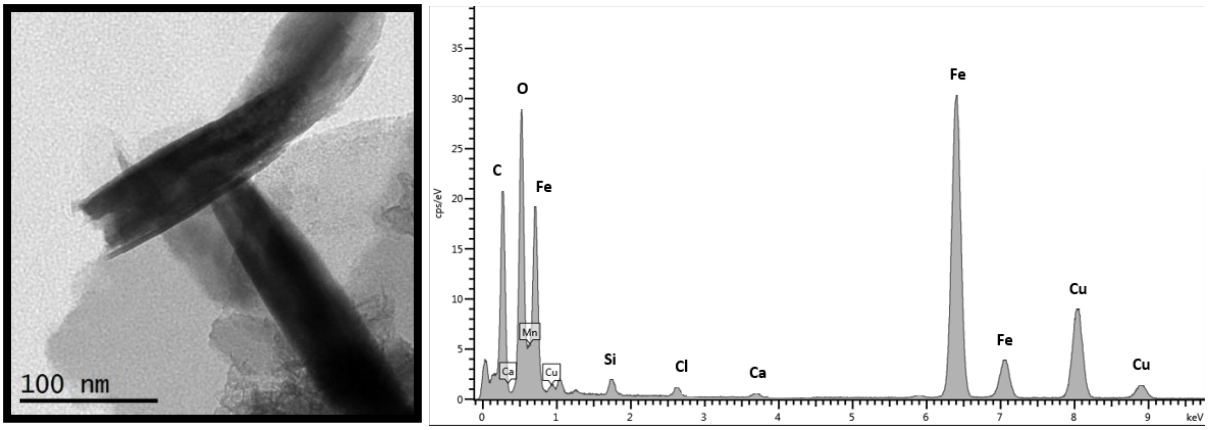

Figure 3-7. TEM image and EDS spectrum of precipitates suspected to be FeII-(hydr)oxides. These precipitates did not have SAED pattern. The Cu signal was from the TEM grid.

The amorphous/poorly crystalline nature of the precipitates produced in our study was attributable to the presence of small amount of oxygen in the solution (< 0.5 mg/L) [186], and the presence of silica, a solute known to inhibit the formation, growth, and crystallization of iron minerals [103,128]. Because more than 97% of the iron in the precipitates were Fe(II) (Figure 3-4), the Fe-(hydr)oxides must be Fe^{II}-(hydr)oxides (*e.g.*, green rust type of minerals). Throughout the course of the experiment, the solution remained hypoxic (DO < 0.5 mg/L, ORP < -200 mV, (Figure 3-9), a condition that has been shown to favor the formation of magnetite and green rust [96].

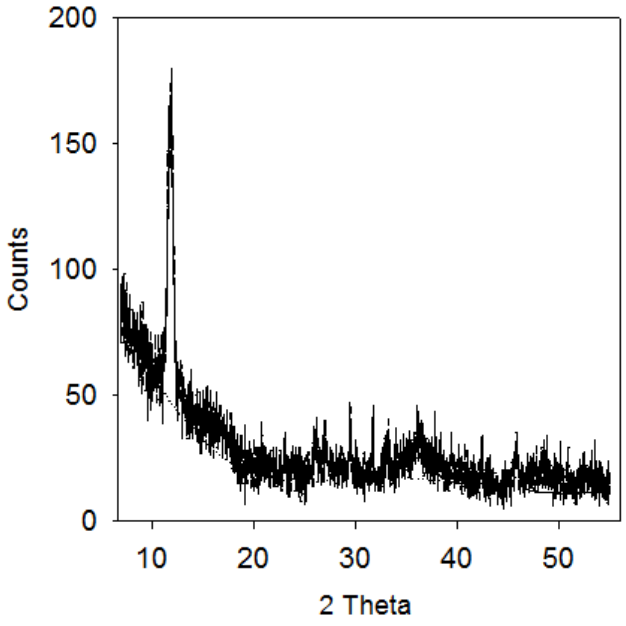

Figure 3-8. XRD pattern of the precipitates produced during the treatment of synthetic solution by Fe-EC.

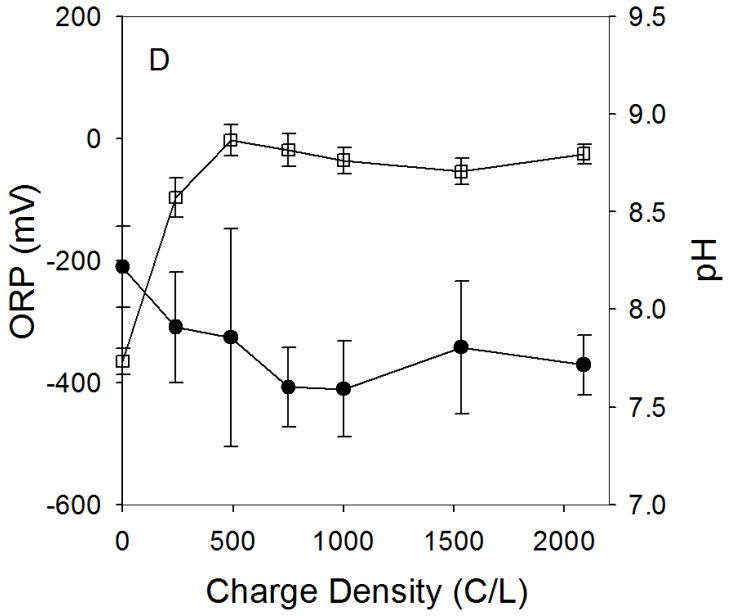

Figure 3-9. pH and ORP of the solution in the experiment presented in Figure 3-2 A.

Also present among the precipitates was elemental sulfur, S^0 (Figure 3-5 F and Figure 3-10). S^0 could have been produced from the anodic oxidation of HS^-, and/or from reactions in the bulk solution [187]:

Anodic oxidation: $HS^- \rightarrow S^0 + 2e^- + H^+$ (E_h = -0.23 V) *(3)*

Bulk solution reaction: $Fe(III) + 2HS^- \rightarrow FeS + S^0 + 2H^+$ *(4)*

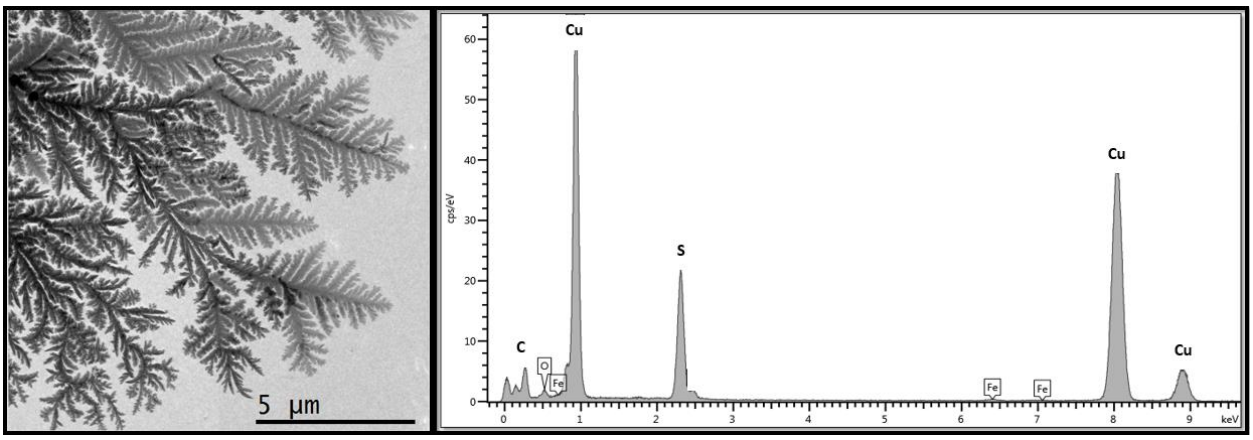

Figure 3-10. TEM image and EDS spectrum of elemental sulfur S^0 produced during the treatment of synthetic solution by Fe-EC. The Cu signal was from the TEM grid.

3.3.4 Removal of Silica, Calcium, and Magnesium

The concentration of dissolved silica in the synthetic solution gradually decreased as charge was passed through the electrochemical cell (Figure 3-5 A). Approximately 65% and 95% of the initial silica was removed when q = 750 C/L (i.e., when FeS was the predominant solid phase) and q = 2090 C/L (i.e., when both FeS and Fe-(hydr)oxides were present), respectively. The removal of silica was attributable to the sorption onto FeS at the initial stage, and onto both FeS and Fe-(hydr)oxides at the later stage. Whereas adsorption of silica onto Fe-(hydr)oxides has been well-studied [127,188–191], reports of adsorption of silica onto FeS have not been seen. It is noted that the removal of silica via other mechanisms cannot be excluded. For example, because the EDS spectrum of the FeS precipitates (Figure 3-5 C) consisted of Si, Fe, and Ca peaks, it could be possible that silica was removed via the precipitation of silicate minerals (e.g., Ca_2SiO_4 or Fe_2SiO_4). The detailed mechanisms through which silica is removed and factors affecting these processes (e.g., solution pH, initial concentration of sulfide) merit further investigation.

Fe-EC was also effective at removing calcium from the synthetic produced water as the concentration of calcium decreased by over 85% when q = 2090 C/L (Figure 3-2 A). In contrast, only less than 25% of the initial magnesium was removed (Figure 3-2 A). The removal of calcium and magnesium was most likely due to the formation of sparingly soluble minerals such as $CaCO_3$, $CaMg(CO_3)_2$, $MgCO_3$, $Mg(OH)_2$, and others (e.g., silicate minerals). During the experiment, the solution pH increased from 7.7 to 8.9 (Figure 3-9). At pH 8.9, speciation calculations predicted that over 99% magnesium existed as dolomite, and over 98% calcium existed as dolomite and calcite (Figure 3-11).

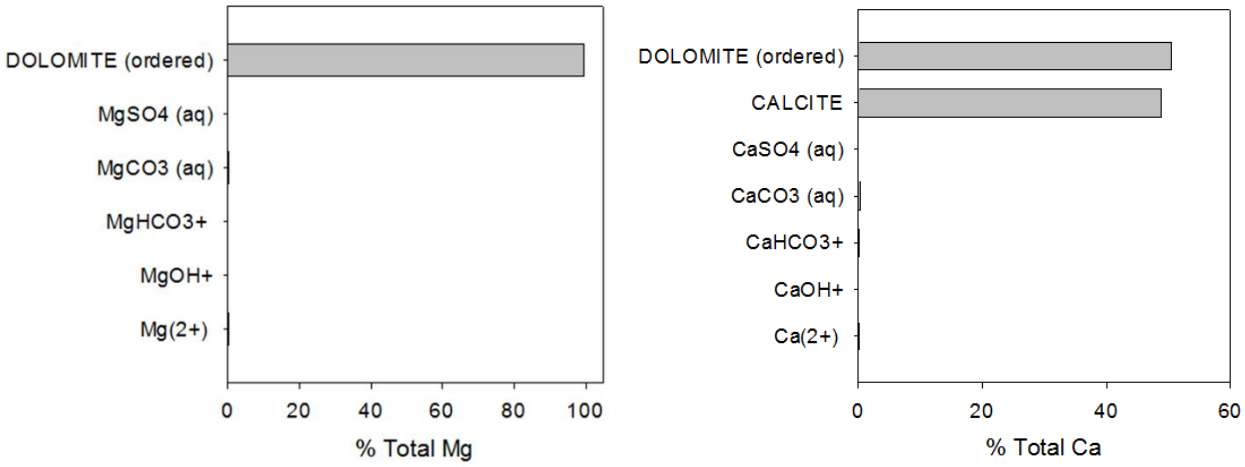

Figure 3-11. Speciation calculations, performed on MINEQL+, predicted that dolomite and calcite were the predominant Ca and Mg species at pH 8.9.

However, dolomite does not form at ambient temperature [192–194]. When dolomite was excluded from the calculation, the equilibrium model predicted that 85% magnesium existed as magnesite, and 99% calcium existed as calcite (Figure 3-12).

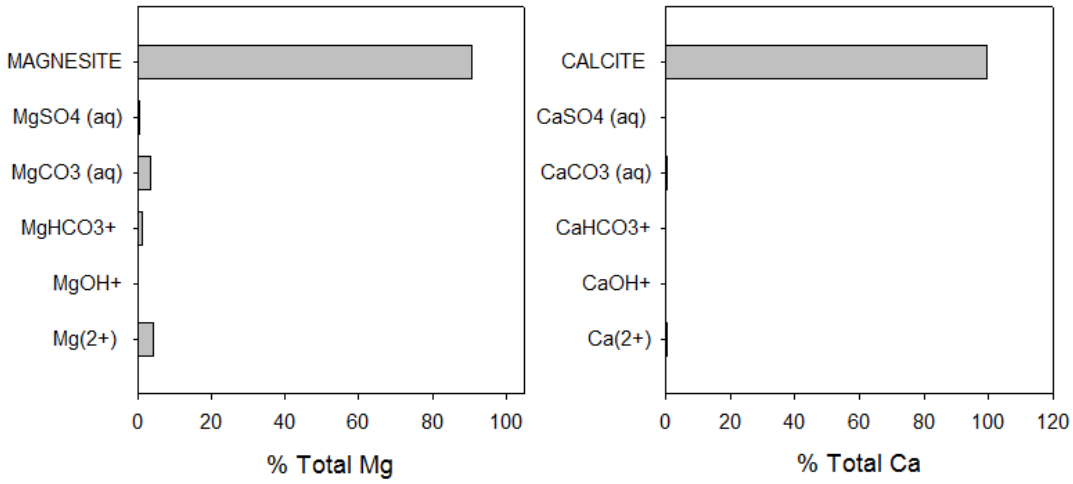

Figure 3-12. When dolomite was excluded from the equilibrium model, MINEQL+ predicted that magnesite and calcite were the predominant Ca and Mg species at pH 8.9.

As with dolomite, magnesite does not form at ambient temperature [193,194]. When both dolomite and magnesite was excluded from the equilibrium calculation, the model predicted that 100% magnesium existed as soluble species.

It is noted that the pH reported in this study is the pH of the bulk solution. However, lower and higher pH regions could have been developed in the vicinity of the anode and cathode, respectively. The rates of calcium and magnesium precipitation in these regions could be significantly different from those in the bulk solution [195–197]. For example, brucite ($Mg(OH)_2$), which precipitates at pH values greater than 10, could have been formed in the alkaline pH regions in the vicinity of the cathode [197]. While the mechanism through which magnesium was removed was not entirely clear, the relatively poor removal of magnesium compared with the removal of calcium may have been due to the slower rates of formation of magnesium minerals than that of calcium minerals.

3.3.5 Effect of Current Density on Contaminant Removal and Energy Consumption

In EC, whereas coagulant dose is determined by *q*, coagulant dosing rate (i.e., the rate at which the coagulant is introduced into the solution) is controlled by the electrolysis current *I*; that is, higher currents result in higher fluxes of Fe(II). Previous studies have reported that with the same charge density, better contaminant removal can be achieved at lower *I* [20,91]. This is because of the higher faradaic efficiency ϕ at lower *I* and/or the increased contact time between coagulant and contaminants due to longer electrolysis time.

The removal of sulfide, dissolved silica, calcium and magnesium at *I* = 0.05 – 0.8 A (*i* = 8.13 – 130 mA/cm^2) was investigated and compared. The results showed that while contaminant removals were dependent on the iron dose (i.e., better removal of Si, calcium and magnesium at *q* = 2090 C/L than at *q* = 750 C/L), they were not appreciably affected by *j* (Figure 3-13 A and B).

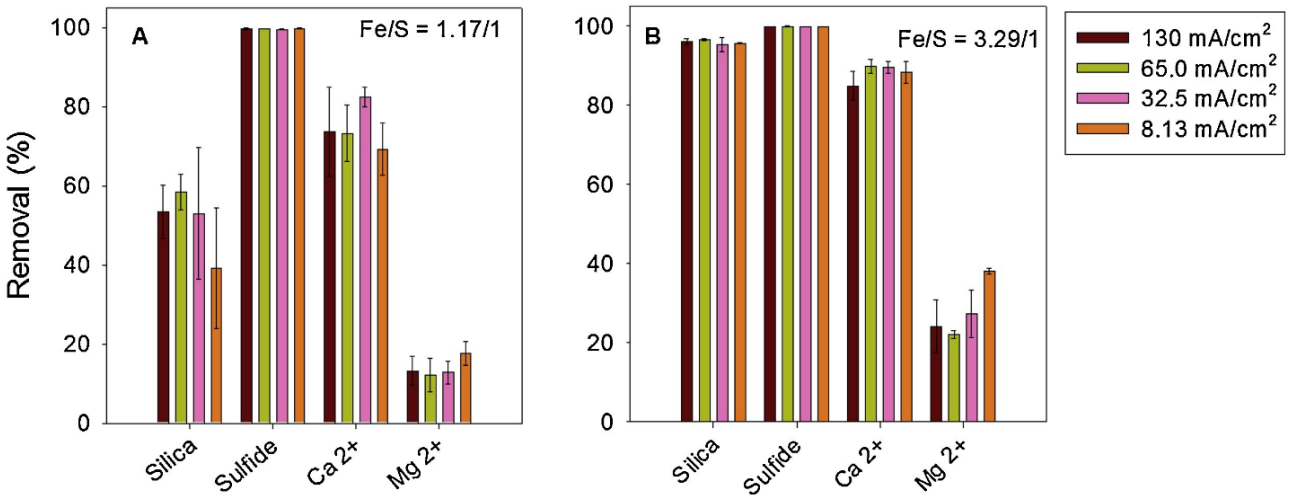

Figure 3-13. Comparison of contaminant removal at different current densities (j = 8.13–130 mA/cm^2) and charge densities (q = 750 C/L and 2090 C/L, which correspond to iron doses of Fe/Sintial = 1.17/1 (A) and 3.29/1 (B), respectively).

At q = 2090 C/L, despite the significantly different electrolysis times (t = 19.5, 78, 156, and 312 min with j = 8.13, 32.5, 65.0, and 130 mA/cm^2, respectively), a similar removal of silica, calcium, and magnesium was achieved in all cases. This observation suggests that the adsorption and/or precipitation of the contaminants took place relatively quickly. The slightly better removal of magnesium at j = 8.13 mA/cm^2 could be due to the longer electrolysis time, which allowed for the formation of the slower-forming magnesium minerals.

The electrolysis current (I) strongly influenced the energy required during the treatment. For the same silica removal percentage, the cumulative energy consumption, $P=(U\times I\times t)/V$ (kWh/m^3, with U being the cell voltage), increased as I increased (Figure 3-14). The higher energy demand was the result of the higher cell voltage U (Figure 3-15), which was caused by increased overpotential and ohmic drop.

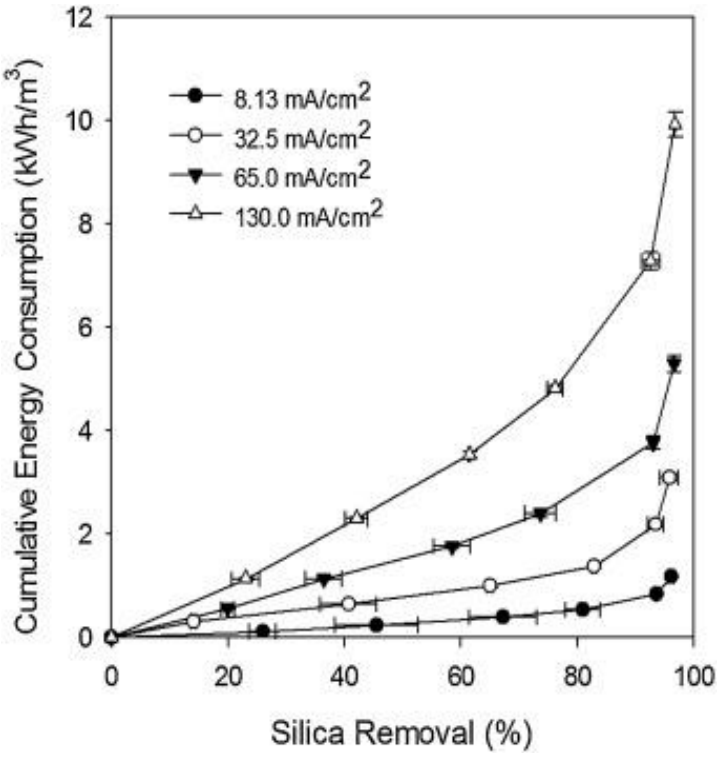

Figure 3-14.Cumulative energy consumption with increasing silica removal at different current densities (i = 8.13–130 mA/cm^2).

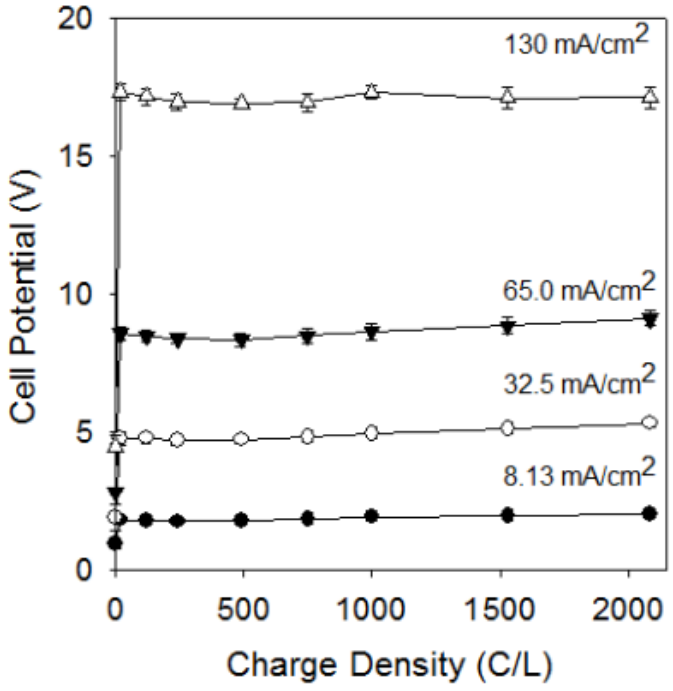

Figure 3-15. Cell voltage profiles in the experiments with synthetic produced water. I = 0.05 – 0.8 A (j = 8.13 – 130 mA/cm^2). Experiments were conducted in triplicate, and the average values along with one standard deviation are presented.

3.3.6 Comparison of Fe-EC with Al-EC

As noted above, the most prominent difference between Fe-EC and Al-EC was that Al-EC was much less effective at removing sulfide (Figure 3-2). In Fe-EC, sulfide was removed via reactions with Fe(II) and Fe(III). Because Al(III) ions do not react with sulfide, the removal in Al-EC was most likely due to (1) the stripping of H_2S, which was accelerated by the generation of gas bubbles at the electrodes; and (2) the electrochemical oxidation of sulfide on the anode. (As in the Fe-EC experiment, the presence of S^0 among the precipitates formed in Al-EC was observed (Figure 3-16). At similar charge density values, the removals of silica, Ca^{2+} and Mg^{2+} by Fe-EC and Al-were comparable (Figure 3-2B), with the removal of Mg^{2+} by Al-EC (50%) being slightly better than by Fe-EC (20%). The removal of these contaminant was attributable to adsorption onto $Al(OH)_3$ and precipitation of carbonate or hydroxide minerals (Figure 3-17). However, considering that Fe-EC was significantly more effective at removing sulfide, and that iron anodes are less expensive than aluminum anodes, Fe-EC appears to be a better choice than Al-EC.

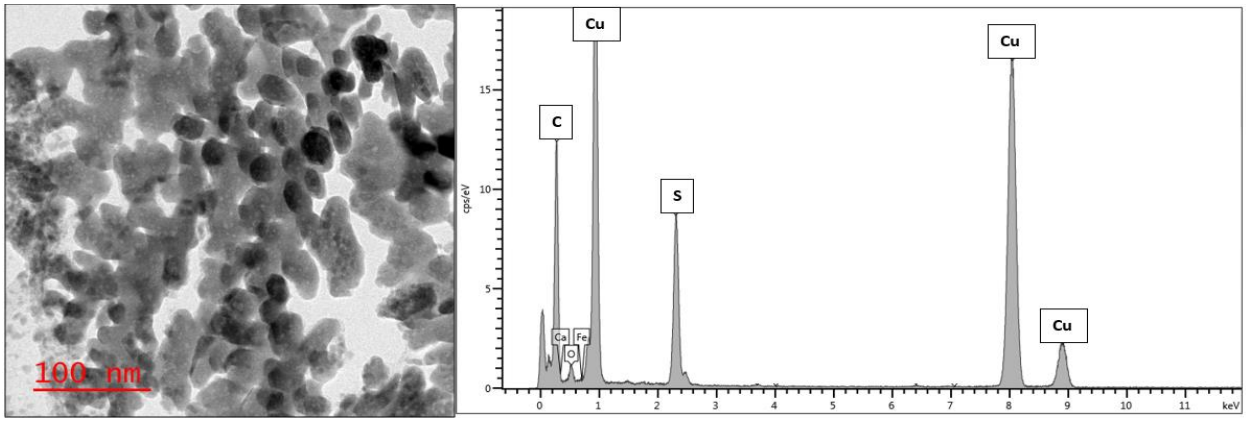

Figure 3-16. TEM image and EDS spectrum of elemental sulfur S^0 produced during the treatment of synthetic solution by Al-EC. The Cu signal was from the TEM grid.

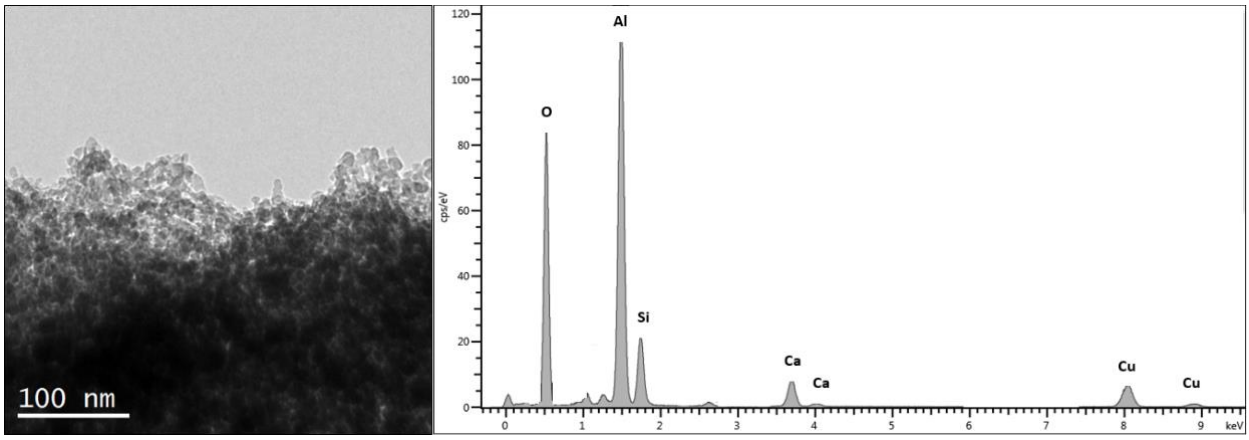

Figure 3-17. TEM image and EDS spectrum of the precipitates produced in Al-EC experiments

3.3.7 Treatment of Authentic In-situ thermal Produced Water by Electrocoagulation

In addition to the inorganic solutes, in situ produced water consists of organic components including oil, grease, and dissolved organic carbon (TOC 200 – 600 mg/L) [24]. The presence of these components could affect the formation of iron precipitates, and the adsorption/precipitation of contaminants of interest.

The utility of Fe-EC was further examined in a series of experiments that employed an authentic in-situ produced water sample, and key observations were as follows. Firstly, the Fe-EC treatment was able to remove sulfide from the produced water. Although it was not possible to quantify the concentration of sulfide in the solution as the presence of organic reduced sulfurs interfered with the Cline method, the removal of sulfide was evidenced by the formation of FeS (Figure 3-18).

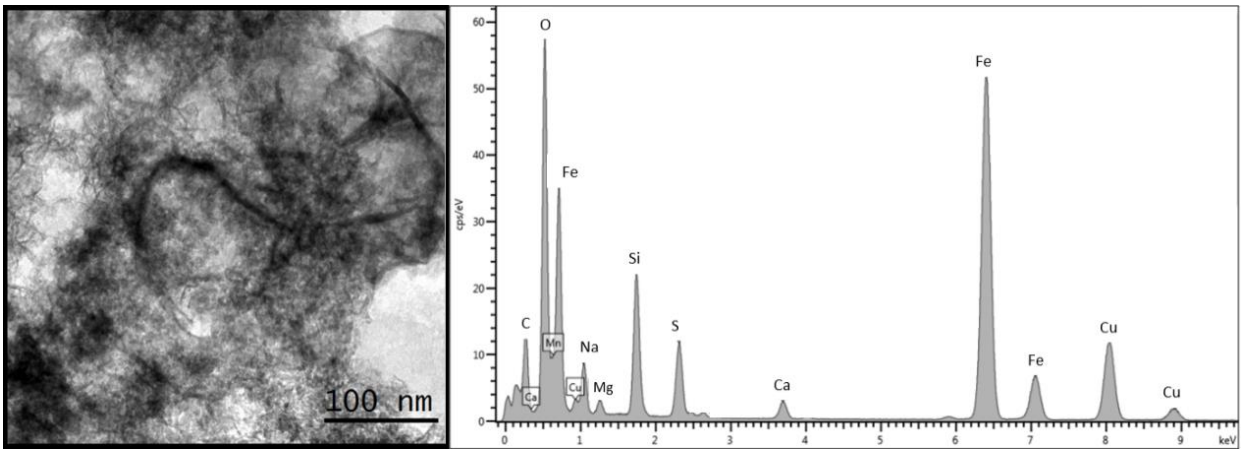

Figure 3-18. TEM image and EDS spectrum of the precipitates produced in the experiment with authentic in situ produced water.

FeS in fact was the predominant precipitate at all *q* values employed because iron (hydr)oxides were not observed by TEM. Secondly, as in the synthetic produced water experiments, an excellent removal of silica was achieved. Treatment with a charge density of *q* = 750 C/L reduced silica concentration by over 60% (Figure 3-19), producing a treated solution containing less than 25 mg/L Si (i.e., the desirable concentration specified by the oil sands industry) [24].

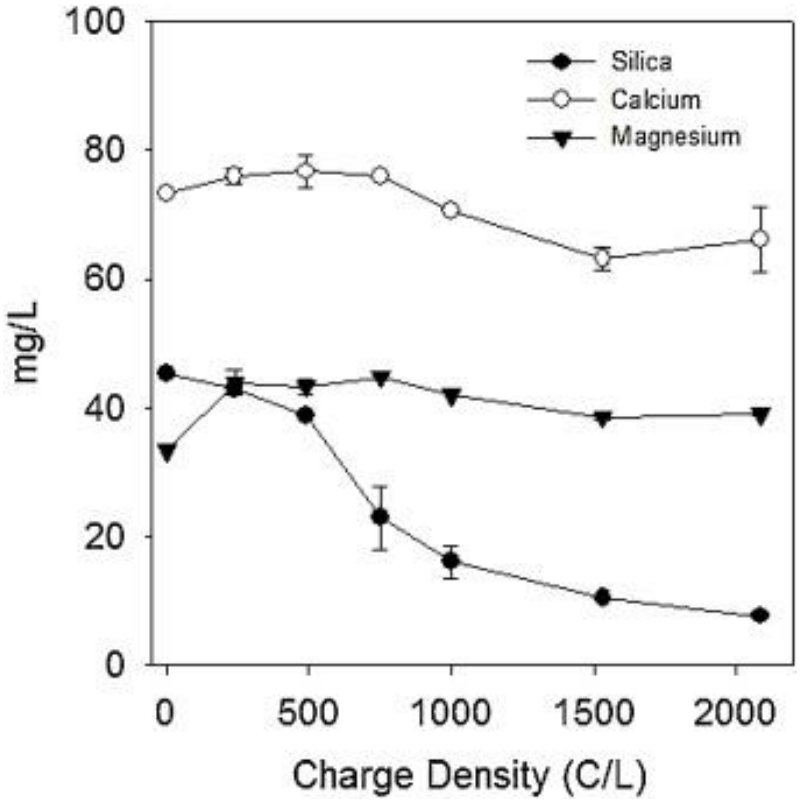

Figure 3-19. Contaminant concentration profiles in the Fe-EC experiment (I = 0.2 A) with the authentic in-situ produced water. Experiments were conducted in duplicate, and the average values along with the range are presented. The increase in the concentrations of Ca^{2+} and Mg^{2+} at the beginning could be due to the presence of high amount of oil and grease in the untreated sample (i.e., corresponding to charge density q = 0 C/L) which interfered with the analysis. The oil and grease components were quickly separated (by foaming) after electric current was passed through the solution, and therefore the subsequent analyses are likely more reliable.

The energy required to achieve this removal level at I = 0.2 A was estimated at approximately 1.1 kWh/m^3 (Figure 3-20). At this rate, EC's energy demand is over 10 times less that of the evaporative treatment technology, which typically consumes 10 – 15 kWh/m^3. It is noted that the energy demand by EC will vary depending on the reactor configuration (e.g., electrode shape, the distance between electrodes, flow condition) and operational parameters (e.g., current density, retention time), further research is needed to optimize the treatment of produced water by EC and reduce energy consumption.

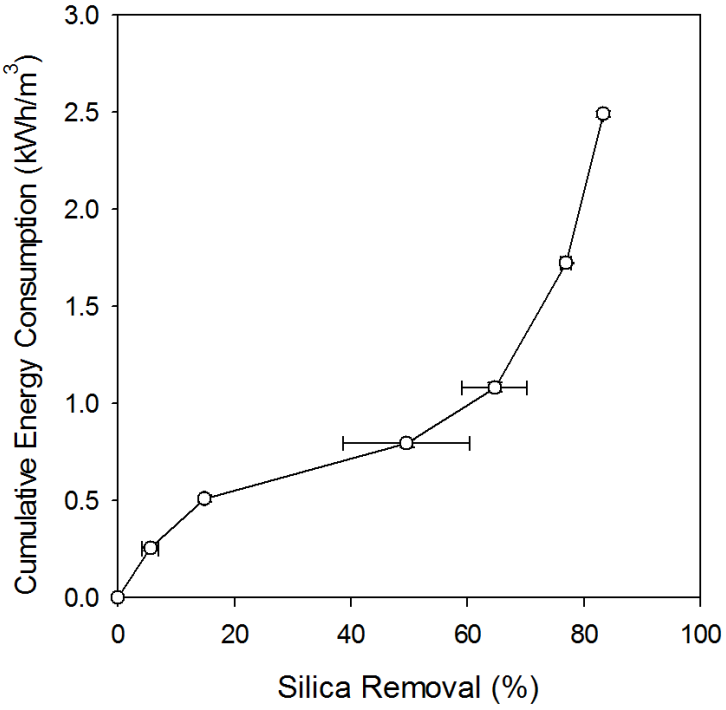

Figure 3-20. Cumulative energy consumption with increasing silica removal at I = 0.2 A in the Fe-EC/authentic produced water system. Experiments were conducted in triplicate, and the average values along with one standard deviation are presented.

Thirdly, both Ca^{2+} and Mg^{2+} were not appreciably removed (Figure 3-19). This was attributable to the complexation of Ca^{2+} by dissolved organic compounds, which inhibited the precipitation of Ca minerals. This hypothesis was supported by an experiment with synthetic water samples that also contained 5 mM of either 1,3-propanedithiol, cysteine, or glutathione. The results of this experiment (Figure 3-21) showed that the presence of each of these organic compounds inhibited/retarded the removal of Ca^{2+}.

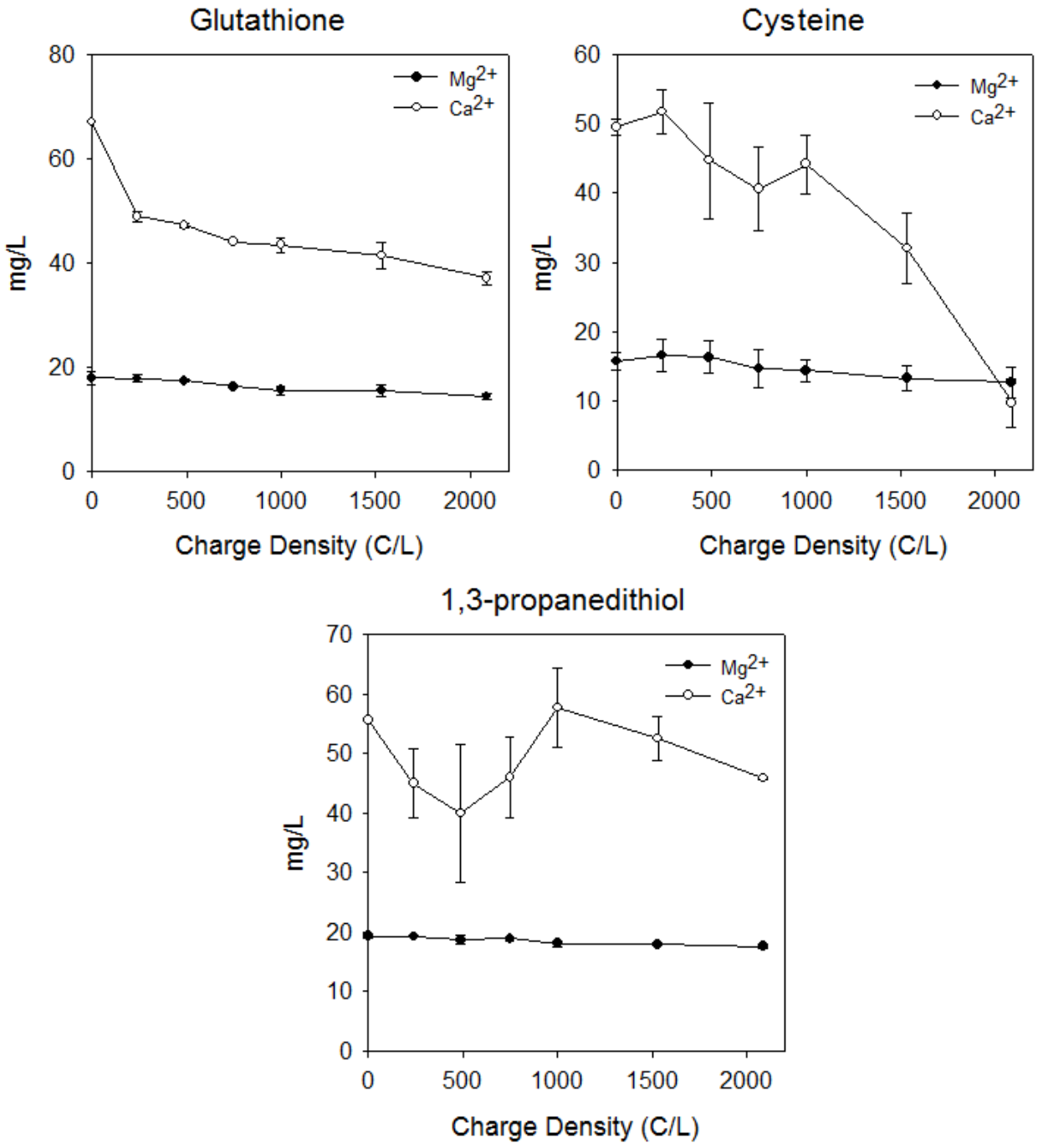

Figure 3-21. Removal of Mg^{2+} and Ca^{2+} from the synthetic solutions that contained 5 mM of either glutathione, cysteine, or 1,3-propanedithiol. Experiments were conducted in triplicate, and the average values along with one standard deviation are presented.

In addition to inhibiting Ca^{2+} removal, it was observed that the organic components influenced the precipitate dynamics. In particular, the precipitates settled much more slowly in the produced water experiments than in the organic-free synthetic water experiments. The precipitates produced in the presence of 1,3-propanedithiol, cysteine, or glutathione also settled at slower rates. This is likely due to the sorption of organic compounds onto the precipitates, which slowed the rate at which the precipitates aggregated into larger flocs. Notably, solution foaming was a common phenomenon in the experiments with the authentic produced water. This was attributable to the foaming of oil and grease caused by the evolution of gas bubbles generated at the electrodes. Foaming often led to incomplete mixing of the solution and, in extreme cases, resulted in precipitate flotation (Figure 3-22). While foaming could present significant operational challenges, flotation could help separate the precipitates from the treated water (a process commonly referred to as electrochemical flotation [198]. Future research investigating the dynamics of the precipitates in the solution may help determine the most appropriate technology for separating the precipitates from the treated water.

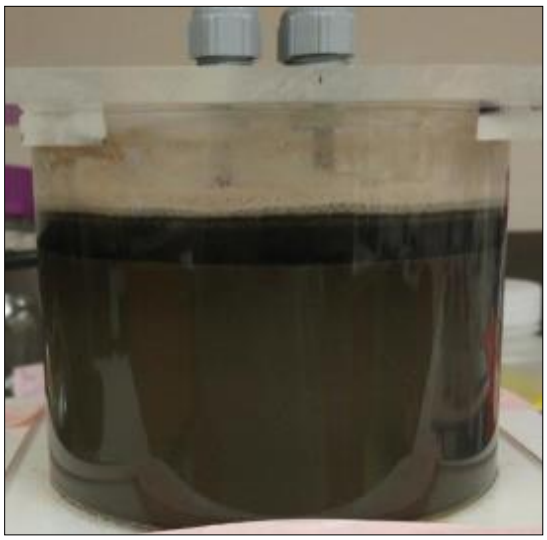

Figure 3-22. Formation of foam and flotation of precipitates in an experiment with authentic produced water.

3.4 Chapter Conclusions

This research explored the treatment of oil sands in-situ produced water by electrocoagulation, focusing particularly on the removal of silica, sulfide, calcium and magnesium. Major findings and their implications are summarized below:

- Both Fe-EC and Al-EC were effective at removing silica, which was the contaminant of primary concern, from the synthetic and authentic produced water. The added benefit of Fe-EC was that it could also effectively remove sulfide. Therefore, Fe-EC seems to be a better choice than Al-EC, especially considering that iron anodes are less expensive than aluminum ones.
- Compared with the two popular silica removal technologies in the oil sands industry, namely warm/hot lime softening and evaporative treatment, Fe-EC consumed less energy than evaporative treatment, and is particularly superior to warm/hot lime-softening because of its ability to remove sulfide. Future research investigating how factors such as reactor configuration and operating parameters influence energy demand will help optimize Fe-EC and reduce treatment cost.
- While silica is the primary scalant of concern, removal of Ca^{2+} and Mg^{2+} is also desirable. Both Ca^{2+} and Mg^{2+} were poorly removed from the authentic produced water, so additional research is needed to improve their removal.
- Additional research is also needed to evaluate other issues including fouling of the electrodes, methods of separating precipitates from the treated water, and disposing and managing of the FeS sludge generated from the treatment.
- In Fe-EC, silica was removed by adsorption onto FeS, a phenomenon reported here for the first time. Future research is needed to investigate the mechanisms of adsorption (e.g.,

surface complexation or electrostatic interaction) as well as adsorption kinetics and isotherm. This further understanding is not only relevant to the Fe-EC/produced water system, but it may also help elucidate geochemical processes in the environments where dissolved Fe(II), sulfide, and silica coexist (e.g., anoxic sediments, hydrothermal vents).

It is important to note that the experiments were conducted in batch reactors, which did not allow for studying the effect of changes in water chemistry or flow conditions on contaminant removal. Understanding these factors will be essential for the scale up of EC for the treatment of authentic produced water. In addition, some of the calculation presented in this study assumed that equilibria existed in the system, which may not be the case in real treatment scenarios.

Chapter 4

Mitigating Electrode Fouling in Electrocoagulation by Means of Polarity Reversal: The Effects of Electrode Type, Current Density, and Polarity Reversal Frequency

This chapter was published in Water Research, Volume 197, Chow H., Pham ALT., Mitigating Electrode Fouling in Electrocoagulation by Means of Polarity Reversal: The Effects of Electrode Type, Current Density, and Polarity Reversal Frequency, 117074, Copyright Elsevier (2021)

4.1 Chapter Introduction

In recent years, electrocoagulation (EC) has become increasingly popular as a means of treating contaminated water streams [3,5,60,71]. EC involves the application of electric current to sacrificial iron a other contaminants in municipal and industrial wastewaters.

Anodic reactions: $Fe \rightarrow Fe(II) + 2e^-$ *(1)*

$Al \rightarrow Al(III) + 3e^-$ *(2)*

Cathodic reactions: $O_2 + 4e^- + 2\,H_2O \rightarrow 4OH^-$ *(3)*

$2H_2O + 2e^- \rightarrow H_{2(g)} + 2OH^-$ *(4)*

A major problem in EC is the build-up of solid materials on the electrode surface, a phenomenon that is often referred to by different terms such as passivation, fouling, or scaling (and will be collectively referred to as fouling going forward)[8,12]. While the mechanism and rate of fouling formation vary depending on factors such as electrode type, solution chemistry, and operating parameters (e.g., current density)[17,133], the primary reactions that are involved in

electrode fouling include 1) the precipitation of iron (hydr)oxides on the anode (reaction 5) [2]), 2) the precipitation of aluminum hydroxides on both the anode and cathode (reaction 6)[115], and 3) the precipitation of Ca and Mg-containing minerals on the cathode (reactions 7, 8, and 9)[129,130,199] where the pH can be highly basic due to the electrochemical production of OH^- via reactions 3 and 4 [2,118,200].

$$4Fe(II) + O_2 + 10H_2O \rightarrow 4Fe(OH)_{3(s)} + 8H^+ \quad (5)$$

$$Al(III) + 3H_2O \rightarrow Al(OH)_3 + 3\,H^+ \quad (6)$$

$$Ca^{2+} + CO_3^{2-} \rightarrow CaCO_{3(s)} \quad (7)$$

$$(1\text{-}x)\,Ca^{2+} + x\,Mg^{2+} + CO_3^{2-} \rightarrow Ca_{1-x}Mg_xCO_{3(s)} \quad (8)$$

$$Mg^{2+} + 2OH^- \rightarrow Mg(OH)_{2(s)} \quad (9)$$

The fouling of the electrodes over time can result in various operating issues, such as decreased coagulant production, increased ohmic resistance and overpotential, increased energy consumption, decreased effective volume of the reactor due to the shrinkage of the gap between the electrodes, and reduced contaminant removal efficiency[6,19–23].

Several approaches have been proposed to deal with electrode fouling, including cleaning the electrodes mechanically or chemically[2,19,22], adding Cl^- to promote pitting corrosion and prevent passivation[17,23,137,138], applying ultrasound to breakdown and dislodge the fouling layers[143,145,147,149], and operating EC with alternating pulsed current (APC, also often referred to as polarity reversal, or PR)[9,17,68,74,84,153,167,201] or sinusoidal alternating current (AC)[97,158,165], such that the fouling layers can be dislodged/dissolved by chemical/electrochemical reactions that take place when the current direction is switched. Of these approaches, PR-EC and AC-EC have gained significant interests due to their ability to remove fouling layers “in situ”, that is, the removal takes place concurrent with the production of coagulants. As the current direction is switched and the

cathode becomes the anode and *vice versa*, the corrosion reactions (reactions 1 and 2) will take place at the electrode that served as the cathode in the previous current cycle, thereby displacing Ca- and Mg-containing precipitates. The dissolution of Ca- and Mg-containing precipitates can also be accelerated by the acidic pH environment developed around the anode as a result of the hydrolysis of iron and aluminum ions (reactions 5 and 6). At the cathode (which served as the anode in the previous current cycle), the evolution of H_2 gas bubbles (produced from reaction 4) can scour loosely-bound $Fe(OH)_{3(s)}$ and $Al(OH)_{3(s)}$ precipitates [9]. PR-EC and AC-EC are particularly attractive because in addition to their ability to remove fouling layers *in situ*, these methods do not require chemical addition, special infrastructure (other than a current switch), or reactor shutdown.

To address the research needs outlined in the background section of this document, the ability of PR-EC to mitigate electrode fouling was investigated in this study. By employing a similar test solution across all experiments, coupled with analyzing cell voltage, anode potential, coagulant production, and SEM images of the electrode surface, new insights have been gained about how current density and reversal frequency (*f*) influence the performance of Fe-EC and Al-EC. As will be discussed in detail later in this paper, it was determined that PR-EC was not effective at preventing the fouling of iron electrodes by Ca- and Mg-containing precipitates under all experimental conditions. This observation motivated us to explore new EC configurations, one of which consisted of an iron (or aluminum) anode and a Ti-IrO_2 cathode (i.e., Fe/Ti-IrO_2 EC and Al/Ti-IrO_2 EC). Ti-based mixed metal oxide electrodes are frequently used in water treatment applications. It has been suggested that the fouling of these electrodes by Ca and Mg-containing precipitates could be mitigated by polarity reversal because the evolution of O_2 gas (produced due to the electrochemical oxidation of H_2O) can dislodge these precipitates [202]. Therefore, it is

hypothesized that operating Fe/Ti-IrO_2 EC and Al/Ti-IrO_2 EC in the DC mode with a periodic switching of the current direction could be an effective way to mitigate electrode fouling by Ca- and Mg-containing precipitates. This hypothesis was tested by conducting such an experiment to compare electrode fouling, coagulant production, and energy consumption in the Fe/Ti-IrO_2 and Al/Ti-IrO_2 systems with those of the conventional Fe-EC and Al-EC.

4.2 Materials and Methods

4.2.1 Materials

All chemicals were of reagent grade and were used without further purification. The electrodes were cylindrical rods (d = 40 mm) of iron (Goodfellow, 98% purity), aluminum (Metal Supermarkets, 95.8% purity), and Ti-IrO_2 (Magneto Special Anodes). Before each experiment, the iron and aluminum electrodes were sonicated in 1 M HCl and rinsed with deionized water. The reaction solution was a synthetic groundwater formulation consisting of 12.6 mg/L dissolved silica (as Si), 110 mg/L Ca^{2+}, 14 mg/L Mg^{2+}, 430 mg/L HCO_3^-, 305 mg/L Na^+, 68 mg/L Cl^-, 220 mg/L SO_4^{2-}, 5.3 mg/L NO_3^- (as N), and 0.25 mg/L phosphate as P [3]. This formulation was chosen because 1) it contains a high concentration of hardness (333.3 mg/L as $CaCO_3$), allowing us to study the fouling of the electrodes by Ca- and Mg-containing precipitates in a practical timescale, and 2) the treatment of groundwater by EC is a topic of interest to researchers investigating the removal of arsenic[1,62,64,65,203]. The synthetic groundwater was prepared by dissolving $Na_2SiO_3.9H_2O$, $MgCl_2.6H_2O$, $CaCl_2$, Na_2SO_4, $NaHCO_3$, $NaNO_3$, and NaH_2PO_4 into 18.2 MΩ·cm water (Millipore System). At elevated pH, Ca^{2+} and Mg^{2+} can react with HCO_3^- and OH^- to form precipitates. To minimize such precipitation, pH was adjusted to 7.4 – 7.5 prior to the addition of $MgCl_2.6H_2O$ and $CaCl_2$, and the solution was immediately used. Within the timeframe of our experiments, no precipitation was observed in the feed solution.

4.2.2 Experimental Setup

EC experiments were carried out at 22 ± 1ºC in a three-electrode flow-through reactor (V = 200 mL). The synthetic groundwater (SGW) was circulated single-pass through the reactor at a rate of 10 mL/min by a peristaltic pump, while the volume within the reactor was stirred

continuously by a magnetic stir bar. The reactor was covered with a lid with three openings that held the working, counter, and reference electrodes (Figure 4-1).

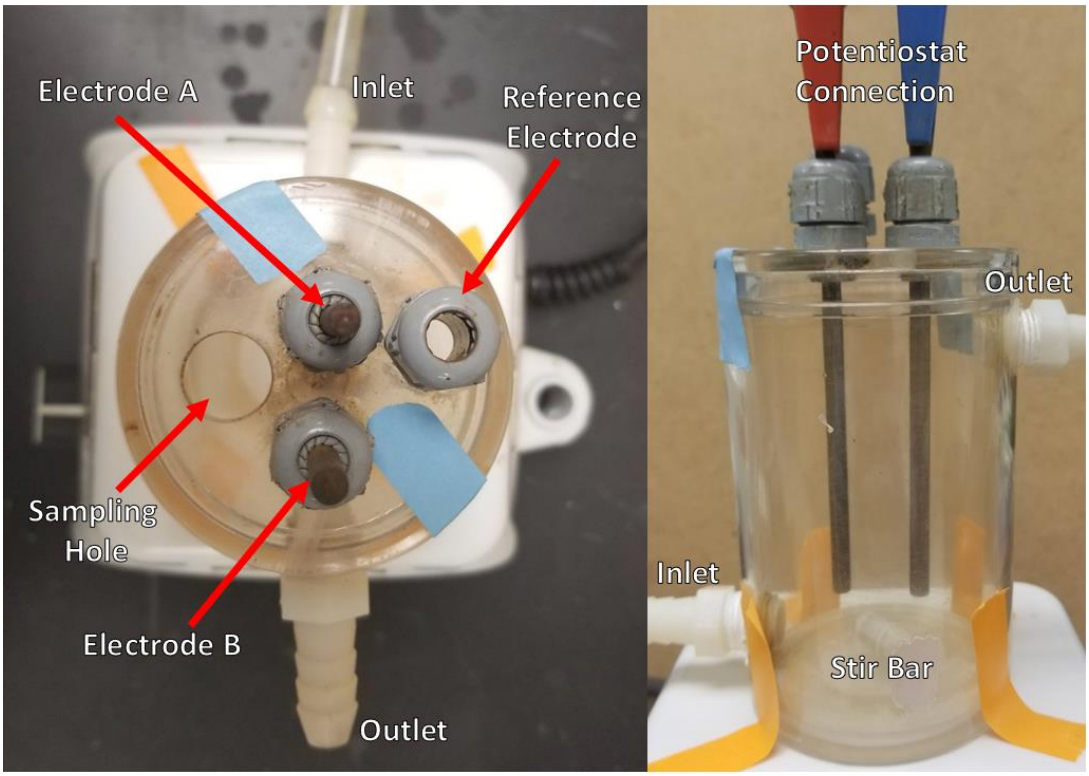

Figure 4-1. Three-electrode electrochemical cell used for flow through EC experiments.

The working and counter electrodes were either iron rods (in the Fe-EC experiments), aluminum rods (in the Al-EC experiments), or an iron or aluminum rod coupled with a Ti-IrO_2 rod. These electrodes were placed 2 cm apart and were submerged into the solution so that the surface area exposed to the solution was 7.6 ± 0.1 cm^2. In addition, a reference electrode (3 M NaCl Ag/AgCl, 0.209 V *versus* SHE) was placed 0.25 cm from one of the other two electrodes. The electrochemical cell was controlled by a VSP potentiostat (Bio-logic Science Instruments), which monitored current (*I*), cell voltage (*U*), and anode potential E_{anode}.

DC-EC and PR-EC experiments were conducted under galvanostatic mode, employing a current value of either I = 8, 50, or 100 mA (i.e., a current density of j = 1, 6.5 or 13 mA/cm^2). In

the PR-EC experiments, the current direction was switched periodically at a *f* of either 0.5 or 10 minutes. A preliminary experiment operated in the DC mode revealed that the cathode, regardless of whether Fe, Al, or Ti-IrO_2 was used, was entirely covered with Ca- and Mg-containing precipitates within the first few hours. As such, all experiments were terminated at t = 6 hours. Subsequently, the surface morphology of the electrodes was analyzed using an FEI Quanta Feg 250 Environmental Scanning Electron Microscope (ESEM) coupled with an Inca Energy Dispersive X-ray Spectrometer (EDX). In addition, the precipitates formed on the surface of the electrodes were scraped off and subjected to X-ray diffraction (XRD) analysis. To determine the amount of coagulant released, an aliquot of the reaction solution was digested with a solution of 3 wt. % HNO_3 and 3 wt. % HCl, and analyzed for aluminum and iron by inductively coupled plasma - optical emission spectroscopy (ICP-OES). The Faradaic efficiency (ϕ) was calculated using the following formula: $\phi = \frac{m \times z \times F}{I \times t \times M}$, where m is the mass of iron or aluminum released into the solution, z is the number of electrons involved in the anodic reaction (z = 2 for Fe, 3 for Al), F is the Faraday's constant (96,485 Coulombs/eq), M is the molecular weight (56 for Fe, 27 for Al) and t is the retention time (20 mins).

The pH of the reaction solution throughout each Fe-EC experiment was 7.5 ± 0.2. In contrast, in all Al-EC experiments the solution pH gradually increased and reached 8 – 8.2 by the end of each experiment. Although the concentration of dissolved oxygen (DO) in the reactor was not monitored, it is expected that the reaction solution always contained some DO because the feed solution (which was saturated with DO) was continuously flown through the reactor. Also, the reactor was opened to the atmosphere. All experiments were conducted in duplicate and average values along with the range are presented.

4.3 Results

4.3.1 Fe-EC

In the experiments operated in the DC mode (i = 13 mA/cm^2), the anode surface quickly turned brown-yellow, a color indicative of Fe(III)(hydr)oxides. Meanwhile, a coarse layer of white-colored precipitates built up on the cathode (Figure 4-2 A). Further inspection of the cathode by SEM-EDX revealed that the white-colored precipitates were rhombohedral-shaped crystals that contained Ca and Mg (Figure 4-2B and Figure 4-3 A). While the XRD spectrum of these crystals (Figure 4-4 A) matches that of pure calcite ($CaCO_3$), their shape and elemental content suggest that they are a magnesian calcite phase ($Ca_{1-x}Mg_xCO_3$) [204].

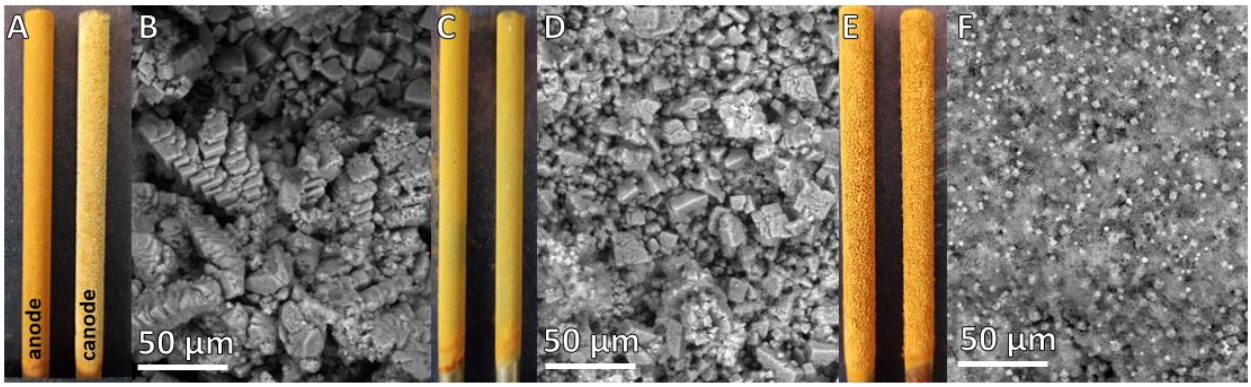

Figure 4-2. Photos and SEM images of Fe electrodes taken at t = 6 h. EC experiments were conducted in the galvanostatic mode (i = 13 mA/cm^2) with direct current (A and B), or current with reversal frequencies of f = 10 min (C and D) and f = 0.5 min (E and F). Note that in the polarity reversal modes there is no designated cathode or anode.

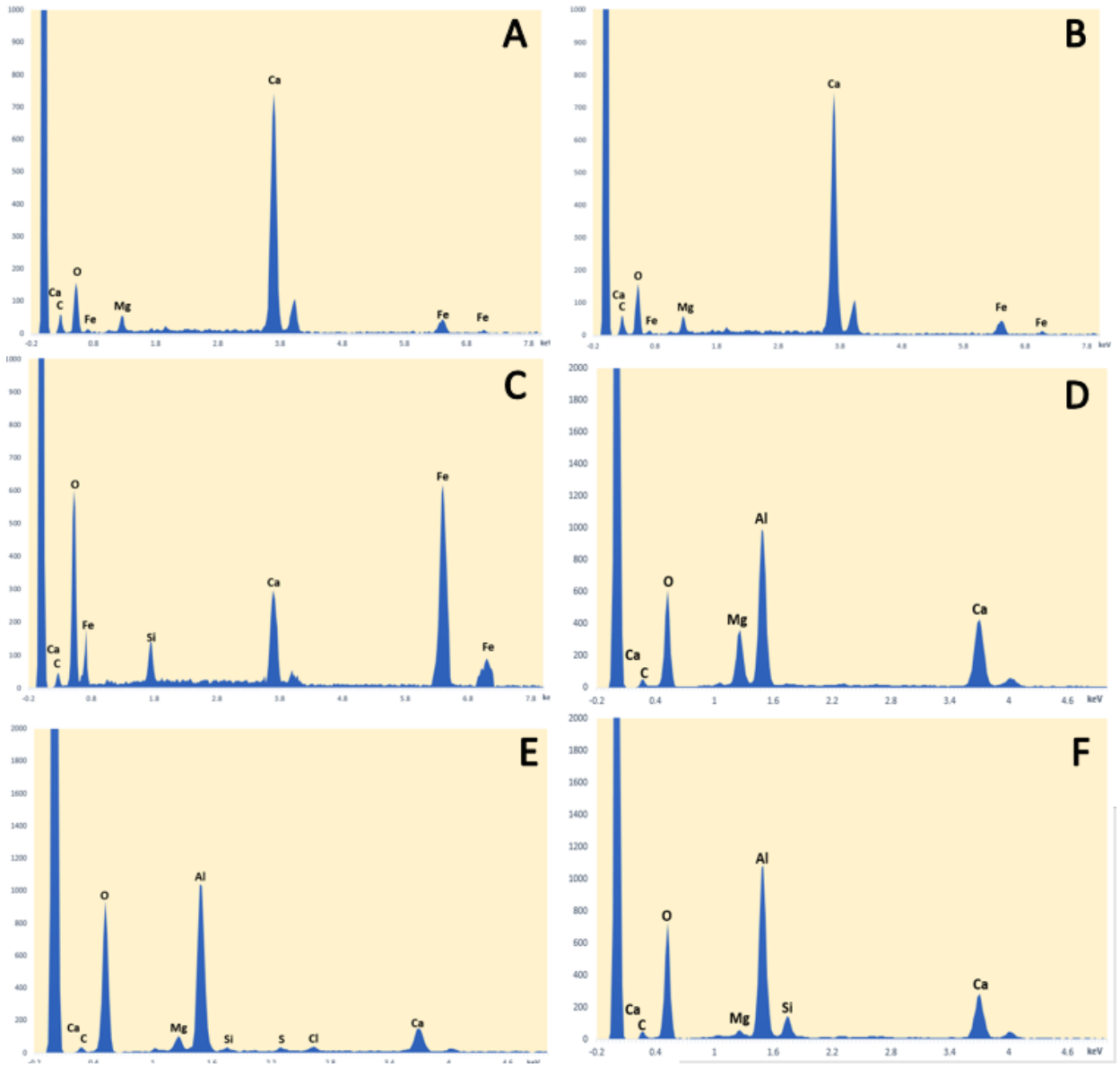

Figure 4-3. EDX spectrum of the surface of the of (A-C) Fe and (D-F) Al cathode or electrodes taken at t = 6 h. EC experiments were conducted in the galvanostatic mode (i = 13 mA/cm^2) with direct current (A and D), or current with reversal frequencies of f = 10 min (B and E) and f = 0.5 min (C and F).

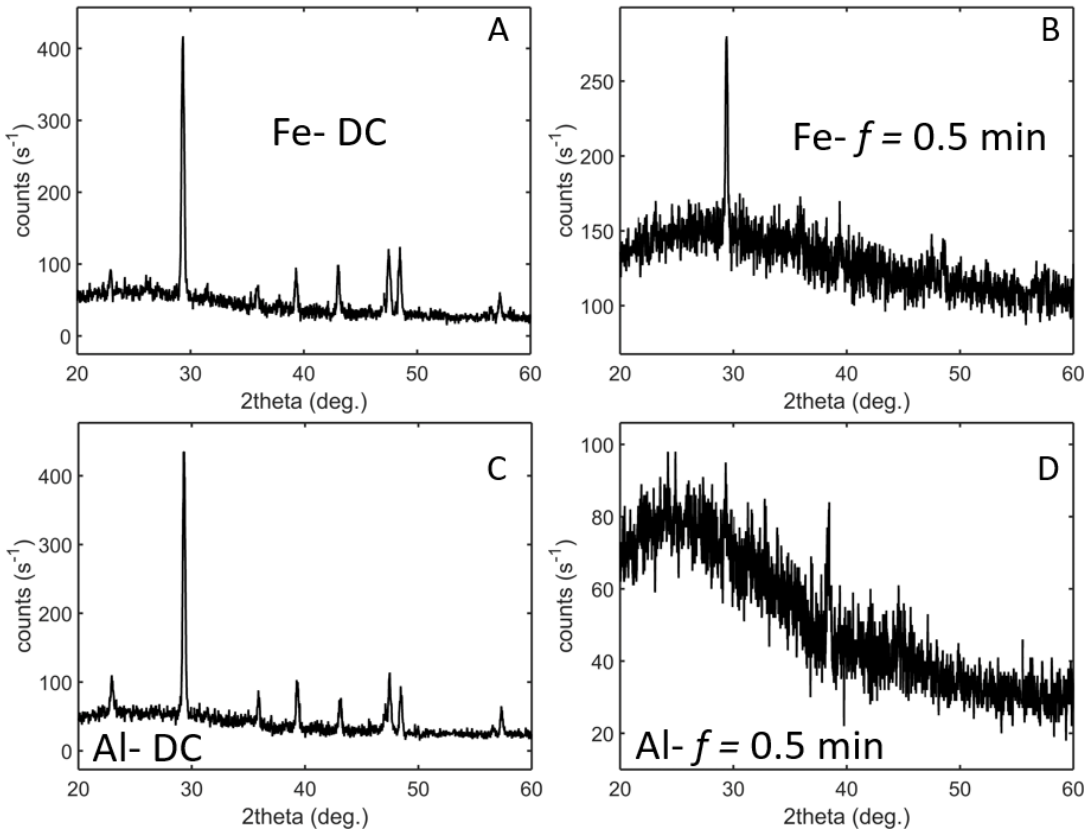

Figure 4-4. XRD spectrum of the fouling layer on the surface of the cathode in DC and electrodes in PR in (A) Fe-EC operated in DC mode (B) Fe-EC operated in PR mode with f = 0.5 min (C) Al-EC operated in DC mode (D) Al-EC operated in PR mode with f = 0.5 min.

Although by the end of the experiment the cathode surface was completely covered with these $Ca_{1-x}Mg_xCO_3$ minerals, the cell voltage U remained constant at ~7.6 V (Figure 4-5 A). The ohmic drop-compensated anode potential, E_{anode} = -0.4 V, also did not vary to any appreciable extent throughout the entire course of the experiment (Figure 4-6 A). The Faradaic efficiency ϕ was 1 ± 0.01 (Table 4-1), indicating that the predominant anodic reaction was the corrosion of iron (reaction 1), and that all iron ions released from the anode migrated into the bulk solution. When a current density of j = 6.5 mA/cm^2 was employed, ϕ was comparable to that in the j = 13 mA/cm^2 experiment. In contrast, ϕ in the j = 1 mA/cm^2 experiment was 20 – 30% lower (Table 4-1). Müller et al [22] also observed a similar trend, that is ϕ (0.66 – 0.85) in a Fe-EC experiment with j = 0.8

mA/cm^2 was lower than those ($\phi > 0.9$) operated at higher j values. They attributed this low ϕ to the accumulation of Fe(II) on the anode, which was the result of the diminished flux of Fe(II) ions released from the anode at low j. It is suspected that for this same reason ϕ in our j = 1 mA/cm^2 experiment was lower than those in the other experiments.

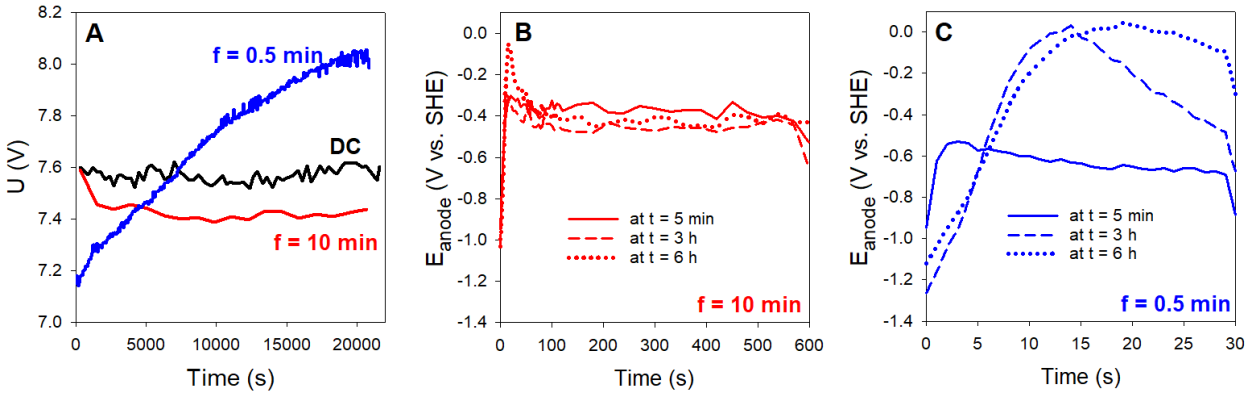

Figure 4-5. Cell voltage U (A), and time profiles of anodic potential E_{anode} within each reversal cycle in PR-EC with f = 10 min (B), and f = 0.5 min (C). Electrodes were Fe, and j = 13 mA/cm^2.

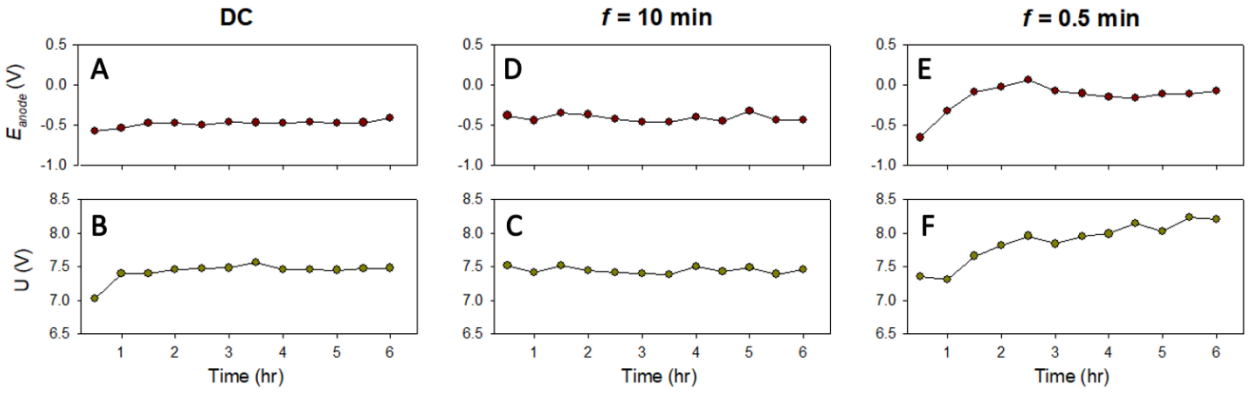

Figure 4-6. Cell voltage U (B C, and F)), and anodic E_{anode} (A, D, and G) potential over the 6-hour experiments in DC (A and B), PR-EC with f = 10 min (D and C)), and f = 0.5 min (E and F). Electrodes were Fe, and j = 13 mA/cm^2.

Table 4-1. Faradaic efficiency in the Fe-EC experiments

Operating Condition	i = 1 mA/cm^2		i = 6.5 mA/cm^2		i = 13 mA/cm^2	
	3 hr	6 hr	3 hr	6 hr	3 hr	6 hr
DC	0.70± 0.01	0.78 ± 0.00	1.02 ± 0.06	0.92 ± 0.01	1.00 ± 0.01	1.02 ± 0.01
f = 10 min	0.46 ± 0.02	0.50 ± 0.06	0.86 ± 0.00	0.86 ± 0.06	0.83 ± 0.04	0.81 ± 0.04
f = 0.5 min	0.13 ± 0.00	0.11 ± 0.00	0.12 ± 0.01	0.06 ± 0.01	0.24 ± 0.01	0.07 ± 0.01

The evolutions of the electrode fouling layers, U, E_{anode}, and ϕ in PR-EC were drastically different from those in DC-EC, and were dependent on the PR f. When f = 10 min and i = 13 mA/cm^2, U decreased from 7.6 V to 7.4 V within the first 20 minutes and remained at this value until the end of the experiment (Figure 4-5 A). At t = 6 h, both electrodes were entirely covered with rhombohedral $Ca_{1-x}Mg_xCO_3$ crystals (Figure 4-2 C and D). When f = 0.5 min, U steadily increased throughout the experiment from 7.2 V to 8.0 V (Figure 4-5 A), and the electrodes were covered with very small cubic minerals that were sparsely dispersed within fluffy iron (hydr)oxide flocs (Figure 4-2 E and F). The EDX spectrum reveals that the fouling layer also contained Si, while the presence of Mg was not detected (Figure 4-3 C). The cubic shape of the Ca-containing precipitates suggests that they are calcite ($CaCO_3$).

In the PR-EC experiments, I dipped whenever the current direction was switched, but subsequently restored to the pre-set value within less than 2 s (Figure 4-7). In contrast, a more complicated change was observed with the anodic potential E_{anode}. (Note that there was no dedicated anode or cathode in PR-EC, since the current direction was constantly changing; therefore, E_{anode} herein refers to the potential of electrode A (Figure 4-1) measured whenever this electrode served as the anode in the cell). In the f = 10 min experiment, E_{anode} measured at t = 5 min increased and peaked at -0.31 V, before decreasing to a steady state value of -0.37 V (the solid

line in Figure 4-5 B). As the experiment progressed, the E_{anode} peak value and the time required for it to reach steady state gradually increased. Toward the end of the experiment, E_{anode} peaked at -0.02 V and decreased to a steady state value of -0.42 V only after 90 s (the dotted line Figure 4-5 B). In the f = 0.5 min experiment, E_{anode} increased over time, ranging from -0.95 V to -0.57 V early on in the experiment (the solid line in Figure 4-5 C), and from -1.12 V to -0.01 V at the end of the experiment (the dotted line in Figure 4-5 C). ϕ in the PR-EC experiments were lower than those of DC-EC, with ϕ = 0.5 – 0.86 and ϕ = 0.06 – 0.24 in the f = 10 min and f = 0.5 min experiments, respectively (Table 4-1). Under f = 0.5 min, ϕ decreased by as much as 3 folds as the experiment progressed (compare ϕ at t = 3 h *versus* at t = 6 h).

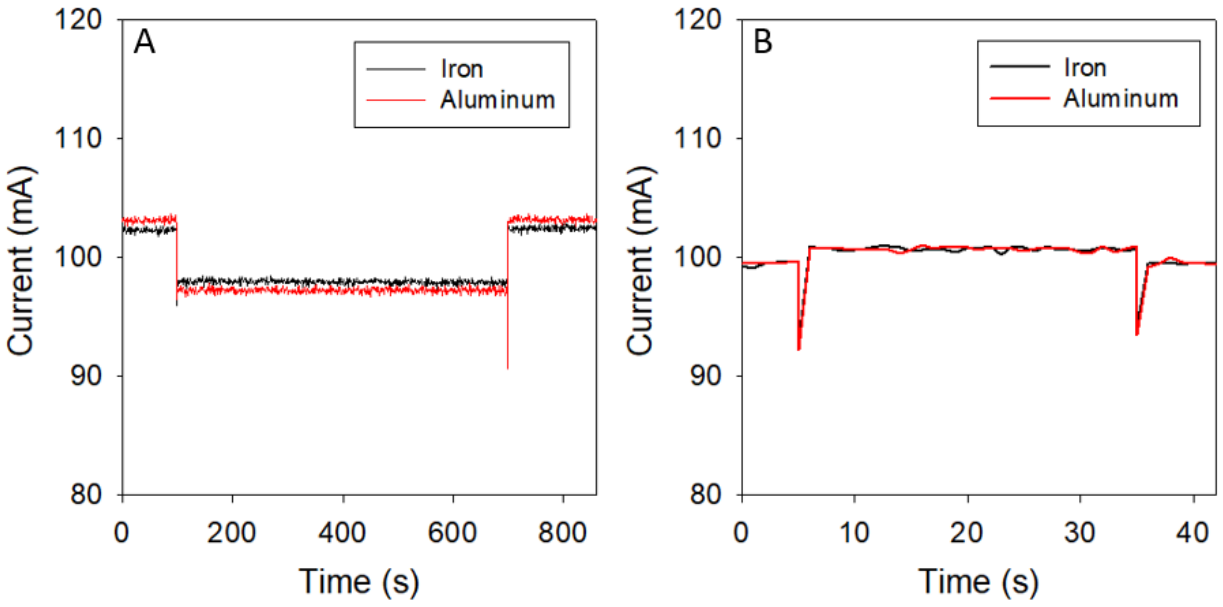

Figure 4-7. Current profiles in Al-EC and Fe-EC with current reversal frequencies of f = (A) 10 min and (B) 0.5 min.

4.3.2 Al-EC

A significant build-up of precipitates on both electrodes was observed in the Al-EC system operated in the DC mode. By the end of the experiment, the anode was covered with fluffy aluminum hydroxide precipitates (Figure 4-8 A). Meanwhile, the cathode was covered with both $Ca_{1-x}Mg_xCO_3$ and aluminum hydroxides (Figure 4-8 B). Throughout the course of the experiment, U steadily increased from 8.1 V to 9.8 V (Figure 4-9 A). E_{anode} also increased steadily over time from -1.75 V to -0.26 V (Figure 4-10 A), indicating that the fouling layer on the anode was responsible for the increase in the cell voltage. The Faradaic efficiency was $\phi = 1.61 – 1.74$ when j = 13 mA/cm^2, 1.83 – 1.92 when j = 6.5 mA/cm^2, and 1.19 – 1.69 when j = 1 mA/cm^2 (Table 4-2).

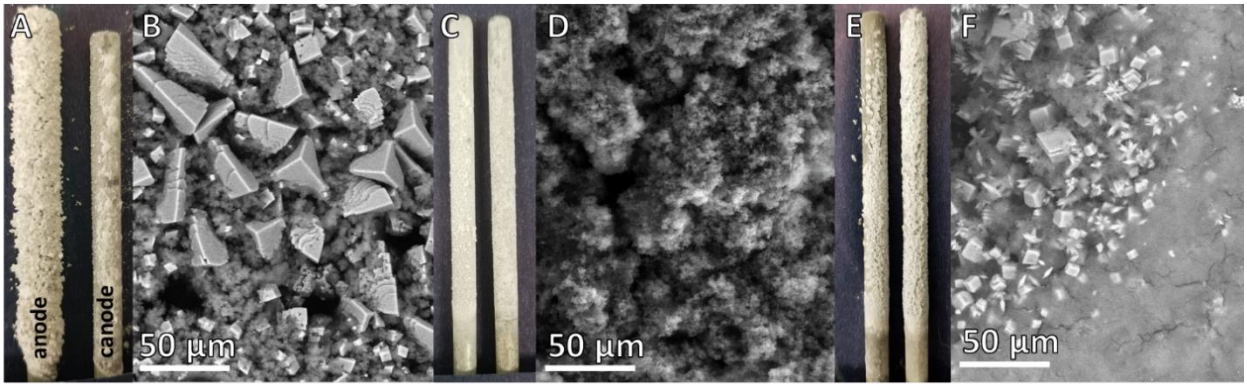

Figure 4-8. Photos and SEM images of Al electrodes taken at t = 6 h. EC experiments were conducted in the galvanostatic mode (i = 13 mA/cm^2) with direct current (A and B), or current with reversal frequencies of f = 10 min (C and D) and f = 0.5 min (E and F). Note that in the polarity reversal modes there is no designated cathode or anode.

A super Faradaic efficiency (i.e., $\phi > 1$) is typical of Al-EC, owing to the combined electrochemical and chemical dissolution of aluminum[107,114,115,166].

Table 4-2. Faradaic efficiency in the Al-EC experiments

Operating Condition	i = 1 mA/cm^2		i = 6.5 mA/cm^2		i = 13 mA/cm^2	
	3 hr	6 hr	3 hr	6 hr	3 hr	6 hr
DC	1.19 ± 0.06	1.69 ± 0.21	1.92 ± 0.01	1.83 ± 0.22	1.74 ± 0.10	1.61 ± 0.03
f = 10 min	1.17 ± 0.17	1.25 ± 0.02	1.75 ± 0.04	1.76 ± 0.06	2.09 ± 0.06	2.13 ± 0.04
f = 0.5 min	0.57 ± 0.00	0.54 ± 0.00	0.67 ± 0.02	0.67 ± 0.10	1.33 ± 0.10	1.40 ± 0.01

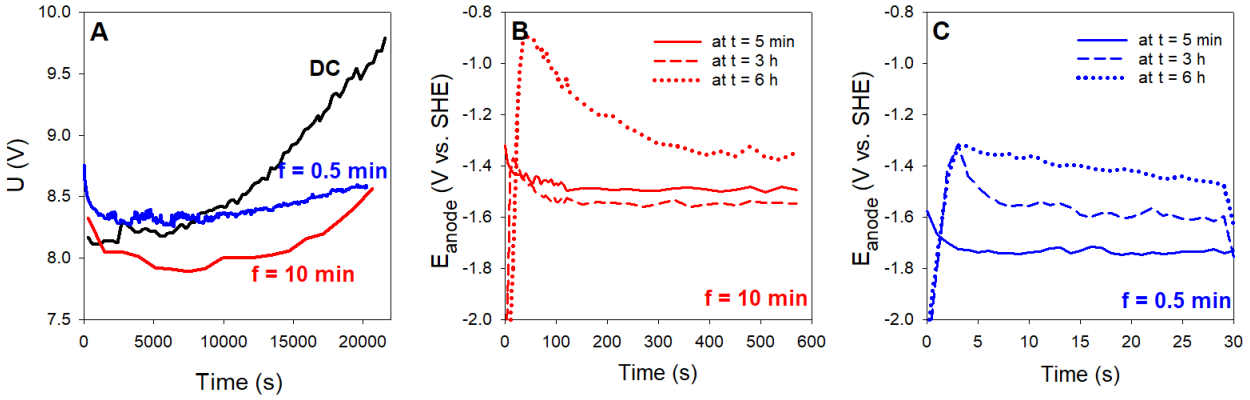

Figure 4-9. Cell voltage U (A), and time profiles of anodic potential E_{anode} within each reversal cycle in PR-EC with f = 10 min (B), and f = 0.5 min (C). Electrodes were Al, and j = 13 mA/cm^2.

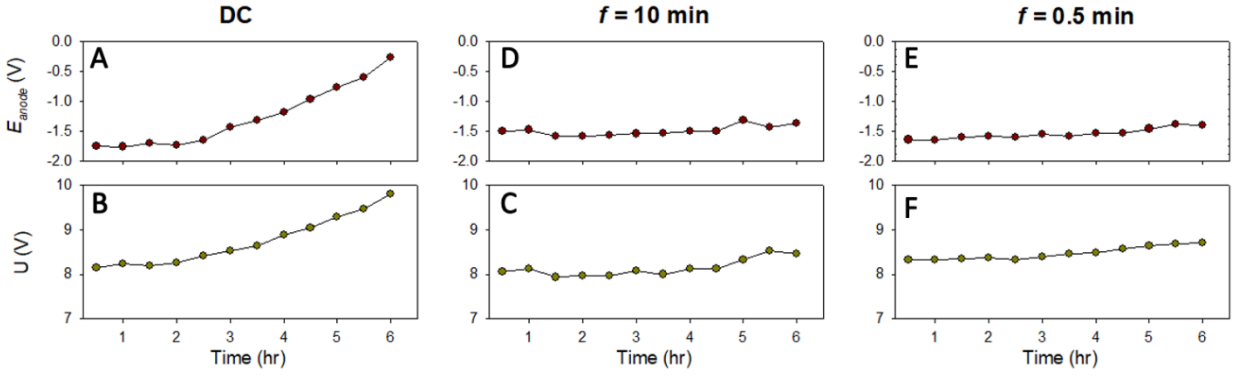

Figure 4-10. Cell voltage U (B C, and F)), and anodic E_{anode} (A, D, and G) potential over the 6-hour experiments in DC (A and B), PR-EC with f = 10 min (D and C)), and f = 0.5 min (E and F). Electrodes were Al, and j = 13 mA/cm^2.

The fouling of the aluminum electrodes substantially decreased in the PR system operated at f = 10 min (Figure 4-8 C). The EDX spectrum reveals the presence of Ca and Mg on the electrode surface (Figure 4-3 E). As such, although not seen in the SEM image (Figure 4-8 D), Ca and Mg-containing precipitates are speculated to be present and must have been enmeshed within the aluminum hydroxide flocs. As seen in Figure 4-9 A, U initially decreased from 8.3 V to 7.9 V, before increasing to 8.5 V by the end of the experiment. Within each PR cycle, E_{anode} rapidly reached a steady state value of -1.5 V early on in the experiment (the solid line in Figure 4-9 B). As the experiment progressed, the time required for E_{anode} to reach a steady state value gradually increased. At t = 6 h, E_{anode} peaked at -0.89 V, and reached a steady state value of -1.3 V after 300 s (the dotted line in Figure 4-9 B).

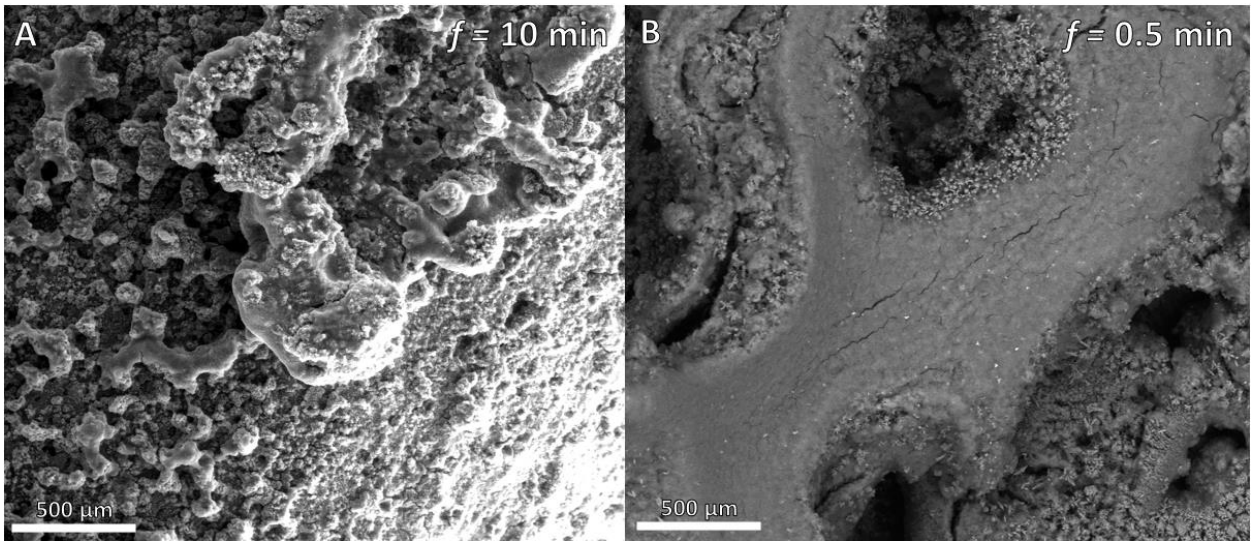

Figure 4-11. Pitting of the aluminum electrodes surfaces with current reversal frequencies of f = (A) 10 min and (B) 0.5 min.

Unlike in the DC and PR f = 10 min experiments, large holes were seen to have formed on both electrodes in the f = 0.5 min experiment (Figure 4-11 B), suggesting that pitting corrosion could be an important mechanism of aluminum dissolution in this case. Also, the surface within each hole was covered with very small spindle and cubic minerals that consisted of Ca, C, and O

(Figure 4-8 F, Figure 4-3 F, and Figure 4-11 B). Although the identity of these minerals could not be elucidated by XRD (since the XRD diffraction spectrum was dominant by that of the amorphous aluminum hydroxide precipitates present in the sample (Figure 4-4 D), the shape and composition of the minerals suggest that they are different polymorphs of $CaCO_3$ (e.g., aragonite, which are spindle-shaped, and calcite, which are cubic-shaped) [205]. In the f = 0.5 min experiment, U ranged between 8.3 V and 8.7 V (Figure 4-9 A), while E_{anode} increased from -1.70 V to -1.47 V (Figure 4-9 C).

As in the Fe-EC experiments, ϕ under f = 0.5 min was the lowest among all Al-EC experiments; notably, ϕ in the j = 1 mA/cm^2 and 6.5 mA/cm^2 experiments were < 1 (Table 4-2).

4.3.3 EC Systems with Ti-IrO_2 Serving as the Cathode

The observation that PR was not effective at preventing the fouling of iron electrodes by Ca- and Mg-containing precipitates motivated us to explore new EC configurations. In a preliminary experiment wherein a Ti-IrO_2 electrode served as the cathode in the Fe-EC system, it was observed that a thick layer of $Ca_{1-x}Mg_xCO_3$ accumulated on this electrode could be completely dislodged within 2 mins upon switching the current direction (Figure 4-12 A and B vs. Figure 4-12 C and D, Figure 4-13). As such, the performance of a combined system of Fe/Al anode and Ti-IrO_2 cathode was further investigated in an experiment in which the cell was operated in the DC mode, but the current direction was intermittently switched so that the Ti-IrO_2 functioned as an anode for 120 s every 30 mins.

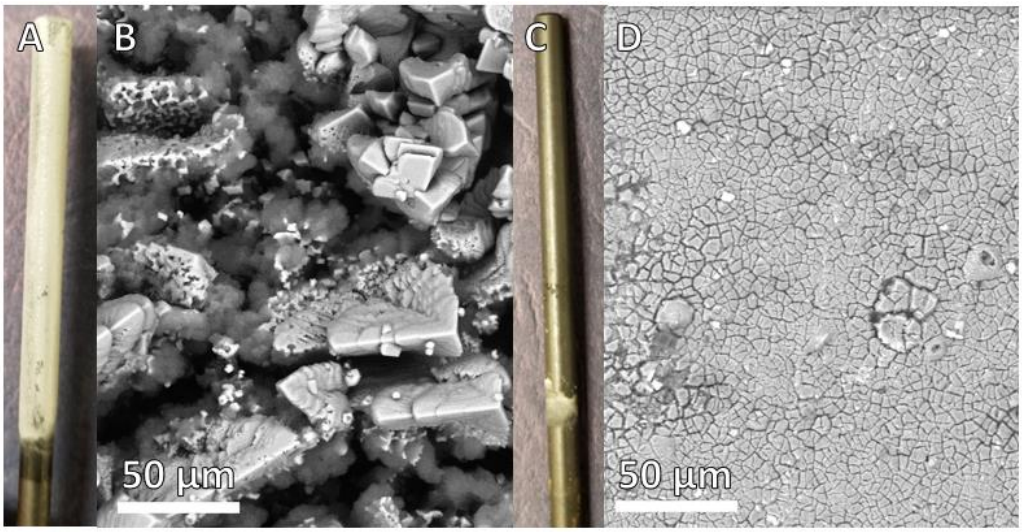

Figure 4-12. Photo and SEM images of a Ti-IrO_2 cathode that was fouled by $Ca_{1-x}Mg_xCO_3$ (A and B). The fouling layer was completely removed (C and D) 30 seconds after the current direct was switched (hence, the Ti-IrO_2 electrode became an anode).

As can be seen from Figure 4-13 A and B, the Ti-IrO_2 electrodes were free of foulants after 6 h of operation. The fouling of the iron and aluminum anodes was also drastically diminished. Notably, the original black color of the iron rod was still visible (Figure 4-13 A). The Faradaic efficiencies were $\phi = 0.87 – 0.95$ and $\phi = 0.82 – 0.90$ in the Fe/Ti-IrO_2 and Al/Ti-IrO_2 systems, respectively (Table 4-3). In both systems, U increased by less than 0.1 V throughout the course of the experiment (Figure 4-13 C).

Table 4-3. Faradaic efficiency in the Fe/Ti-IrO_2 and Al/Ti-IrO_2 EC experiments

Fe/Ti-IrO_2 EC		Al/Ti-IrO_2 EC	
i = 13 mA/cm^2		i = 13 mA/cm^2	
ϕ (3 h)	ϕ (6 h)	ϕ (3 h)	ϕ (6 h)
0.87 ± 0.020	0.95 ± 0.004	0.82 ± 0.01	0.900 ± 0.01

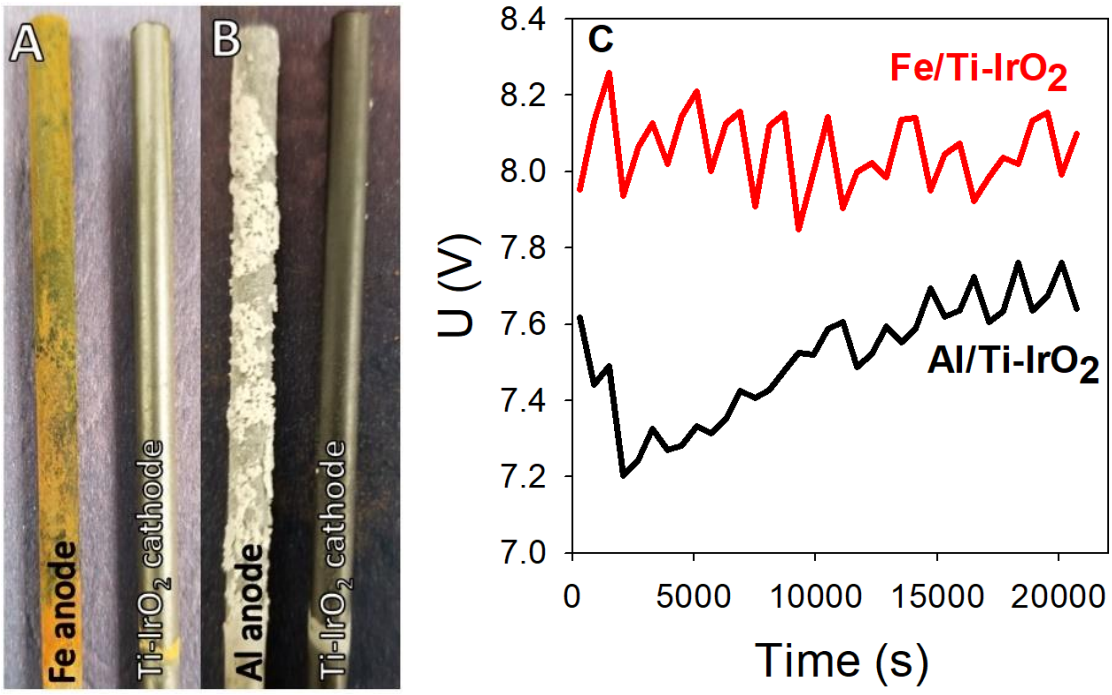

Figure 4-13. Photo and SEM images of the electrodes in the Fe/Ti-IrO_2 (A) and Al/Ti-IrO_2 (B) EC systems. In these systems, Fe or Al served as the anode while Ti-IrO_2 served the cathode. Electrocoagulation experiments were operated in the DC mode (i = 13 mA/cm^2). Every 30 minutes, the current direction was reversed for that the Ti-IrO_2 served as the anode for 120s, before the current direction was reversed back. (C): Time profile of cell voltage in the Fe/Ti-IrO2 and Al/Ti-IrO_2.

4.4 Discussion

A major finding of this study is that operating EC in the PR mode did not always result in a lower energy consumption and/or greater coagulant production efficiency. In the Fe-EC system operated under the PR f = 10 min mode, a slightly lower U compared with that in DC-EC (and hence lower energy consumption P, since $P = U \times I \times t$) came at the expense of a ϕ that decreased by 10 – 35%. In the PR f = 0.5 min system, not only did the energy consumption increase over time, but ϕ also drastically decreased by as much as 90%. Moreover, while it has been suggested that operating EC in the PR mode can reduce electrode fouling [153,159], this was not the case in our Fe-EC experiments. As was mentioned earlier, the iron electrodes were fully covered with $Ca_{1-x}Mg_xCO_3$ (Figure 4-2 D), $CaCO_3$ and iron (hydr)oxides (Figure 4-2 F). Although U remained constant in the PR f = 10 min system, it is speculated that U may ultimately increase if $Ca_{1-x}Mg_xCO_3$ continues to accumulate on both electrodes. In the PR f = 0.5 min, the increase in U (Figure 4-5 A) is attributable to the surface accumulation of iron (hydr)oxides, which passivated the surface of iron[22,133]. Iron (hydr)oxides are several orders of magnitude less conductive than metallic iron[128].

There are several possible explanations for the lower coagulant production in the iron PR-EC experiments. *First,* following each current switching event, the cathode will exert an electrostatic attraction force on the cationic iron species that have just been released from the same electrode. (This electrode served as the anode in the preceding current cycle). This attractive force would retard the migration of the cationic iron species into the bulk solution. Subsequently, upon encountering the OH^- ions that are now generated via cathodic reactions 3 and 4, these cationic iron species would precipitate on the surface of the electrode, resulting in a lower ϕ. This hypothesis is speculated to be particularly relevant to the PR f = 0.5 min system wherein a rapid

current cycling means that there would be less time for cationic iron species to migrate away from the electrodes. This hypothesis is also consistent with the formation of fluffy iron (hydr)oxide flocs on the electrode surface (Figure 4-2 E and F). *Second*, the lower ϕ could be due to electrochemical side reactions that if present will divert the current away from the iron corrosion reaction (i.e., reaction 1). In previous studies, $\phi < 1$ was attributable to the electrochemical oxidation of H_2O and Cl^- [8,17,22,66,96,113,206–208]. However, since $E^0_{H(w),\ O2/H2O}$ = +0.81 V and $E^0_{H(w),\ Cl2/Cl-}$ = +1.34 V, the presence of these reactions can be ruled out from our system. This is because E_{anode} in our experiments were always < +0.81 V. (Note that due to the acidic environment in the anodic boundary layer, E_{anode} must be greater than $E^0_{H(w),\ O2/H2O}$ and $E^0_{H(w),\ Cl2/Cl-}$ to trigger the oxidation of H_2O and Cl^-). Under PR f = 10 min, that ϕ = 0.81 – 0.86 as well as E_{anode} mostly ranged between -0.37 and -0.42 V suggest that the predominant anodic reaction was the oxidation of iron ($E^0_{H(w),\ Fe/Fe2+}$ = -0.44 V). Under PR f = 0.5 min, E_{anode} ranged between -1.12 V and -0.02 V. Within this range, in addition to the oxidation of Fe, other reactions that are thermodynamically possible include the oxidation of $H_{2(g)}$ ($E^0_{H(w),\ H2O/H2}$ = - 0.41 V), the oxidation of $Fe(OH)_2$, ($E^0_{H,\ green\ rust/Fe(OH)2}$ = -0.5 to -0.6 V when pH = 7 – 10 [209,210]; $E^0_{H,\ Fe2O3/Fe(OH)2}$ = -0.5 to -1.0V when pH = 9 – 14 [211], and the oxidation of Fe_3O_4 ($E^0_{H,\ Fe2O3/Fe3O4}$ = -0.2 to -0.5 V when pH = 8 – 14 [211]. In these experiments, the formation of $H_{2(g)}$ bubbles whenever each of the two electrodes served as the cathode was observed. Some bubbles detached from the electrode, while some remained on the electrode surface. Therefore, it is hypothesized that the oxidation of these adsorbed $H_{2(g)}$ (or dissolved H_2 present in the vicinity of the electrodes), which would take place when the current direction is switched and a cathode becomes an anode, is an important side reaction. However, since E_{anode} in the PR f = 0.5 min system varied over a wide range (Figure 4-5 C), it is likely that multiple oxidation side reactions were occurring. In addition to the oxidation side reactions, the

electrochemical reduction on the cathode of Fe(II) ions [212](released from the same electrode when it served as the anode in the preceding current cycle) could have resulted in a low ϕ in PR-EC. *Third*, the lower ϕ also could be due to the build-up of precipitates on the surface of both electrodes, which would prevent the migration into the bulk solution of the iron ions that are released from the electrode base beneath the fouling layer. *Lastly*, the lower coagulant production in PR-EC could be due to the current interruption period between each PR cycle. However, since current was restored to the pre-set value within less than 2 s (Figure 4-7), the effect of current interruption on ϕ should be minimal.

If PR is detrimental to Fe-EC, it is appeared to be beneficial to the performance of Al-EC. *Firstly*, electrode fouling was significantly reduced in all aluminum PR-EC experiments (compare Figure 4-8 C and E with Figure 4-8 A). A notable difference between the Fe-EC and Al-EC systems is that the aluminum hydroxide precipitates were observed to be more loosely bound to the anode, and more easily dislodged by the $H_{2(g)}$ bubbles that were produced whenever the current direction was switched. *Secondly*, *U* in the PR experiments were lower than that of Al-DC (Figure 4-9 A), which increased substantially as the experiment progressed. *Finally*, of all the PR conditions tested, only under f = 0.5 min/i = 1 mA/cm^2 and f = 0.5 min/i = 6.5 mA/cm^2 did the aluminum PR-EC system exhibit a significant decrease in ϕ (by as much as 75%). Under the other PR conditions, ϕ is either equal to (f = 10 min/i = 6.5 mA/cm^2), slightly higher (f = 10 min/i = 13.5 mA/cm^2), or slightly lower (f = 0.5 min/i = 13 mA/cm^2 and f = 10 min/i = 1 mA/cm^2) than ϕ in the Al-DC counterparts.

Another important difference between Al-EC and Fe-EC is that the anode and cathode in Al-EC can undergo chemical corrosion, owing to the low and high pH regions developed in the

vicinity of each electrode [107,114,115,166]. The chemical dissolution of the cathode would dislodge Ca- and Mg-containing precipitates – as can be seen by comparing Figure 4-2 B and Figure 4-8 B, the aluminum cathode was not covered by $Ca_{1-x}Mg_xCO_3$ to the same extent as was the iron cathode. The chemical oxidation of aluminum electrodes also resulted in $\phi > 1$, with the exception of the f = 0.5 min/i = 6.5 mA/cm^2 (ϕ = 0.67) and the f = 0.5 min/i = 1 mA/cm^2 (ϕ = 0.54) systems. As in the iron PR-EC system, possible explanations for the lower ϕ in the aluminum PR-EC f = 0.5 min systems include (1) decreased migration into the bulk solution of cationic aluminum species because of the rapid current cycling, and (2) electrochemical side reactions, particularly the oxidation of adsorbed $H_{2(g)}$. Another reason for the lower ϕ could be that the rapid current cycling in the f = 0.5 min system resulted in less acidic/basic pH environments in the vicinity of each electrode, thereby decreasing the chemical dissolution of aluminum [200].

Compared with the Fe-EC and Al-EC systems, the fouling of the electrodes in the Fe/Ti-IrO_2 and Al/Ti-IrO_2 systems was diminished (the iron and aluminum electrodes) or prevented altogether (the Ti-IrO_2 electrode). As was mentioned earlier, the Fe/Ti-IrO_2 and Al/Ti-IrO_2 systems were operated under the DC mode (iron or aluminum was the anode while Ti-IrO_2 was the cathode), with an occasional current switching that reversed the role of the two electrodes for a short period (120 s). Following each current switching event, the $Ca_{1-x}Mg_xCO_3$ precipitates accumulated on the Ti-IrO_2 electrode was rapidly dislodged by the evolution of $O_{2(g)}$ bubbles (produced from the electrochemical oxidation of H_2O on Ti-IrO_2). In the Fe/Ti-IrO_2 system, ϕ decreased only by 5 – 13%, which is attributable to the interruption of coagulant production whenever the Ti-IrO_2 electrode served as an anode (13.3% of the overall operating time). From the operational perspective, this slightly lower ϕ could be outweighed by the potential benefits that the diminished electrode fouling may provide (e.g., lower ohmic drop, sustained coagulant production, less

frequent replacement of electrodes). In contrast, ϕ in the Al/Ti-IrO_2 system decreased by 40 – 60% compared with ϕ in the aluminum DC-EC counterpart. This significant decrease of ϕ in the Al/Ti-IrO_2 system highlights the importance of the chemical dissolution of the aluminum cathode in the aluminum DC-EC system to the overall coagulant production. It also suggests that the Al/Ti-IrO_2 system might not be an attractive alternative to conventional Al-EC systems, considering that the amount of energy consumed in the former system is only 10 – 20% lower (compare U_{cell} = 7.2 – 7.6 V of the Al/Ti-IrO_2 system (Figure 4-13 C) versus U_{cell} = 8.0 – 8.5 V of the aluminum PR-EC f = 10 min (Figure 4-9 A). Of all the Al-EC systems tested in this study, the aluminum PR-EC/f = 10 min appeared to provide the greatest balance of high coagulant production efficiency, reduced energy consumption, and diminished electrode fouling.

4.5 Chapter Conclusions

This study compared the performance of Fe- and Al-EC systems that operated in the direct current and polarity reversal modes. By systematically examining the effects of electrode type, current density, and PR *f* on the coagulant production efficiency, electrode fouling, energy consumption, and anodic potential, the following insights have been gained:

- Under the experimental conditions employed in this study, Fe-EC operated in the polarity reversal mode consumed more energy but generated less coagulant than the iron DC-EC counterpart. The fouling of the iron electrodes also was not reduced under all conditions, which is contrary to what has been suggested in the literature.
- In general, polarity reversal was beneficial to the performance of Al-EC. In all but one experiment, the coagulant production of aluminum PR-EC was comparable to that of aluminum DC-EC. Notably, aluminum PR-EC systems consumed less energy and did not suffer from electrode fouling to the same extent as aluminum DC-EC.
- Under a rapid rate of polarity reversal (f = 0.5 mins), the coagulant production efficiency decreased by as much as 90% in Fe-EC, and by 40 – 50% in Al-EC. This decrease was attributable to electrochemical side reactions (e.g., the oxidation of adsorbed $H_{2(g)}$), the retardation of the iron and aluminum ion migration into the bulk solution, and the precipitation of these ions on the electrodes. It is suspected that, for these same reasons, the coagulant production efficiencies in EC systems operated with alternating current (AC-EC) were lower than those of DC-EC [155,157]. In AC-EC systems, the migration of iron and aluminum ions into the bulk solution is expected to be further retarded since the current direction is constantly changing.

- An EC system that employed a iron anode and a Ti-IrO_2 cathode, and operated under the DC mode with an occasional current switching, was shown to result in not only effective coagulant production but also minimal electrode fouling. This combined Fe/Ti-IrO_2 electrode system has the potential to be an effective EC configuration.

As a concluding remark, it is noted that all experiments in this study were conducted under a similar flow dynamic and employed one solution formulation. Since the nature of the fouling layer and the coagulant production efficiency are dependent on the solution composition (e.g., the corrosion of iron is accelerated by Cl^- but inhibited by oxyanions such as SO_4^{2-} and phosphate[17,134–136] and cell design [101,132,213], additional research is needed to compare the performance of DC-EC and PR-EC under different solution chemistry and flow dynamics.

Chapter 5

The Effect of Polarity Reversal on Faradaic Efficiency, Contaminant Removal, and Precipitate Separation

Portions of this chapter (figures (Figure 5-1, Figure 5-3, Figure 5-4), tables (Table 5-1), and texts (sections 5.2 and 5.3.1)) were published in Water Research, Volume 203, Chow H., Ingelsson M., Pham A. L. T., Roberts E. P. L., How does periodic polarity reversal affect the faradaic efficiency and electrode fouling during iron electrocoagulation?, 117497, Copyright Elsevier (2021)

All other materials have not been published.

5.1 Chapter Introduction

Electrochemical water treatment technologies, such as electrocoagulation (EC), electrochemical oxidation, and electroflotation, have been growing in popularity owing to their ability to remove a wide variety of pollutants without the need for chemical addition [202,214]. Of these technologies, EC has been proposed as an alternative to the traditional chemical coagulation (CC), namely the process in which chemical coagulants such as alum or ferric chloride are added to destabilize and precipitate out contaminants [21,36,118,215]. EC has several advantages over CC, including little to no chemical addition, less sludge generation, improved coagulant mixing, and smaller space requirements [6,8–11]. In EC, coagulant is added via the application of electric current to metal electrodes to release metal ions into the surrounding water. The most common electrode materials for EC applications are iron and aluminum, which have been shown to effectively remove a wide variety of contaminants while being relatively low cost [8,21,55]. In iron-based EC (Fe-EC), iron ions are released into solution through the electrochemical production of Fe(II) at the

anode (reaction 1) [2,17]. These ions subsequently form various iron oxyhydroxides (reaction 2). Aluminum-based EC (Al-EC) functions similarly, with the Al(III) ions produced via electrochemical dissolution at the anode (reaction 3) undergoing hydrolysis to produce $Al(OH)_3$ precipitates (reaction 4) [107,166]. In addition to producing the precipitates necessary for contaminant removal, the hydrolysis reactions also produce H^+, resulting in an acidic environment in the vicinity of the anode. On the cathode side, the reduction of water produces OH^- (reaction 5), creating an alkaline region. These localized acidic and alkaline pH environments further promote the dissolution of aluminum electrodes, resulting in coagulant doses that are often higher than what would have been expected based on the faradaic law; this phenomenon is often referred to as super faradaic efficiency [107,114,115,166].

$$Fe \rightarrow Fe(II) + 2e- \quad (1)$$

$$4Fe(II) + O_2 + 10H_2O \rightarrow 4Fe(OH)_3 + 8H^+ \quad (2)$$

$$Al \rightarrow Al(III) + 3e- \quad (3)$$

$$Al(III) + 3H_2O \rightarrow Al(OH)_3 + 3\,H^+ \quad (4)$$

$$2H_2O + 2e^- \rightarrow 2OH^- + H_{2(g)} \quad (5)$$

One major problem in EC is the build-up of materials on the surface of the electrodes, a phenomenon that is often referred to as fouling [8,177]. While anodic fouling is caused primarily by the precipitation of metal hydroxides onto the surface of the electrode, cathodic fouling can be due to the precipitation of metal hydroxides as well as Ca- and Mg- containing minerals [177]. The precipitation of Ca- and Mg- containing minerals directly onto the cathode is attributable to the high pH at the cathode (reactions 6-8) [129,130].

$$Ca^{2+} + CO_3^{2-} \rightarrow CaCO_{3(s)} \quad (6)$$

$$(1\text{-}x)\ Ca^{2+} + x\ Mg^{2+} + CO_3^{2-} \rightarrow Ca_{1-x}Mg_xCO_{3(s)} \qquad (7)$$

$$Mg^{2+} + 2OH^- \rightarrow Mg(OH)_{2(s)} \qquad (8)$$

Fouling can negatively impact the long-term performance of EC by decreasing coagulant production, decreasing electrode gap, increasing energy consumption, and reducing contaminant removal efficiency[6,20–23,203]. Therefore, researchers have put significant efforts into finding techniques to prevent/mitigate fouling. One technique that has gained great deal of interest is polarity reversal (PR), which involves periodically switching the direction of the current such that the anode becomes the cathode and *vice versa* [9,17,68,74,84,153,177,201]. It has been hypothesized that as the current direction is switched, the removal of fouling layers will be promoted by various chemical/electrochemical processes, including 1) the production of hydrogen gas from water reduction, which can displace precipitates that are loosely bound to the electrode surface [9,216], 2) metal hydrolysis, which creates low pH environments around the electrode and facilitates the dissolution of Ca- and Mg- containing minerals, and 3) electrochemical dissolution of the underlying electrode, which can dislodge fouling layers accumulated on the surface [216]. Compared with other fouling removal techniques (e.g., mechanical/chemical cleaning, pre-treatment by ion exchange to remove Ca^{2+} and Mg^{2+}), PR is especially appealing because it allows for the removal of fouling to occur concurrently with the production of coagulant. PR also does not require chemical addition, reactor shutdown, or additional infrastructure (other than a current switch).

In Chapter 4, it was found that Fe-EC operated in the PR mode consumed more energy but generated less coagulant than the iron DC-EC counterpart. The fouling of the iron electrodes also was not reduced, which is contrary to what has been suggested in the literature. In contrast to Fe-EC, it was found that PR was beneficial to the performance of Al-EC because the coagulant production in aluminum PR-EC was comparable to that of aluminum DC-EC in all but one

experiment. Notably, aluminum PR-EC systems consumed less energy and did not suffer from electrode fouling to the same extent as aluminum DC-EC. As was noted in the Conclusions section of Chapter 4, all experiments employed one solution formulation (i.e., a synthetic groundwater formulation containing high concentrations of Ca^{2+} and Mg^{2+}). Since the nature of the fouling layer and the coagulant production efficiency are dependent on the solution composition (e.g., Cl^- can induce pitting corrosion and prevent passivation [17,134,135]; SO_4^{2-} and PO_4^{3-} can inhibit corrosion and increase overpotentials [17,135,136]; Ca^{2+}, Mg^{2+}, and dissolved silica can accelerate electrode fouling[19], additional research is needed to compare the performance of DC-EC and PR-EC under different solution chemistry.

To this end, the first objective of this study was to determine the impacts of water chemistry and PR frequency on the coagulant production in Fe-EC and Al-EC. As will be discussed in detail later in this chapter, it was found that Fe-EC suffered severe electrode fouling and low coagulant production efficiency under most conditions, especially when Fe-EC was employed for the treatment of oil sands in-situ synthetic produced water (SPW). This result suggests that even though Fe-EC can remove both silica and sulfide from produced water (as reported in Chapter 3), the treatment effectiveness would decrease over time. Therefore, the other objective of this study is to re-examine the efficacy of Al-EC to treat SPW, focusing specifically on the effects of PR on contaminant removal and the separation of precipitates post EC.

5.2 Materials and Methods

5.2.1 Materials

All chemicals were of reagent grade and were used without further purification. The electrodes were iron rods (4.8 mm diameter, 98%+ purity) and aluminum rods (d = 4.8 mm, 96%+ purity) obtained from Metal Supermarkets.

Four types of synthetic water samples were used to study the effect of solution chemistry on coagulant production:

- NaCl in deionized water
- Na_2SO_4 in deionized water
- Synthetic groundwater (SGW)
- Synthetic produced water (SPW), emulating the chemical profile of produced water associated with in-situ bitumen extraction

These solutions were chosen for their increasing complexity and varying effects on EC performance. For example, the SGW and SPW solutions contained buffers (e.g., HCO_3^-), which have previously been reported to affect EC performance by creating a passive layer at the electrode surfaces and thereby preventing the release of Fe(II/III) [17]. In the NaCl solution, the coagulant production is expected to be high because Cl^- can help dissolve the electrode surface layers and facilitate pitting [137]. In contrast, SO_4^{2-} has been shown to promote iron and aluminum passivation [17]. In the SGW and SPW solutions, Ca^{2+} and Mg^{2+} are expected to contribute to the fouling of the cathode in DC-EC [72], and on both electrodes in PR-EC (Chapter 4). Lastly, the SPW contains HS^-, which can be electrochemically oxidized into elemental sulfur (S^0), and/or can react with Fe^{2+} to generate sparingly soluble iron sulfide minerals (FeS) (Chapter 3).

The ionic compositions of the tested solutions are presented in Table 5-1. Characteristics of test solutions[1]. The chemicals used to prepare the solutions were Na_2SiO_3 (or $Na_2SiO_3 \cdot 9H_2O$), $NaHS \cdot H_2O$, $MgCl_2$ (or $MgCl_2 \cdot 6H_2O$), $CaCl_2$, Na_2SO_4, $NaHCO_3$, $NaNO_3$, $Na_3PO_4 \cdot H_2O$ (or $Na_3PO_4 \cdot 12H_2O$), and NaCl. The pH of the solutions was adjusted to their initial pH using 1 M HCl. All solutions were prepared using 18.2 MΩ·cm water.

Table 5-1. Characteristics of test solutions[1]

	NaCl	**Na_2SO_4**	**SGW[2]**	**SPW[3]**
Cl^-	758		68	1,945
NO_3^- (as N)			5.3	
HCO_3^-			430	1,700
SO_4^{2-}		676	220	40
Phosphate (as P)			0.25	
Silica (as Si)			12.6	58
Na^+	492	324	305	1,900
Mg^{2+}			14	20
Ca^{2+}			110	65
HS^-				110
pH	7	7	7.3-7.4	7.6-7.8
Conductivity (mS/cm)	2.46	1.60	1.89	8.22

1. *Concentration of solutes are presented in mg/L*
2. *Pan C, Troyer LD, Catalano JG, Giammar DE. Dynamics of chromium(VI)removal from drinking water by iron electrocoagulation. Environ Sci Technol. 2016;50(24):13502-13510. doi:10.1021/acs.est.6b03637* [3]
3. *Chapter 3 SPW formulation*

5.2.2 Continuous Flow-Through Experiments

The effects of PR frequency (f) and water chemistry on coagulant production were examined using the continuous flow-through reactor (V = 200 mL) similar to that described in Chapter 4 (Figure 4-1). The reaction solution was supplied to the reactor by a peristaltic pump at a flow rate of 10 mL min^{-1}, resulting in a retention time of 20 min. Within the reactor, the solution was continuously mixed by a magnetic stir bar. The reactor was covered with a lid with three openings, two that held iron and aluminum rods and one for solution sampling. The rods were spaced 2 cm apart, and were submerged to a depth of 6 cm, resulting in an active surface area of 7.6 cm^2 ± 0.1 cm. Before each experiment, the electrodes were sonicated in 1 M HCl, polished with sandpaper, and rinsed with deionized water.

The reactor was controlled by a potentiostat (VSP, Bio-logic Science Instruments), which applied a constant current of I = 0.1 A (j = 13 mA cm^{-2}). Experiments were conducted either in the DC mode, or in the PR mode with f = 0.5, 1 or 2 min. At t = 3 and 6 h, liquid samples were withdrawn from the reactor, and were digested in a solution consisting of 3 wt. % HNO_3 and 3 wt. % HCl. Subsequently, the digested solution was subjected to inductively coupled plasma-optical emission spectroscopy (ICP-OES) analysis. To examine the electrode surface morphology and elemental composition, the electrodes were removed from the reactor at the end of the experiments, air dried, and analyzed using an FEI Quanta FEG 250 Environmental Scanning Microscope (ESEM) that was coupled with an Inca energy dispersive X-ray (EDX) spectrometer.

5.2.3 Batch Experiments with Synthetic Produced Water

The treatment of SPW by Al-EC operated under DC and PR was further investigated. In these experiments, a taller (30 cm) reactor was employed to allow sufficient distance for the precipitates to settle, in order to examine the effects of DC and PR on the settling of the precipitates

post EC. The reactor, which was operated in the batch mode, consisted of 1.9 L of SPW solution that was constantly stirred by a magnetic stir bar. The cell was covered with a lid that has two openings, which held two aluminum electrodes, and openings for sampling. The aluminum rods were spaced 2 cm apart, and were submerged to a depth of 11 cm, resulting in an active surface area of approximately 17.5 cm^2 ± 0.1 cm (Figure 5-1).

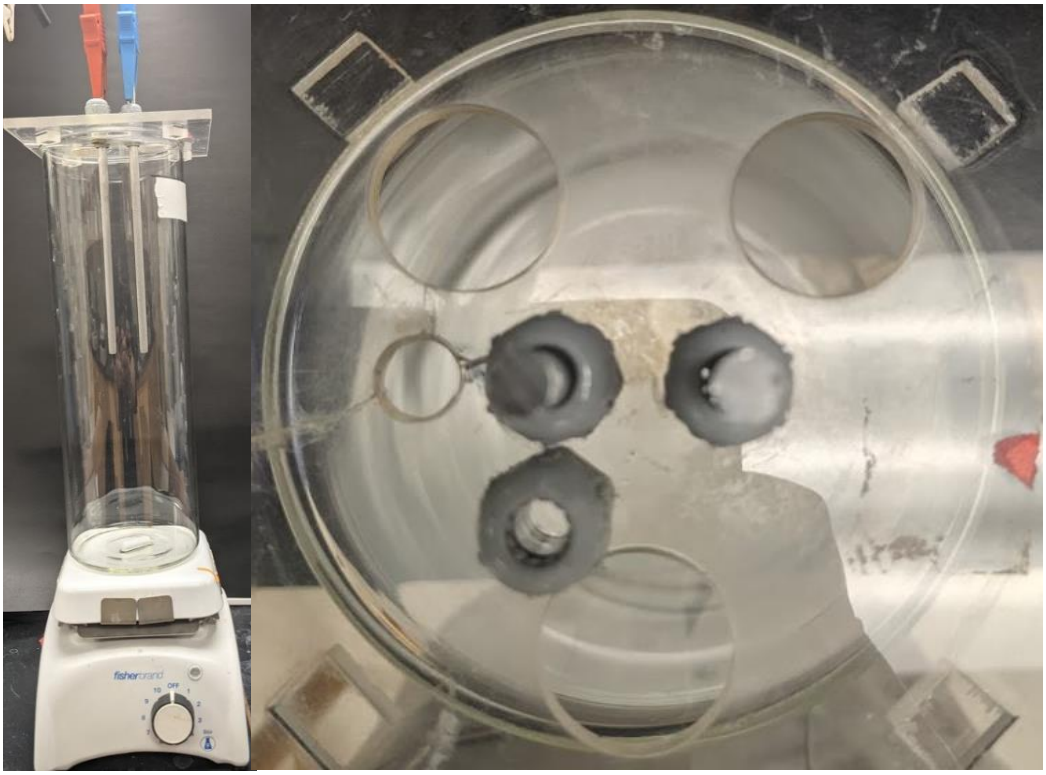

Figure 5-1. Electrochemical cell used for batch EC experiments

Current was supplied to the system galvanostatically (i = 5.7 mA cm^{-2}) for a total of 1.5 hrs. Experiments were conducted either in the DC mode, or in the PR mode with f = 10 or 0.5 min. At pre-determined time intervals, 20 mL of solution was removed from the reactor. Of this 20 mL, 5 mL was digested in a solution consisting of 3 wt. % HNO_3 and 3 wt. % HCl, and the digested solution was then subjected to ICP-OES analysis to measure Al. The remaining 15 mL was filtered

through a 0.2-μm nylon filter. Subsequently, the filtered solution was subjected to ICP-OES analysis to measure Si, Ca, Mg and Al.

To characterize the precipitates produced in these experiments, the treated solution was subsampled and deposited on a transmission electron microscopy (TEM) grid, blotted with a kimwipes paper, allowed to dry at room temperature, and subjected to TEM analysis. In addition, the treated solution was filtered through a filter paper (pore size of 10 μm, active filter area of 10.2 cm^2) using a vacuum pump (pressure = -0.8 bar). The solids collected on the filter were allowed to air dry and were subsequently characterized by X-ray diffraction (XRD) and SEM to examine crystal structure, surface morphology, and elemental composition. The surface area of the precipitates was also measured by the Brunauer–Emmett–Teller (BET) N_2 physisorption method. Lastly, during the collection of the precipitates by filtration, the time needed to filter the solution was recorded, which was used to calculate filtration flux (mL/cm^2s).

Due to the sample preparation requirements, the characterization methods described above are prone to artifacts. For example, it is not possible to capture the particles' aggregation structure by SEM and TEM since the samples were dried prior to analysis. As such, liquid samples were also taken directly from the solution and examined with a Zeiss Axioskop II light microscope to investigate the floc structure.

At the end of the experiments (i.e., at t = 1.5 hrs), the potentiostat and the magnetic stirrer were turned off and the precipitates were allowed to settle. At predetermined time intervals, a 15-mL aliquot was taken at a height of 13 cm from the bottom of the reactor and was analyzed on a HACH portable turbidity meter. All data presented were for experiments conducted in triplicate with averages and standard deviations presented.

5.2.4 Faradaic Efficiency

The applied current governs the electrochemical reaction rates at the electrodes. Therefore, the amount of anodic metal dissolution can be predicted by Faraday's Law (Equation 3):

$$\text{Theoretical mass of coagulant metal dissolved} = \frac{ItM}{zF}$$

where I (A) is current, t (s) is electrolysis time, M is the atomic mass of the metal (M = 55.485 g mol^{-1} for Fe), z is electron transfer number (z = 2 for Fe, z = 3 for Al), and F is Faraday's constant (96,485 C mol^{-1}). In this study, the faradaic efficiency (ϕ) was calculated as the ratio of the measured to the theoretically predicted (electrochemical produced by Faraday's law) (from Equation 4) mass of coagulant dissolved:

$$\text{Faradaic efficiency } (\phi) = \frac{\text{Observed Coagulant}}{\text{Theoretical Coagulant}} = \frac{zFm}{ItM}$$

where m (g) is the experimentally measured mass of iron or aluminum released into the bulk solution.

5.2.5 Statistical Analysis

To determine if the difference in coagulant production, contaminant removal, turbidity, and filtering flux between PR and DC operation were statistically significant, a two tailed student's t-test for samples with equal variances was performed. This test was performed for a significance level of 5%. The degrees of freedom, variance, and the t value were calculated using equations 5, 6, and 7.

$$\sigma^2 = \frac{\sum_{i=1}^{n}(x_i-\mu)^2}{n-1}$$

Equation 5 Variance

$$df = \frac{\left(\frac{{\sigma_1}^2}{n_1} + \frac{{\sigma_2}^2}{n_2}\right)^2}{\frac{1}{n_1 - 1}\left(\frac{\sigma_1^2}{n_1}\right) + \frac{1}{n_2 - 1}\left(\frac{\sigma_2^2}{n_2}\right)}$$

Equation 6. Degrees of Freedom

$$t = \frac{\bar{x}_1 - \bar{x}_2}{\sqrt{\frac{\sigma_1^2}{n_1} + \frac{\sigma_2^2}{n_2}}}$$

Equation 7 t-Value

The null hypothesis (H_0) tested is: $\mu_1 = \mu_2$ and the alternative hypothesis (H_a) is: $\mu_1 \neq \mu_2$, where μ_1 and μ_2 are the means of the two experimental points. Relevant statistical parameters are reported in Appendix I: Statistics.

5.3 Results and Discussion

5.3.1 The PR Fe-EC System

In the continuous-flow system, ϕ in PR-EC were always lower than those in DC-EC (Figure 5-2). Notably, ϕ progressively decreased as *f* decreased from 2 min to 0.5 min. The extent to which *f* influenced ϕ was dependent on the solution chemistry. For example, the lowest ϕ observed with the NaCl solution was 80%, while the lowest ϕ in other solutions ranged between 5 and 50%. In the PR-EC experiments with SPW, ϕ was < 20% at all *f*.

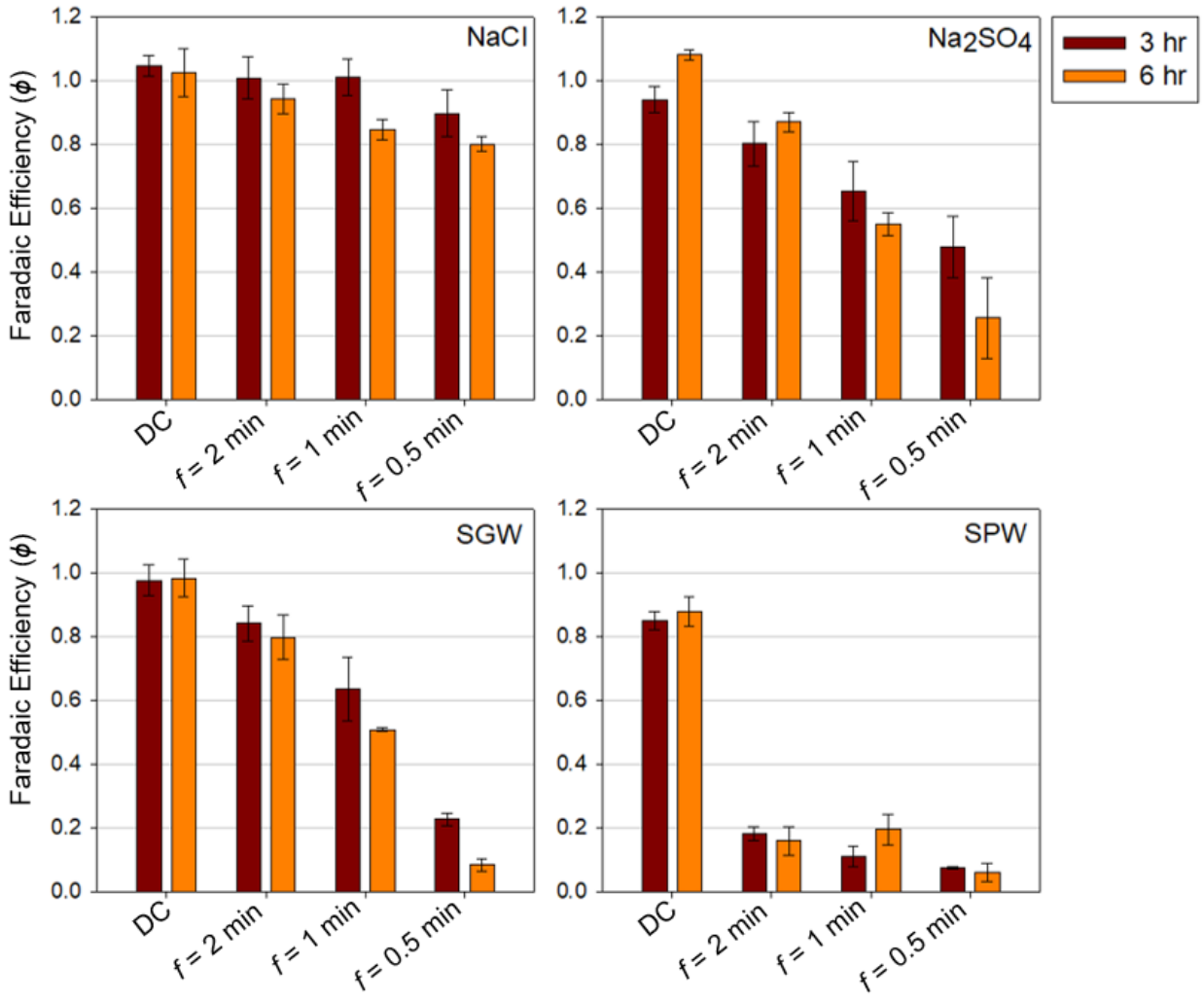

Figure 5-2. The effects of PR f and water chemistry on ϕ in Fe-EC. Experiments were conducted in triplicate with averages and standard deviations presented.

Possible explanations for the diminished ϕ in PR-EC include (1) Fe ions precipitated on the electrode surfaces instead of migrating into the bulk solution, and (2) there are electrochemical side reactions that diverted the current away from reaction 1. The first hypothesis is supported by the visual observation that more materials accumulated on the electrodes in PR-EC than in DC-EC, especially in experiments with f = 0.5 min. Notably, the electrodes quickly turned black in the experiments with SPW — this is attributable to the reaction between Fe(II) and HS^-, which produced sparingly soluble FeS minerals (Chapter 3). This reaction is known to be much faster than the hydrolysis and oxidation of Fe(II) [217]:

$$Fe^{2+} + HS^- \rightarrow FeS + H^+ \qquad (9)$$

The presence of FeS on the electrode surface is corroborated by a clear signal of S in the EDS spectrum (Figure 5-3).

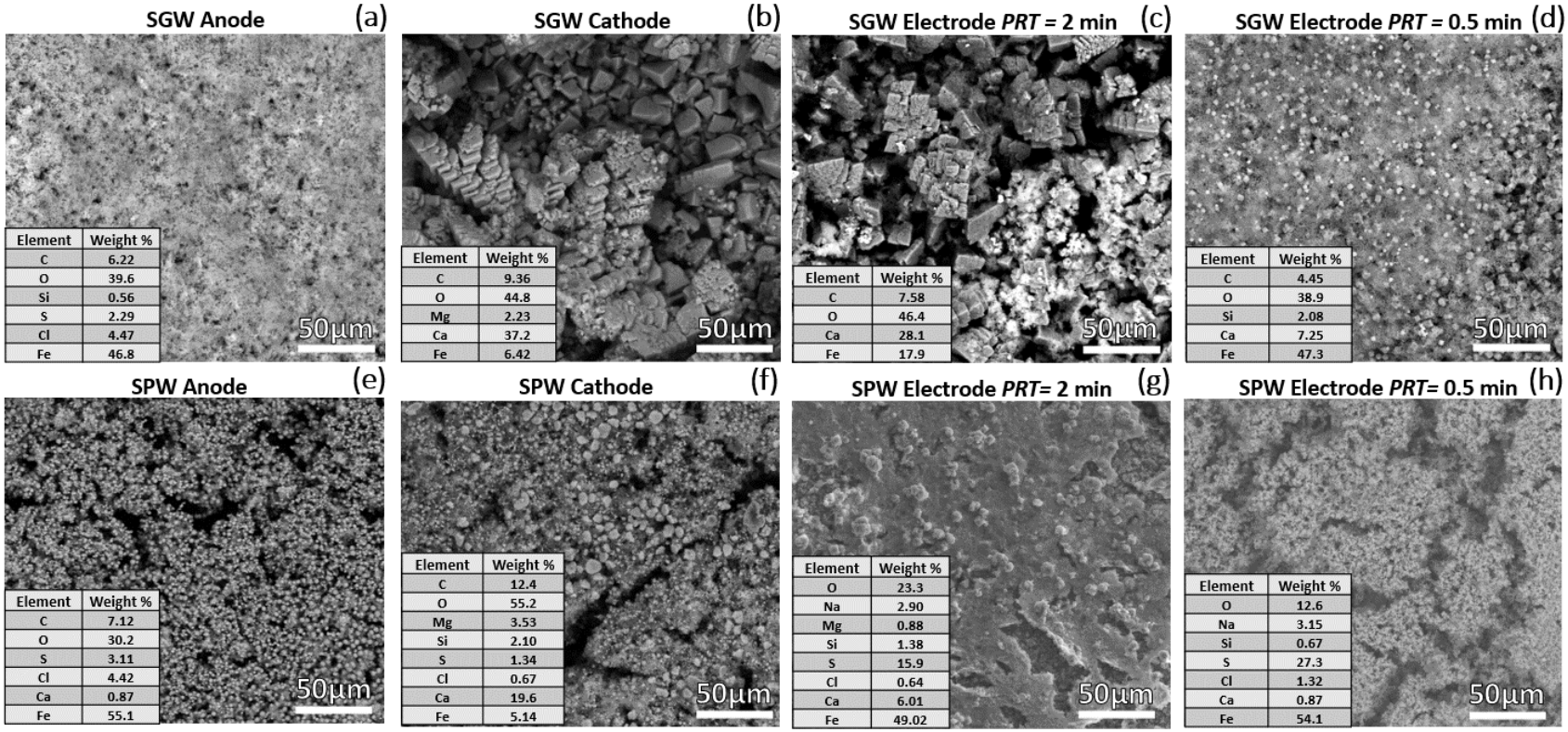

Figure 5-3. SEM images of the Fe electrodes after 6 hours.

(a) and (b): The anode and cathode in the DC-EC experiment that employed synthetic groundwater (SGW)

(c) and (d): The electrode in the PR-EC experiments that employed SGW

(e) and (f): The anode and cathode in the DC-EC experiment that employed synthetic produced water (SPW)

(g) and (h): The electrode in the PR-EC experiments that employed SPW.

Note that there is no dedicated cathode and anode in PR-EC because the current was intermittently reversed.

The build-up of Fe in the fouling layer in the SPW and SGW experiments could also have been caused by Ca- and Mg-containing minerals, which covered the surface of the electrodes (Figure 5-3) and trapped more Fe in the fouling layer [22]. Ca- and Mg-containing minerals, such as $CaCO_3$, $Mg(OH)_2$, and $CaMg(CO_3)_2$, can precipitate under alkaline conditions developed in the boundary layer of the cathode [129,130]. Because both electrodes in PR-EC intermittently served as the cathode as the polarity alternated, Ca- and Mg-containing minerals were seen to be present on both electrodes (Figure 5-3).

Regarding the second hypothesis, side reactions that could have occurred include the electrochemical oxidation of H_2O to $O_{2(g)}$, and HS^- to S^0. As reported in Chapter 3, the electrochemical oxidation of HS^- to S^0 was observed when SPW was treated by Fe-EC operated in the DC mode. In the PR-EC/Na_2SO_4 system, gas evolution was observed on both electrodes, suggesting that the oxidation of H_2O was occurring (reaction 10). Dubrawski et al also attributed the low ϕ in their Fe-EC experiment to the oxidation of H_2O, which was triggered by the passivation of the electrodes by SO_4^{2-} [96]:

$$2H_2O \rightarrow O_2 + 4H^+ + 4e^- \qquad (10)$$

The higher ϕ and lower electrode fouling layers observed in the experiments with the NaCl solution is attributable to the ability of Cl^- to inhibit electrode passivation via pitting corrosion [137]. (Although SGW and SPW also contained Cl^-, the depassivation effect of Cl^- must have been outcompeted by ions that can inhibit corrosion (i.e., SO_4^{2-}, NO_3^-, silicate and phosphate). SGW and SPW also contained Ca^{2+} and Mg^{2+}, which can further foul the electrode surfaces via the mechanism discussed above.

5.3.2 The PR Al-EC System

Sulfate ions are known to passivate Al electrodes [107,112,139]. Presumably due to this passivation effect, a voltage surge occurred almost immediately after the Al-EC experiments with the Na_2SO_4 solution started, resulting in the shut down of the potentiostat. As such, only data from the experiments with the three other solutions could be collected (Figure 5-4).

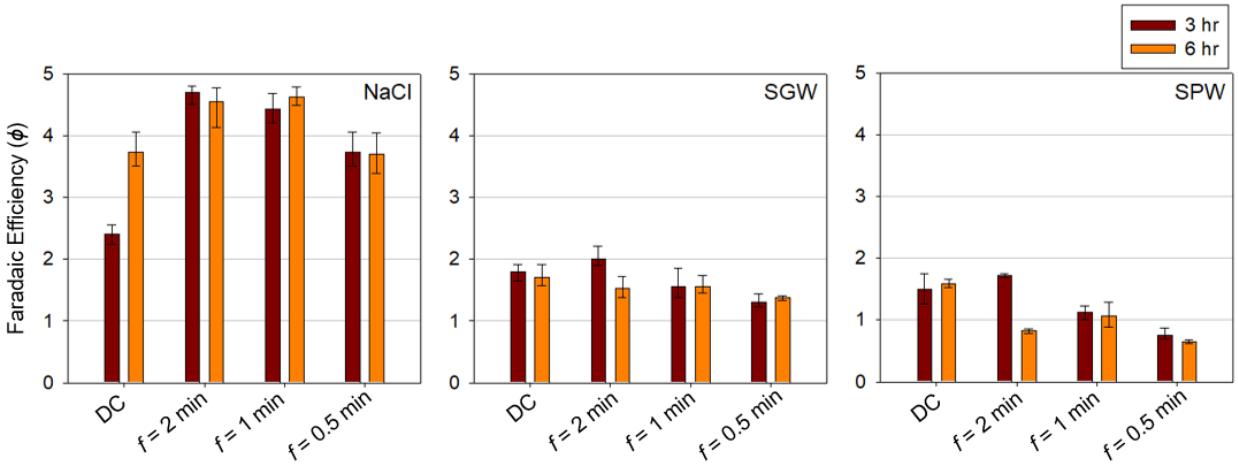

Figure 5-4. The effect of PR f and solution chemistry on ϕ in Al-EC. Experiments were conducted in triplicate with averages and standard deviations presented.

Contrary to the results in the Fe-EC system (Figure 5-2), there was no clear trend between ϕ and PR *f* in the Al-EC system (Figure 5-4). Compared to DC-EC, the application of PR resulted in an increase in ϕ in the NaCl experiments, no effect on ϕ in the SGW experiments, and a decrease in ϕ in the SPW experiments. As in the Fe-EC system, the high coagulant production in the NaCl experiments was likely the result of pitting corrosion facilitated by Cl^- ions [90,218,219]. While SGW also contained Cl^-, the depassivation effect of Cl^- is hypothesized to be counteracted by SO_4^{2-}, Ca^{2+}, Mg^{2+}, and phosphate, which passivated the electrodes (Figure 5-5). Lastly, the decreased in ϕ in the SPW solution is hypothesized to be caused by sulfide. As reported in Chapter 3, sulfide ions can be electrochemically oxidized into S^0 during Al-EC.

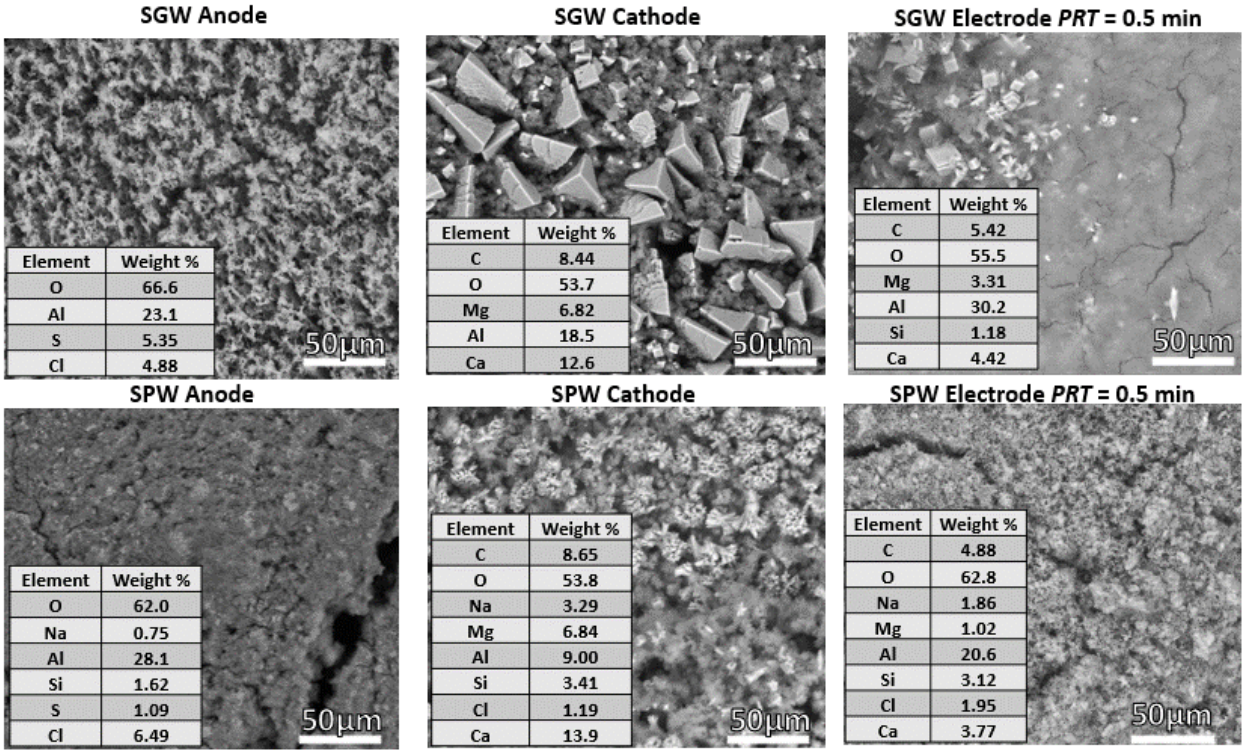

Figure 5-5. Figure 5 5. SEM images of the Al electrodes after 6 hours in SGW and SPW.

5.3.3 The Treatment of SPW by PR-EC

Based on the results presented above, along with the results reported in Chapter 3, the following conclusions can be deduced about the treatment of SPW by EC. First, while Fe-EC is effective at removing sulfide, the reaction between Fe(II) and sulfide in the electrode boundary layer could result in severe electrode fouling. Second, the mitigation of electrode fouling in the Fe-EC/SPW system by PR does not appear to be a promising strategy, as the application of PR resulted in a very low ϕ. A low ϕ is detrimental not only to the removal of silica, but also to the removal of sulfide. In contrast, while Al-EC is not as effective as Fe-EC at removing sulfide, Al-EC may be a more effective option for the treatment of oil sands in-situ produced water, because Al electrodes will not be fouled rapidly by sulfide (since aluminum ions do not react directly with

sulfide). Additionally, if Al electrodes are fouled by $Al(OH)_3$ and hardness, PR could potentially be used to remove fouling layers without significantly compromising coagulant production.

Since maintaining a high coagulant production is paramount to the removal of silica (i.e., the main target contaminant in the oil sands in-situ produced water), Al-EC was deemed more promising for the treatment oil sands in-situ produced water. Therefore, the subsequent sections discuss the effect of PR on 1) the removal of silica, calcium, and magnesium in SPW by Al-EC, 2) precipitate separation post EC treatment, and 3) precipitate characteristics.

Contaminant removal. As presented in Figure 5-6 A and B, silica removal was proportional to the coagulant production. The lowest amount of coagulant production and silica removal were observed in the PR f = 0.5 min system. In contrast, coagulant production and silica removal were comparable in the DC-EC and the PR f = 10 min systems. These results are consistent with those reported in previous studies, which showed that silica was removed in Al-EC via adsorption onto $Al(OH)_3$ [14,15,28].

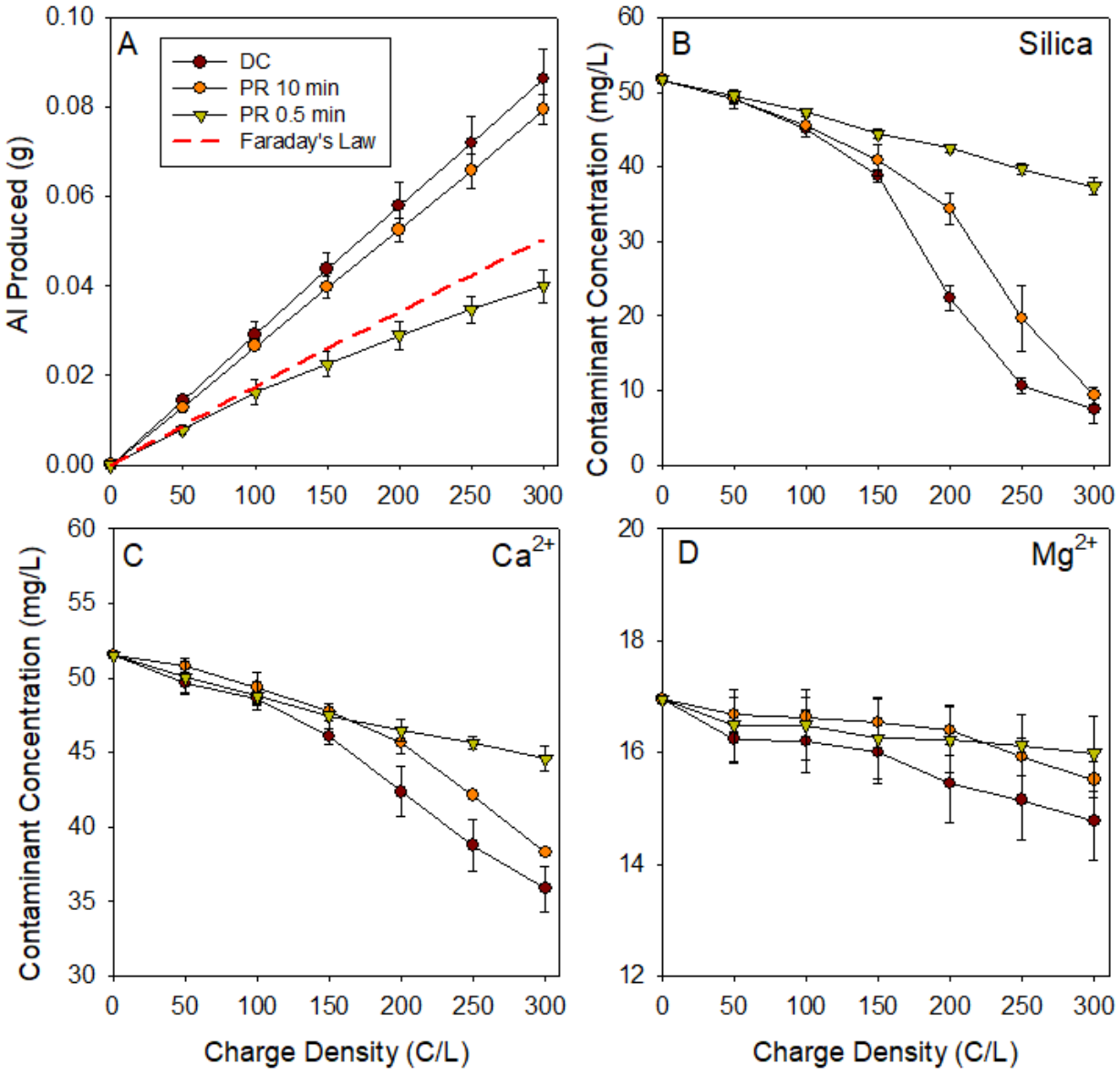

Figure 5-6. (A) The mass f aluminum removed and (B-D) contaminant removal profiles for (B) silica, (C) calcium, and (D) magnesium vs. charge density. Experiments were conducted in SPW employing a current density of j = 5.7 mA/cm^2. Experiments were conducted in triplicates, and average values along with one standard deviation (i.e., error bar) are presented.

The removals of calcium and magnesium were also affected by the application of PR. While 30% of calcium was removed in DC-EC, the removal efficiency decreased to 26% and 11% in PR *f* = 10 min and PR *f* = 0.5 min, respectively (Figure 5-6 C). (The removals of calcium in DC-EC (i.e., 30%) and PR *f* = 10 min (i.e., 26%) were statistically different). In the case of magnesium,

the removals were 13%, 8.8%, and 6% in DC-EC, PR f = 10 min, and PR f = 0.5 min, respectively (Figure 5-6 D), although the removals were not statistically different. Since calcium and magnesium are mainly removed from the solution via reactions 6 – 8, the difference between the removals in DC-EC and PR-EC can be explained as follows. In DC-EC, a high pH region conducive to reactions 6 – 8 is developed around the cathode [14,86,220,221]. In contrast, the constant production of OH^- and H^+ at each electrode as the current direction was switched in PR would result in the more neutral pH environment in the electrode boundary layer (i.e., a condition that is less favorable for reactions 6 – 8). When PR f = 0.5 min was employed, the rapid current cycling would have created the most neutral pH environment surrounding each electrode, resulting in the lowest removal efficiency.

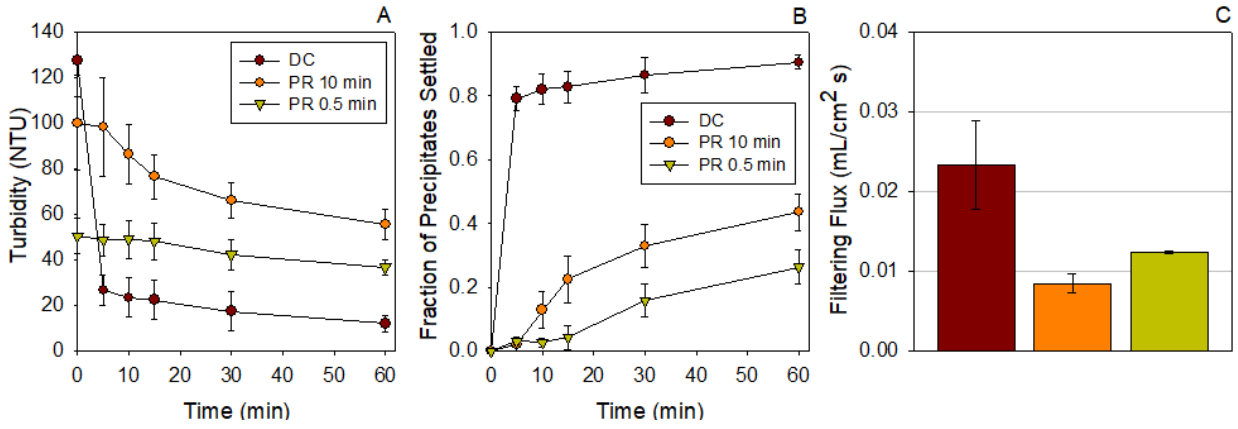

Figure 5-7. Solids separation post Al-EC via settling, measured by turbidity, and filtration

Precipitate separation by settling and vacuum filtration. The precipitates produced with PR f = 0.5 min settled at the slowest rate (Figure 5-7 A and B). This could be partly due to the lowest coagulant amount produced in this experiment (Figure 5-6 A) — a low coagulant dose would result in a low particle collision frequency and, thus, slower aggregation and settling rates. However, the settling rates in the DC and PR f = 10 min were drastically different, even though the amounts of coagulant produced in these experiments were comparable (Figure 5-6 A and Figure 5-7 A).

Therefore, it is hypothesized that the particles produced under DC and PR may have different physical/chemical properties. This hypothesis is supported by three lines of evidence. *First*, the BET surface areas of the precipitates produced in the PR experiments were higher that those produced in the DC experiment (Table 5-2). Between the PR f = 10 min and f = 0.5 min experiments, the precipitates produced in the latter experiment possessed a higher surface area per mass. *Second*, when the treated solutions were filtered through a quantitative filter paper, the filtration flux was the lowest in the solution treated under PR f = 0.5 min (Figure 5-7 C). This

result suggests that the filter was clogged to the greatest extent during the filtration of this solution, even though the amount of coagulant produced in the PR f = 0.5 min experiment was the lowest (Figure 5-6 A). *Third*, the precipitates collected on the filter were visually different: while the precipitates produced in the DC experiment were white, those that were produced in the PR experiments were grey (Figure 5-8).

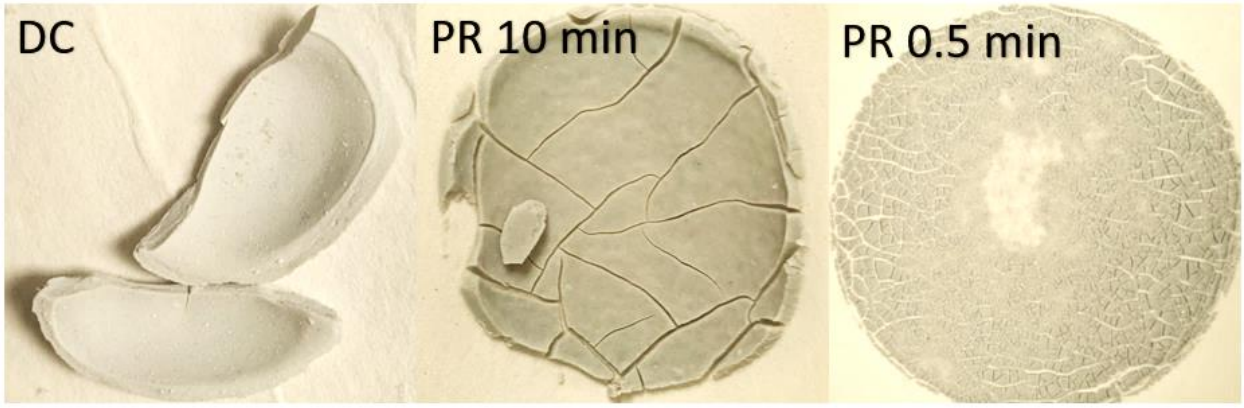

Figure 5-8. The effect of PR on precipitate colour in SPW

Table 5-2. BET surface area of the aluminum precipitates produced in the experiments with SPW

	Surface Area (m^2/g)
DC	149.6
PR f = 10 min	281.7
PR f = 0.5 min	319.8

Precipitate characteristics. The discussion presented above supports the hypothesis that PR changes the characteristics of the precipitates produced. To gain further insights into their physical/chemical properties, the precipitates were further characterized by XRD, TEM, SEM, and light microscopy. Somewhat surprisingly, these characterization methods reveal little if any differences among the precipitates. Specifically, the surface of the precipitates produced in the DC experiment appeared to be smoother than the surface of those produced in the PR experiments (Figure 5-9), although the difference is relatively subtle. In contrast, XRD spectra (Figure 5-10) and TEM images (Figure 5-11) suggest that all precipitates were amorphous in nature and were flocs of 10 – 20 nm particles. However, it is noted that the aggregation of particles could have changed during the drying process required for sample prep for TEM analysis. Therefore, a light microscope was employed to further examined the floc structure in liquid aliquots subsampled from the solution. The light microscope images (Figure 5-12) reveal that the particles produced in the DC experiment aggregated into much larger flocs compared to those produced in the PR experiments.

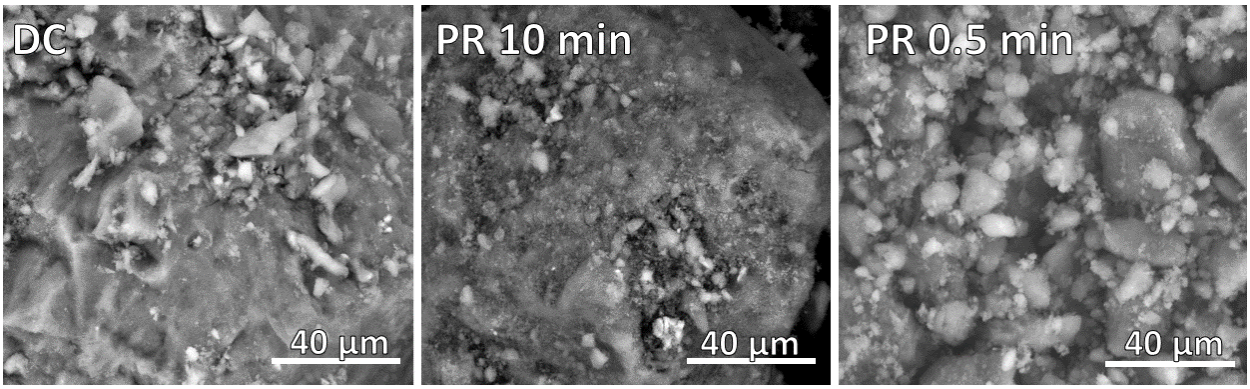

Figure 5-9. SEM images of the aluminum precipitates produced in SPW with DC and PR operation.

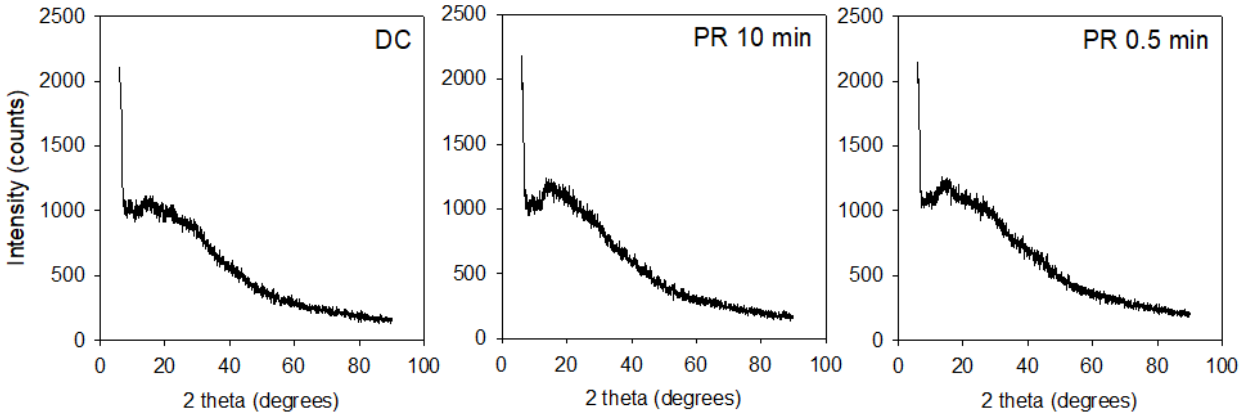

Figure 5-10. XRD spectrum of the aluminum precipitates produced in SPW with DC and PR operation.

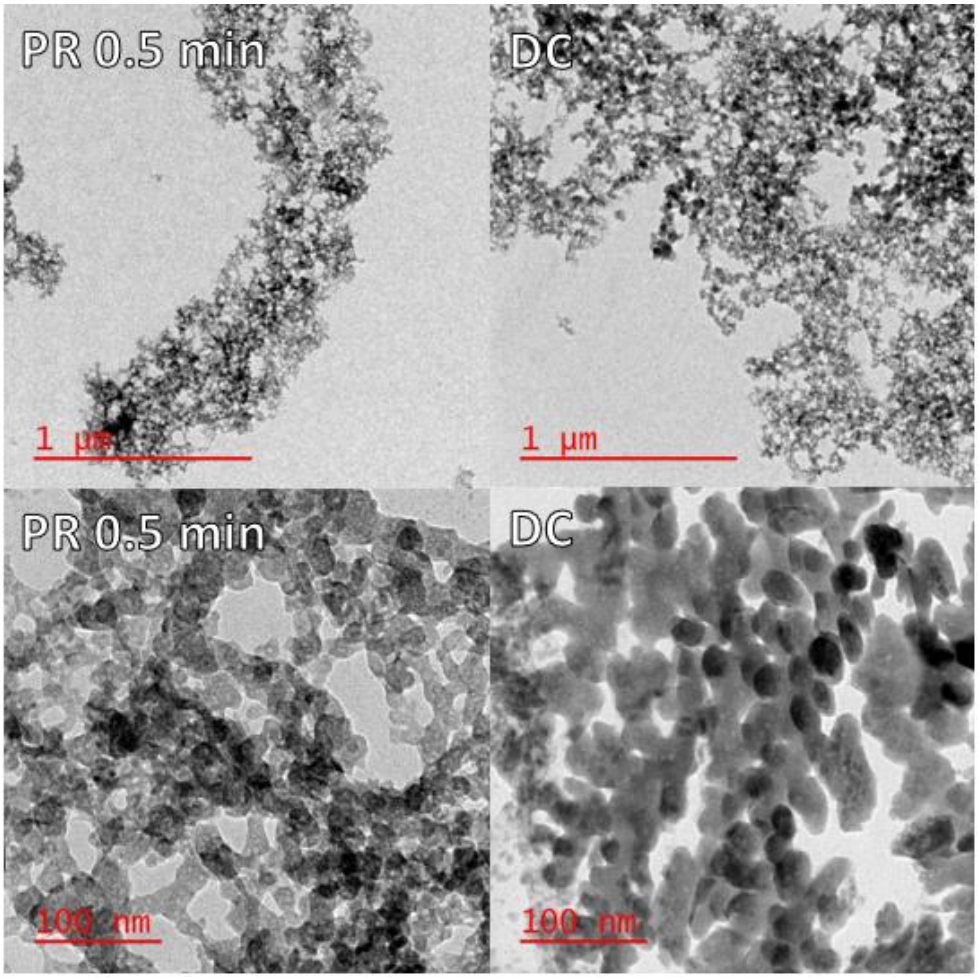

Figure 5-11. TEM images of the aluminum precipitates produced in SPW with DC and PR operation

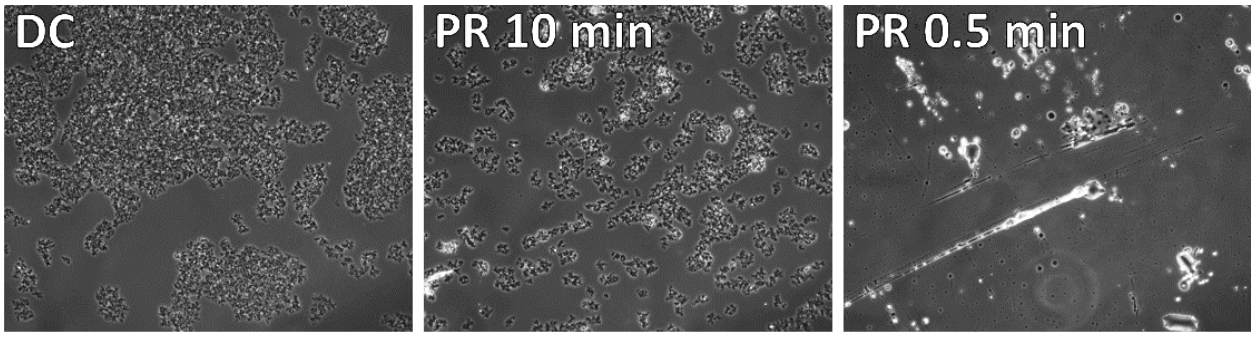

Figure 5-12. Light microscope images of the aluminum precipitates produced in SPW with DC and PR operation with a magnification of 100x

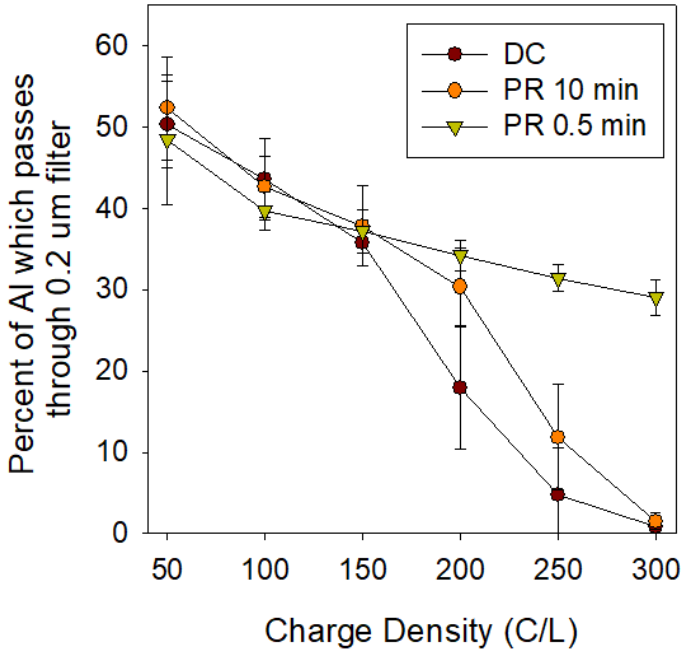

Figure 5-13. Percent of aluminum precipitates, generated in SPW, which passed through a 0.2 μm filter with DC and PR operation.

Besides potential artifacts resulted from sample drying, another potential pitfall of the XRD and SEM analyses could be that the precipitates were collected using a 10-μm filter. As such, these analyses may not have captured particles/aggregates smaller than 10 μm not retained by the filter. Thus, another set of experiments was conducted wherein the treated solutions were fractionated using a 0.2-μm nylon filter. It was observed that the fraction of aluminum that passed through the 0.2-μm filter in the PR f = 0.5 min experiment varied between 30 – 50% throughout the course of

the experiment (Figure 5-13). In comparison, these fractions in the DC and PR f = 10 min experiments decreased from 50% to less than 2%. These results suggest that the particles/flocs produced in the PR f = 0.5 min were smaller than those produced in the other two experiments.

Collectively, the characterization results presented above suggest that while the precipitates produced in all experiments were amorphous in nature, those produced in PR-EC were smaller in size and possessed higher surface area per mass than those produced in DC-EC. The effect of PR on the physical characteristics of the precipitates is hypothesized to be as follows. When EC is operated in the DC mode, an acidic and a basic pH zone are formed around the anode and cathode, respectively. Under either acidic or basic conditions, a high proportion of aluminum released from the electrodes would remain in the dissolved form within the electrode boundary layers. Once the dissolved aluminum migrates from the boundary layers to the bulk solution (i.e., where the pH is more neutral), the precipitation of $Al(OH)_3$ would occur. This two-stage process would create "reaction limited aggregation" conditions, resulting in more dense flocs that would grow and settle more readily. Conversely, the aluminum ions produced in the PR experiments would precipitate within the electrode boundary layers where the pH is more neutral. The simultaneous dissolution of Al from the electrodes and precipitation of $Al(OH)_3$ would create a "diffusion limited aggregation" condition, resulting in the formation of smaller particles as well as looser and more fragile flocs that settle at a slower rate. Due to the alternating production of H^+ and OH^- at both electrodes, the pH of the boundary layers in PR f = 0.5 min are expected to be the most neutral. Thus, the precipitates/flocs formed in this experiment were smallest and settled at the slowest rate.

Generally, smaller particles have higher surface area per mass, which is consistent with the BET results (Table 5-2).

Overall, the results presented above suggest that a low PR *f* (i.e., 0.5 min in this study) would result in decreased coagulant production (hence, decreased silica removal efficiency), decreased calcium and magnesium removal, and smaller precipitates that are more challenging to separate. Therefore, PR *f* should be optimized to minimize electrode fouling while not compromising contaminant removal and particle separation post EC.

5.4 Chapter Conclusions

This study explored the effect of water chemistry and PR on EC's key performance parameters, including coagulant production, contaminant removal, and precipitate separation. It was found that the application of PR in Fe-EC resulted in a decreased coagulant production under all solution chemistry conditions. In general, the coagulant production decreased as PR frequency increased. Notably, the coagulant production ranged between 10 – 20% in the experiments with produced water. This result suggests that while Fe-EC is capable of removing both silica and sulfide from produced water, the removal efficiency would decrease over time. In comparison, ϕ was above 100% (i.e., super faradaic efficiency) in most Al-EC experiments. Given that maintaining a high coagulant production is paramount to the removal of silica (i.e., the main target contaminant in the oil sands in-situ produced water), Al-EC was deemed more promising for the treatment oil sands in-situ produced water. While operating Al-EC under PR can mitigate electrode fouling, the use of high PR frequency should be avoided, as this would result in decreased coagulant production (hence, decreased silica removal), decreased calcium and magnesium removal, and smaller precipitates that would be more challenging to separate post EC treatment.

Chapter 6

Conclusions

6.1 Summary of Results

This research aimed to investigate some of the major barriers that hamper the adoption of EC. Investigating these barriers, and the underlying fundamental mechanisms which control the processes in EC, will facilitate the use of EC as a water treatment technology. The two questions this research aimed to answer were: (1) Can EC effectively treat heavily contaminated wastewater streams consisting of different types of contaminants? and (2) How can electrode fouling in EC be mitigated without disrupting the treatment process? To answer these questions, this thesis was divided into three main objectives, 1) gain insights into the removal of multiple contaminants from PW, 2) determine how PR affects electrode fouling and coagulant production, and 3) investigate the effect of solution chemistry in conjunction with PR on coagulant production, contaminant removal, and precipitate characteristics.

Under Objective 1, several insights were gained into the effectiveness of Al- and Fe-EC for the treatment of PW. Firstly, it was determined that both Al and Fe-EC could remove silica, which is the primary contaminant in PW. Secondly, the removal of sulfide in Fe-EC was found to be the result of iron sulfide formation and, since this was the dominant iron precipitate in solution, the removal of silica was attributed to adsorption onto iron sulfides. While the removal of silica by EC has been investigated by other researchers, this research was the first to show its removal by adsorption onto iron sulfides. In contrast, the removal of silica in Al-EC occurred via adsorption onto aluminum hydroxides, while the removal of sulfide was due to stripping and electrochemical oxidation. Since the removal of sulfide via the formation of FeS in Fe-EC was much greater than

that by stripping and electrochemical oxidation in Al-EC, sulfide removal may be an important advantage of Fe-EC over Al-EC. Additionally Ca and Mg removal was observed in the organic-free SPW solution in both systems but was hampered by the presence of organics in the authentic PW. Experiments conducted in the Fe-EC system also revealed that contaminant removal in this system was controlled by charge density (i.e., coagulant dosing) but not current density (i.e., the rate of dosing). While this portion of the research suggests that EC may be an effective treatment technology for the removal of silica from PW, further work into the issue of electrode fouling still needed to be investigated.

Under Objective 2, it was found that during the treatment of SGW with DC Fe-EC and Al-EC, the electrodes were fouled by metal oxyhydroxides (on the anode), and calcium and magnesium minerals (on the cathode.) When PR was applied at low *f* to remove fouling, calcium and magnesium minerals were removed from the surface of the electrodes in Al-EC but not Fe-EC. In an attempt to eliminate the calcium and magnesium minerals, a higher *f* PR was employed. However, high *f* PR not only was unable to entirely eliminate fouling but also resulted in higher metal oxyhydroxide accumulation on both electrodes, both in Al-EC and Fe-EC. Moreover, PR also negatively impacted coagulant production in Fe-EC, with less coagulant production observed with increased PR *f*.

Building upon the investigation with SGW, the research expanded into examining the effect of PR on coagulant production in NaCl, Na_2SO_4, and SPW solutions (Objective 3). As in the SGW case, PR was detrimental to ϕ in Fe-EC in these solutions, with ϕ being inversely proportional to PR frequency. Contrary to in the Fe-EC system, the application of PR had no consistent effect on ϕ in Al-EC: ϕ increased in the NaCl solution, remained unchanged in SGW, and slightly decreased

in SPW. These results demonstrated the importance of testing different operating conditions and electrode materials for the specific treatment application.

Due to the lower ϕ observed in Fe-EC with PR operation, it was determined that if fouling control by PR is necessary, Al-EC may be a more appropriate electrode material. In particular, high ϕ is important for the treatment of PW by EC, since the removal of silica (and sulfide in Fe-EC) is dependent on coagulant dose. Therefore, the effect of PR on precipitate characteristics and contaminant removal in SPW was further investigated with Al-EC. In this research portion, it was observed that the flocs produced under PR were smaller and settled at a slower rate. Furthermore, the application of PR at high *f* resulted in decreased removal of silica, calcium and magnesium. The less effective contaminant removal was attributable to the decreased coagulant production and the more neutral pH condition within the electrode boundary layers, which is less conducive to the precipitation of calcium and magnesium minerals. Overall, this portion of the research demonstrated that PR impacts not only coagulant production and electrode fouling but also contaminant removal as well as the separation of the precipitates post-EC. As a result, careful optimizing of the use of PR will be critical to the proper implementation of PR as a fouling mitigation strategy in EC.

In addition to the new insights gained into Al- and Fe-EC operation with PR, a novel EC reactor design, which used a Ti-IrO_2 electrode as a cathode and an iron or aluminum electrode as the anode with occasional PR was tested. Experiments conducted in the Fe/Ti-IrO_2 system maintained coagulant production over time and exhibited minimal electrode fouling, making it a promising solution for mitigating electrode fouling in Fe-EC. This new reactor design may be a way to ensure sulfide removal from PW, while also controlling electrode fouling.

Overall, this research showed the importance of investigating the mechanisms that control the performance of EC. An understanding of the processes that control the production of coagulant, contaminant removal, and electrode fouling, specifically how they are impacted by different water chemistry conditions, electrode materials, and EC operating conditions, will aid in the design and operation of full-scale EC treatment systems.

6.2 Limitations and Future Research

While this thesis met the objectives set, there are still limitations to this research and many avenues left to explore. As discussed in Chapter 3, silica is the primary scalant of concern for the oil sands industry. However, the removal of calcium and magnesium is also desirable. While calcium and magnesium were removed to some extent when EC was employed to treat SPW, the removal was significantly lower in authentic PW, presumably due to the complexation of calcium and magnesium with organic solutes. Additional research is needed to improve the removal of hardness from produced waters.

The research reported in Chapters 4 and 5 revealed how dependent PR performance is on water chemistry, highlighting the need to study the performance of PR for the specific water to be treated. Additionally, Chapter 5 also showed that precipitate characteristics change with PR operation. It is likely that this effect would also change with water chemistry and would have different outcomes, depending on what contaminant is targeted for removal. Therefore, future work should focus on more solution chemistries with varying contaminants of interest.

Another limitation of this research is the scale of the experiments conducted and the design of the reactors used. The experiments in this thesis were all lab-scale experiments with small reactor sizes, slow flow rates, uniform mixing, and short experimental durations. While experiments at this scale help create a controlled environment that allows for the isolation of different parameters, they are not representative of a full-scale EC treatment plant. Therefore, it is recommended that the insights gained in these experiments be used to inform the design of pilot scale experiments, which would help further elucidate factors that control EC performance. One of the factors known to affect EC, which was not studied in this thesis, is flow dynamics. The flow paths and flow velocity through the EC reactor can impact EC performance by controlling the

migration of ions from the electrodes to the bulk solution. It has even been suggested that fouling can be controlled by subjecting the electrodes to enough shear force such that the fouling layer is physically removed [9,177]. However, increasing the flow rate may have a detrimental effect on the coagulation/flocculation process and, consequently, the contaminant removal performance. The optimal flow characteristics will also be highly situation-dependent, as it will impact the size of the reactor, the shape of the electrodes, and residence time. Additionally, pilot-scale experiments conducted for longer time periods (day, weeks, months) will be helpful in determining the long-term applicability of PR as a fouling mitigation strategy.

Finally, this research investigated the use of two electrode materials, namely aluminum and iron. While these electrodes are some of the most common materials used, PR-EC studies employing other electrode types would be valuable for situations where different electrode materials are more well suited to the EC application. For example, magnesium-based EC can be used for the removal of phosphorus from wastewater [222,223]. Additionally, hybrid systems with a mix of electrodes, such as the Al and Fe - Ti-IrO_2 system suggested in Chapter 4, should be studied and optimized for different solution chemistry and operating conditions.

Despite the limitations and the need for future work, this study added to the growing body of literature on EC and helped filled several knowledge gaps that were present prior to this study. This thesis helped elucidate some of the fundamental factors that control the removal of contaminants and the use of PR in EC. The conclusions drawn from this work will help inform future engineers and researchers to empower them to design appropriate experiments and EC reactors to save money and improve water treatment.

References

1. Wan W, Pepping TJ, Banerji T, Chaudhari S, Giammar DE. Effects of water chemistry on arsenic removal from drinking water by electrocoagulation. *Water Res*. 2011;45(1):384-392. doi:10.1016/j.watres.2010.08.016

2. Lakshmanan D, Clifford DA, Samanta G. Ferrous and ferric ion generation during iron electrocoagulation. *Environ Sci Technol*. 2009;43(10):3853-3859. doi:10.1021/es8036669

3. Pan C, Troyer LD, Catalano JG, Giammar DE. Dynamics of chromium(VI)removal from drinking water by iron electrocoagulation. *Environ Sci Technol*. 2016;50(24):13502-13510. doi:10.1021/acs.est.6b03637

4. Rickard D, Luther GW. Chemistry of iron sulfides. *Chem Rev*. 2007;107(2):514-562. doi:10.1021/cr0503658

5. Emamjomeh MM, Sivakumar M. Review of pollutants removed by electrocoagulation and electrocoagulation/flotation processes. *J Environ Manage*. 2009;90(5):1663-1679. doi:10.1016/j.jenvman.2008.12.011

6. Garcia-Segura S, Eiband MMSG, de Melo JV, Martínez-Huitle CA. Electrocoagulation and advanced electrocoagulation processes: A general review about the fundamentals, emerging applications and its association with other technologies. *J Electroanal Chem*. 2017;801:267-299. doi:10.1016/j.jelechem.2017.07.047

7. Mollah MYA, Schennach R, Parga JR, Cocke DL. Electrocoagulation (EC) — science and applications. *J Hazard Mater*. 2001;84(1):29-41. doi:10.1016/S0304-3894(01)00176-5

8. Mollah M, Morkovsky P, Gomes J, Kesmez M, Parga J, Cocke D. Fundamentals, present and future perspectives of electrocoagulation. *J Hazard Mater*. 2004;114(1-3):199-210. doi:10.1016/j.jhazmat.2004.08.009

9. Timmes TC, Kim HC, Dempsey BA. Electrocoagulation pretreatment of seawater prior to ultrafiltration: Pilot-scale applications for military water purification systems. *Desalination*. 2010;250(1):6-13. doi:10.1016/j.desal.2009.03.021

10. Vik EA, Carlson DA, Eikum AS, Gjessing ET. Electrocoagulation of potable water. *Water Res*. 1984;18(11):1355-1360. doi:10.1016/0043-1354(84)90003-4

11. Mollah MYA, Schennach R, Parga JR, Cocke DL. Electrocoagulation (EC)- Science and applications. *J Hazard Mater*. 2001;84(1):29-41. doi:10.1016/S0304-3894(01)00176-5

12. Moussa DT, El-Naas MH, Nasser M, Al-Marri MJ. A comprehensive review of electrocoagulation for water treatment: Potentials and challenges. *J Environ Manage*. 2017;186:24-41. doi:10.1016/j.jenvman.2016.10.032

13. Cañizares P, Jiménez C, Martínez F, Sáez C, Rodrigo MA. Study of the electrocoagulation process using aluminum and iron electrodes. *Ind Eng Chem Res*. 2007;46(19):6189-6195. doi:10.1021/ie070059f

14. Liao Z, Gu Z, Schulz MC, Davis JR, Baygents JC, Farrell J. Treatment of cooling tower

blowdown water containing silica, calcium and magnesium by electrocoagulation. *Water Sci Technol*. 2009;60(9):2345-2352. doi:10.2166/wst.2009.675

15. Schulz MC, Baygents JC, Farrell J. Laboratory and pilot testing of electrocoagulation for removing scaleforming species from industrial process waters. *Int J Environ Sci Technol*. 2009;6(4):521-526. doi:10.1007/bf03326091

16. Guzmán A, Gutiérrez S, Nava J, Coreño O, Rodríguez I. Arsenic and fluoride removal from groundwater by electrocoagulation using a continuous filter-press reactor. *j*. 2016;144. doi:10.1016/j.chemosphere.2015.10.108

17. Van Genuchten CM, Dalby KN, Ceccato M, Stipp SLS, Dideriksen K. Factors affecting the Faradaic efficiency of Fe(0) electrocoagulation. *J Environ Chem Eng*. 2017;5(5):4958-4968. doi:10.1016/j.jece.2017.09.008

18. Hakizimana JN, Gourich B, Vial C, et al. Assessment of hardness, microorganism and organic matter removal from seawater by electrocoagulation as a pretreatment of desalination by reverse osmosis. *Desalination*. Published online 2016. doi:10.1016/j.desal.2015.12.025

19. Bandaru SRS, Roy A, Gadgil AJ, Van Genuchten CM. Long-term electrode behavior during treatment of arsenic contaminated groundwater by a pilot-scale iron electrocoagulation system. *Water Res*. 2020;175:115668. doi:10.1016/j.watres.2020.115668

20. Holt PK, Barton GW, Mitchell CA. The future for electrocoagulation as a localised water treatment technology. *Chemosphere*. 2005;59(3):355-367. doi:10.1016/j.chemosphere.2004.10.023

21. Holt PK, Barton GW, Wark M, Mitchell CA. A quantitative comparison between chemical dosing and electrocoagulation. *Colloids Surfaces A Physicochem Eng Asp*. 2002;211(2-3):233-248. doi:10.1016/S0927-7757(02)00285-6

22. Müller S, Behrends T, Van Genuchten CM. Sustaining efficient production of aqueous iron during repeated operation of Fe(0)-electrocoagulation. *Water Res*. 2019;155:455-464. doi:10.1016/j.watres.2018.11.060

23. Yang ZH, Xu HY, Zeng GM. The behavior of dissolution/passivation and the transformation of passive films during electrocoagulation: Influences of initial pH, Cr(VI) concentration, and alternating pulsed current. *Electrochim Acta*. 2015;153:149-158. doi:10.1016/j.electacta.2014.11.183

24. Canada's Oil Sands Innovation Alliance. *Alternative Silica Removal Technologies.*; 2014. Accessed May 20, 2021. https://cosia.ca/sites/default/files/attachments/New Water Treatment Technologies_0.pdf

25. Fakhru'l-Razi A, Pendashteh A, Abdullah LC, Biak DRA, Madaeni SS, Abidin ZZ. Review of technologies for oil and gas produced water treatment. *J Hazard Mater*. 2009;170(2-3):530-551. doi:10.1016/j.jhazmat.2009.05.044

26. Allen EW. Process water treatment in Canada's oil sands industry: I. Target pollutants and treatment objectives. *J Environ Eng Sci*. 2008;7(2):123-138. doi:10.1139/S07-038

27. Smith JS, Miller JDA. Nature of sulphides and their corrosive effect on ferrous metals: A review. *Br Corros J*. 1975;10(3):136-143. doi:10.1179/000705975798320701

28. Den W, Wang CJ. Removal of silica from brackish water by electrocoagulation pretreatment to prevent fouling of reverse osmosis membranes. *Sep Purif Technol*. 2008;59(3):318-325. doi:10.1016/j.seppur.2007.07.025

29. Zhao S, Huang G, Cheng G, Wang Y, Fu H. Hardness, COD and turbidity removals from produced water by electrocoagulation pretreatment prior to reverse osmosis membranes. *Desalination*. 2014;344:454-462. doi:10.1016/j.desal.2014.04.014

30. Murugananthan M, Bhaskar Raju G, Prabhakar S. Removal of sulfide, sulfate and sulfite ions by electro coagulation. *J Hazard Mater*. 2004;109(1-3):37-44. doi:10.1016/j.jhazmat.2003.12.009

31. Lin HW, Kustermans C, Vaiopoulou E. Electrochemical oxidation of iron and alkalinity generation for efficient sulfide control in sewers. *Water Res*. 2017;118:114-120. doi:10.1016/j.watres.2017.02.069

32. Chow H, Pham ALT. Effective removal of silica and sulfide from oil sands thermal in-situ produced water by electrocoagulation. *J Hazard Mater*. 2019;380:120880. doi:10.1016/j.jhazmat.2019.120880

33. Chow H, Pham ALT. Mitigating Electrode Fouling in Electrocoagulation by Means of Polarity Reversal: The Effects of Electrode Type, Current Density, and Polarity Reversal Frequency. *Water Res*. Published online March 19, 2021:117074. doi:10.1016/j.watres.2021.117074

34. Chow H, Ingelsson M, Roberts EPL, Pham ALT. How does periodic polarity reversal affect the faradaic efficiency and electrode fouling during iron electrocoagulation? *Water Res*. 2021;203:117497. doi:10.1016/J.WATRES.2021.117497

35. Peter J, Bruce J, and Parsons SA. Breakage, Regrowth, and Fractal Nature of Natural Organic Matter Flocs. *Environ Sci Technol*. 2005;39(7):2307-2314. doi:10.1021/ES048854X

36. Bagga A, Chellam S, Clifford DA. Evaluation of iron chemical coagulation and electrocoagulation pretreatment for surface water microfiltration. *J Memb Sci*. 2008;309(1-2):82-93. doi:10.1016/J.MEMSCI.2007.10.009

37. Heng L, Jun N, Wen-jie H, Guibai L. Algae removal by ultrasonic irradiation–coagulation. *Desalination*. 2009;239(1-3):191-197. doi:10.1016/J.DESAL.2007.12.035

38. Ghernaout B, Ghernaout D, Saiba A. Algae and cyanotoxins removal by coagulation/flocculation: A review. *New pub Balaban*. 2012;20(1-3):133-143. doi:10.5004/DWT.2010.1202

39. Xagoraraki I, Harrington GW, Assavasilavasukul P, Standridge JH. Removal of Emerging Waterborne Pathogens and Pathogen Indicators by Pilot-Scale Conventional Treatment. *J Am Water Works Assoc*. 2004;96(5):102-113. doi:10.1002/J.1551-8833.2004.TB10632.X

40. Xie W, Wang Q, Ma H, Ohsumi Y, Ogawa HI. Study on phosphorus removal using a

coagulation system. *Process Biochem*. 2005;40(8):2623-2627. doi:10.1016/J.PROCBIO.2004.06.056

41. Tibebe D, Kassa Y, Bhaskarwar AN. Treatment and characterization of phosphorus from synthetic wastewater using aluminum plate electrodes in the electrocoagulation process. *BMC Chem*. 2019;13(1):1-14. doi:10.1186/s13065-019-0628-1

42. Arnaldos M, Pagilla K. Effluent dissolved organic nitrogen and dissolved phosphorus removal by enhanced coagulation and microfiltration. *Water Res*. 2010;44(18):5306-5315. doi:10.1016/J.WATRES.2010.06.066

43. Lee W, Westerhoff P. Dissolved organic nitrogen removal during water treatment by aluminum sulfate and cationic polymer coagulation. *Water Res*. 2006;40(20):3767-3774. doi:10.1016/J.WATRES.2006.08.008

44. Wickramasinghe SR, Han B, Zimbron J, Shen Z, Karim MN. Arsenic removal by coagulation and filtration: comparison of groundwaters from the United States and Bangladesh. *Desalination*. 2004;169(3):231-244. doi:10.1016/J.DESAL.2004.03.013

45. Scott KN, Green JF, Do HD, McLean SJ. Arsenic removal by coagulation. *J Am Water Works Assoc*. 1995;87(4):114-126. doi:10.1002/J.1551-8833.1995.TB06347.X

46. Johnson PD, Girinathannair P, Ohlinger KN, Ritchie S, Teuber L, Kirby J. Enhanced Removal of Heavy Metals in Primary Treatment Using Coagulation and Flocculation. *Water Environ Res*. 2008;80(5):472-479. doi:10.2175/106143007X221490

47. Gong WX, Qu JH, Liu RP, Lan HC. Effect of aluminum fluoride complexation on fluoride removal by coagulation. *Colloids Surfaces A Physicochem Eng Asp*. 2012;395:88-93. doi:10.1016/J.COLSURFA.2011.12.010

48. Patil DS, Chavan SM, Oubagaranadin JUK. A review of technologies for manganese removal from wastewaters. *J Environ Chem Eng*. 2016;4(1):468-487. doi:10.1016/J.JECE.2015.11.028

49. Charerntanyarak L. Heavy metals removal by chemical coagulation and precipitation. *Water Sci Technol*. 1999;39(10-11):135-138. doi:10.1016/S0273-1223(99)00304-2

50. Latour I, Miranda R, Blanco A. Silica removal from newsprint mill effluents with aluminum salts. *Chem Eng J*. 2013;230:522-531. doi:10.1016/J.CEJ.2013.06.039

51. Hermosilla D, Ordóñez R, Blanco L, et al. pH and Particle Structure Effects on Silica Removal by Coagulation. 2012;35(9):1632-1640. doi:10.1002/CEAT.201100527

52. Castañeda LF, Coreño O, Nava JL, Carreño G. Removal of fluoride and hydrated silica from underground water by electrocoagulation in a flow channel reactor. *Chemosphere*. Published online 2020. doi:10.1016/j.chemosphere.2019.125417

53. Kobya M, Soltani RDC, Omwene PI, Khataee A. A review on decontamination of arsenic-contained water by electrocoagulation: Reactor configurations and operating cost along with removal mechanisms. *Environ Technol Innov*. 2020;17:100519. doi:10.1016/j.eti.2019.100519

54. Roberts LC, Hug SJ, Ruettimann T, Billah M, Khan AW, Rahman MT. Arsenic Removal with Iron(II) and Iron(III) in Waters with High Silicate and Phosphate Concentrations. *Environ Sci Technol*. 2004;38(1):307-315. doi:10.1021/es0343205

55. Devlin T, Kowalski M, Pagaduan E, Zhang X, Wei V, Oleszkiewicz J. Electrocoagulation of wastewater using aluminum, iron, and magnesium electrodes. *j*. Published online 2019. doi:10.1016/j.jhazmat.2018.10.017

56. Yadav JS, Dikshit AK. Stabilized old landfill leachate treatment using electrocoagulation. *EnvironmentAsia*. Published online 2017. doi:10.14456/ea.2017.4

57. Moraes PB, Bertazzoli R. Electrodegradation of landfill leachate in a flow electrochemical reactor. *Chemosphere*. 2005;58(1):41-46. doi:10.1016/j.chemosphere.2004.09.026

58. Khorram AG, Fallah N. Treatment of textile dyeing factory wastewater by electrocoagulation with low sludge settling time: Optimization of operating parameters by RSM. 2018;6(1):635-642. doi:10.1016/j.jece.2017.12.054

59. Mansoorian HJ, Mahvi AH, Jafari AJ. Removal of lead and zinc from battery industry wastewater using electrocoagulation process: Influence of direct and alternating current by using iron and stainless steel rod electrodes. *Sep Purif Technol*. 2014;135:165-175. doi:10.1016/j.seppur.2014.08.012

60. Van Genuchten CM, Addy SEA, Peña J, Gadgil AJ. Removing arsenic from synthetic groundwater with iron electrocoagulation: An Fe and As K-edge EXAFS study. *Environ Sci Technol*. 2012;46(2):986-994. doi:10.1021/es201913a

61. Lakshmanan D, Clifford DA, Samanta G. Comparative study of arsenic removal by iron using electrocoagulation and chemical coagulation. *Water Res*. 2010;44(19):5641-5652. doi:10.1016/j.watres.2010.06.018

62. Delaire C, Amrose S, Zhang M, Hake J, Gadgil A. How do operating conditions affect As(III) removal by iron electrocoagulation? *Water Res*. 2017;112:185-194. doi:10.1016/j.watres.2017.01.030

63. Graça NS, Ribeiro AM, Rodrigues AE. Modeling the electrocoagulation process for the treatment of contaminated water. *Chem Eng Sci*. 2019;197. doi:10.1016/j.ces.2018.12.038

64. Amrose S, Gadgil A, Srinivasan V, et al. Arsenic removal from groundwater using iron electrocoagulation: Effect of charge dosage rate. *J Environ Sci Heal - Part A Toxic/Hazardous Subst Environ Eng*. 2013;48(9):1019-1030. doi:10.1080/10934529.2013.773215

65. Amrose SE, Bandaru SRS, Delaire C, et al. Electro-chemical arsenic remediation: Field trials in West Bengal. *Sci Total Environ*. 2014;488-489(1):539-546. doi:10.1016/j.scitotenv.2013.11.074

66. Heidmann I, Calmano W. Removal of Cr(VI) from model wastewaters by electrocoagulation with Fe electrodes. *Sep Purif Technol*. 2008;61(1):15-21. doi:10.1016/j.seppur.2007.09.011

67. Ölmez T. The optimization of Cr(VI) reduction and removal by electrocoagulation using

response surface methodology. *J Hazard Mater*. 2009;162(2-3):1371-1378. doi:10.1016/j.jhazmat.2008.06.017

68. Keshmirizadeh E, Yousefi S, Rofouei MK. An investigation on the new operational parameter effective in Cr(VI) removal efficiency: A study on electrocoagulation by alternating pulse current. *J Hazard Mater*. 2011;190(1-3):119-124. doi:10.1016/j.jhazmat.2011.03.010

69. Khaled B, Wided B, Béchir H, Elimame E, Mouna L, Zied T. Investigation of electrocoagulation reactor design parameters effect on the removal of cadmium from synthetic and phosphate industrial wastewater. *Arab J Chem*. 2019;12(8). doi:10.1016/j.arabjc.2014.12.012

70. Merzouk B, Gourich B, Sekki A, Madani K, Chibane M. Removal turbidity and separation of heavy metals using electrocoagulation-electroflotation technique. A case study. *J Hazard Mater*. 2009;164(1):215-222. doi:10.1016/j.jhazmat.2008.07.144

71. Rincón GJ, La Motta EJ. Simultaneous removal of oil and grease, and heavy metals from artificial bilge water using electro-coagulation/flotation. *J Environ Manage*. 2014;144:42-50. doi:10.1016/j.jenvman.2014.05.004

72. Doggaz A, Attoura A, Le Page Mostefa M, Côme K, Tlili M, Lapicque F. Removal of heavy metals by electrocoagulation from hydrogenocarbonate-containing waters: Compared cases of divalent iron and zinc cations. *J Water Process Eng*. 2019;29(November 2018):100796. doi:10.1016/j.jwpe.2019.100796

73. Al-Qodah Z, Al-Shannag M. Heavy metal ions removal from wastewater using electrocoagulation processes: A comprehensive review. *Sep Sci Technol*. 2017;52(17). doi:10.1080/01496395.2017.1373677

74. Eyvaz M, Kirlaroglu M, Aktas TS, Yuksel E. The effects of alternating current electrocoagulation on dye removal from aqueous solutions. *Chem Eng J*. 2009;153(1-3):16-22. doi:10.1016/j.cej.2009.05.028

75. Cañizares P, Martínez F, Jiménez C, Lobato J, Rodrigo MA. Coagulation and electrocoagulation of wastes polluted with dyes. *Environ Sci Technol*. 2006;40(20):6418-6424. doi:10.1021/es0608390

76. Secula MS, Crežescu I, Petrescu S. An experimental study of indigo carmine removal from aqueous solution by electrocoagulation. *Desalination*. Published online 2011. doi:10.1016/j.desal.2011.04.031

77. Pi KW, Xiao Q, Zhang HQ, Xia M, Gerson AR. Decolorization of synthetic Methyl Orange wastewater by electrocoagulation with periodic reversal of electrodes and optimization by RSM. *Process Saf Environ Prot*. 2014;92(6):796-806. doi:10.1016/j.psep.2014.02.008

78. Nandi B, Patel S. Effects of operational parameters on the removal of brilliant green dye from aqueous solutions by electrocoagulation. *j*. 2017;10. doi:10.1016/j.arabjc.2013.11.032

79. Kalivel P, Singh RP, Kavitha S, Padmanabhan D, Krishnan S kumar, Palanichamy J.

Elucidation of electrocoagulation mechanism in the removal of Blue SI dye from aqueous solution using Al-Al, Cu-Cu electrodes - A comparative study. *Ecotoxicol Environ Saf*. 2020;201:110858. doi:10.1016/j.ecoenv.2020.110858

80. Moneer AA, El Nemr A. Electro-Coagulation for textile dyes removal. In: *Non-Conventional Textile Waste Water Treatment*. ; 2012.

81. Yang B, Han Y, Yu G. Efficient removal of perfluoroalkyl acids (PFAAs) from aqueous solution by electrocoagulation using iron electrode. *Chem Eng J*. Published online 2016. doi:10.1016/j.cej.2016.06.011

82. Liu Y, Hu X-M, Zhao Y. Removal of perfluorooctanoic acid in simulated and natural waters with different electrode materials by electrocoagulation. *Chemosphere*. 2018;201:303-309. doi:10.1016/j.chemosphere.2018.02.129

83. Lin H, Wang Y, Niu J, Yue Z, Huang Q. Efficient Sorption and Removal of Perfluoroalkyl Acids (PFAAs) from Aqueous Solution by Metal Hydroxides Generated in Situ by Electrocoagulation. *Environ Sci Technol*. 2015;49(17):10562-10569. doi:10.1021/acs.est.5b02092

84. Bao J, Yu W-J, Liu Y, Wang X, Liu Z-Q, Duan Y-F. Removal of perfluoroalkanesulfonic acids (PFSAs) from synthetic and natural groundwater by electrocoagulation. *Chemosphere*. 2020;248:125951. doi:10.1016/j.chemosphere.2020.125951

85. Belongia BM. Treatment of Alumina and Silica Chemical Mechanical Polishing Waste by Electrodecantation and Electrocoagulation. *J Electrochem Soc*. 1999;146(11):4124. doi:10.1149/1.1392602

86. Jin H, Yu Y, Zhang L, Yan R, Chen X. Polarity reversal electrochemical process for water softening. *Sep Purif Technol*. 2019;210:943-949. doi:10.1016/j.seppur.2018.09.009

87. Malakootian M, Mansoorian HJ, Moosazadeh M. Performance evaluation of electrocoagulation process using iron-rod electrodes for removing hardness from drinking water. *Desalination*. 2010;255(1-3):67-71. doi:10.1016/j.desal.2010.01.015

88. Naim MM, Moneer AA, El-Said GF. Predictive equations for the defluoridation by electrocoagulation technique using bipolar aluminum electrodes in the absence and presence of additives: a multivariate study. *Desalin Water Treat*. Published online 2016. doi:10.1080/19443994.2015.1007487

89. López-Guzmán M, Alarcón-Herrera MT, Irigoyen-Campuzano JR, Torres-Castañón LA, Reynoso-Cuevas L. Simultaneous removal of fluoride and arsenic from well water by electrocoagulation. *Sci Total Environ*. 2019;678. doi:10.1016/j.scitotenv.2019.04.400

90. Hu CY, Lo SL, Kuan WH. Effects of co-existing anions on fluoride removal in electrocoagulation (EC) process using aluminum electrodes. *Water Res*. 2003;37(18):4513-4523. doi:10.1016/S0043-1354(03)00378-6

91. Dubrawski KL, Mohseni M. Standardizing electrocoagulation reactor design: Iron electrodes for NOM removal. *Chemosphere*. 2013;91(1):55-60. doi:10.1016/j.chemosphere.2012.11.075

92. Sillanpää M, Ncibi MC, Matilainen A, Vepsäläinen M. Removal of natural organic matter in drinking water treatment by coagulation: A comprehensive review. *Chemosphere*. 2018;190. doi:10.1016/j.chemosphere.2017.09.113

93. Barişçi S, Turkay O. Domestic greywater treatment by electrocoagulation using hybrid electrode combinations. *J Water Process Eng*. 2016;10. doi:10.1016/j.jwpe.2016.01.015

94. Núñez J, Carrasco C, Yeber M, Medina P, Cisternas N, Thibaut R. Application of electrocoagulation for the efficient pollutants removal to reuse the treated wastewater in the dyeing process of the textile industry. *j*. 2019;371. doi:10.1016/j.jhazmat.2019.03.030

95. Elazzouzi M, Haboubi K, Elyoubi MS. Electrocoagulation flocculation as a low-cost process for pollutants removal from urban wastewater. *Chem Eng Res Des*. 2017;117. doi:10.1016/j.cherd.2016.11.011

96. Dubrawski KL, Van Genuchten CM, Delaire C, Amrose SE, Gadgil AJ, Mohseni M. Production and transformation of mixed-valent nanoparticles generated by Fe(0) electrocoagulation. *Environ Sci Technol*. 2015;49(4):2171-2179. doi:10.1021/es505059d

97. Kamaraj R, Ganesan P, Lakshmi J, Vasudevan S. Removal of copper from water by electrocoagulation process-effect of alternating current (AC) and direct current (DC). *Environ Sci Pollut Res*. 2013;20(1):399-412. doi:10.1007/s11356-012-0855-7

98. Vasudevan S, Lakshmi J, Packiyam M. Electrocoagulation studies on removal of cadmium using magnesium electrode. *J Appl Electrochem*. 2010;40(11):2023-2032. doi:10.1007/s10800-010-0182-y

99. Safwat SM, Matta ME. Performance evaluation of electrocoagulation process using zinc electrodes for removal of urea. *Sep Sci Technol*. 2020;55(14):2500-2509. doi:10.1080/01496395.2019.1636067

100. Ali I, Asim M, Khan TA. Arsenite removal from water by electro-coagulation on zinc-zinc and copper-copper electrodes. *Int J Environ Sci Technol*. 2013;10(2):377-384. doi:10.1007/s13762-012-0113-z

101. Dubrawski KL, Mohseni M. In-situ identification of iron electrocoagulation speciation and application for natural organic matter (NOM) removal. *Water Res*. 2013;47(14):5371-5380. doi:10.1016/j.watres.2013.06.021

102. Kinsela AS, Jones AM, Bligh MW, et al. Influence of Dissolved Silicate on Rates of Fe(II) Oxidation. *Environ Sci Technol*. 2016;50(21):11663-11671. doi:10.1021/acs.est.6b03015

103. Anderson PR, Benjamin MM. Effects of Silicon on the Crystallization and Adsorption Properties of Ferric Oxides. *Environ Sci Technol*. 1985;19(11):1048-1053. doi:10.1021/es00141a004

104. King DW, Lounsbury HA, Millero FJ. Rates and Mechanism of Fe(II) Oxidation at Nanomolar Total Iron Concentrations. *Environ Sci Technol*. 1995;29(3):818-824. doi:10.1021/es00003a033

105. Stefánsson A. Iron(III) hydrolysis and solubility at 25°C. *Environ Sci Technol*.

2007;41(17):6117-6123. doi:10.1021/es070174h

106. David A. Dzombak FMMM. *Surface Complexation Modeling: Hydrous Ferric Oxide | Wiley*. Wiley; 1990. Accessed May 19, 2021. https://www.wiley.com/en-ca/Surface+Complexation+Modeling%3A+Hydrous+Ferric+Oxide-p-9780471637318

107. Mouedhen G, Feki M, Wery MDP, Ayedi HF. Behavior of aluminum electrodes in electrocoagulation process. *J Hazard Mater*. 2008;150(1):124-135. doi:10.1016/j.jhazmat.2007.04.090

108. Mansouri K, Ibrik K, Bensalah N, Abdel-Wahab A. Anodic Dissolution of Pure Aluminum during Electrocoagulation Process: Influence of Supporting Electrolyte, Initial pH, and Current Density. *Ind Eng Chem Res*. 2011;50(23):13362-13372. doi:10.1021/ie201206d

109. Chellam S, Sari M. Aluminum electrocoagulation as pretreatment during microfiltration of surface water containing NOM: A review of fouling, NOM, DBP, and virus control. *j*. 2016;304. doi:10.1016/j.jhazmat.2015.10.054

110. Sari MA, Chellam S. Mechanisms of boron removal from hydraulic fracturing wastewater by aluminum electrocoagulation. *J Colloid Interface Sci*. 2015;458:103-111. doi:10.1016/j.jcis.2015.07.035

111. Tanneru CT, Rimer JD, Chellam S. Sweep flocculation and adsorption of viruses on aluminum flocs during electrochemical treatment prior to surface water microfiltration. *Environ Sci Technol*. 2013;47(9):4612-4618. doi:10.1021/es400291e

112. Huang CH, Chen L, Yang CL. Effect of anions on electrochemical coagulation for cadmium removal. *Sep Purif Technol*. 2009;65(2):137-146. doi:10.1016/j.seppur.2008.10.029

113. Cañizares P, Carmona M, Lobato J, Martínez F, Rodrigo MA. Electrodissolution of aluminum electrodes in electrocoagulation processes. *Ind Eng Chem Res*. 2005;44(12):4178-4185. doi:10.1021/ie048858a

114. Mechelhoff M, Kelsall GH, Graham NJD. Electrochemical behaviour of aluminium in electrocoagulation processes. *Chem Eng Sci*. 2013;95:301-312. doi:10.1016/j.ces.2013.03.010

115. Mechelhoff M, Kelsall GH, Graham NJD. Super-faradaic charge yields for aluminium dissolution in neutral aqueous solutions. *Chem Eng Sci*. 2013;95:353-359. doi:10.1016/j.ces.2013.03.016

116. Crittenden JC, Hand DW, Howe KJ, Tchobanoglous G, Trussell RR. *MWH's Water Treatment : Principles and Design.* 3rd ed. John Wiley & Sons; 2012.

117. Liu Y, Zhang X, Jiang WM, Wu MR, Li ZH. Comprehensive review of floc growth and structure using electrocoagulation: Characterization, measurement, and influencing factors. *Chem Eng J*. 2021;417:129310. doi:10.1016/J.CEJ.2021.129310

118. Harif T, Khai M, Adin A. Electrocoagulation versus chemical coagulation: Coagulation/flocculation mechanisms and resulting floc characteristics. *Water Res*.

2012;46(10):3177-3188. doi:10.1016/j.watres.2012.03.034

119. Harif T, Adin A. Characteristics of aggregates formed by electroflocculation of a colloidal suspension. *Water Res*. 2007;41(13):2951-2961. doi:10.1016/J.WATRES.2006.11.055

120. Spicer PT, Pratsinis SE, Raper J, Amal R, Bushell G, Meesters G. Effect of shear schedule on particle size, density, and structure during flocculation in stirred tanks. *Powder Technol*. 1998;97(1):26-34. doi:10.1016/S0032-5910(97)03389-5

121. Nasrullah M, Singh L, Krishnan S, Sakinah M, Mahapatra DM, Zularisam AW. Electrocoagulation treatment of raw palm oil mill effluent: Effect of operating parameters on floc growth and structure. *J Water Process Eng*. 2020;33:101114. doi:10.1016/J.JWPE.2019.101114

122. Zodi S, Potier O, Lapicque F, Leclerc JP. Treatment of the textile wastewaters by electrocoagulation: Effect of operating parameters on the sludge settling characteristics. *Sep Purif Technol*. 2009;69(1):29-36. doi:10.1016/J.SEPPUR.2009.06.028

123. Ulu F, Barişçi S, Kobya M, Särkkä H, Sillanpää M. Removal of humic substances by electrocoagulation (EC) process and characterization of floc size growth mechanism under optimum conditions. *Sep Purif Technol*. 2014;133:246-253. doi:10.1016/J.SEPPUR.2014.07.003

124. Nasrullah M, Zularisam A, Krishnan S, Sakinah M, Singh L, Fen Y. High performance electrocoagulation process in treating palm oil mill effluent using high current intensity application. *j*. 2019;27(1). doi:10.1016/j.cjche.2018.07.021

125. Chen X, Chen G, Yue PL. Separation of pollutants from restaurant wastewater by electrocoagulation. *Sep Purif Technol*. 2000;19(1-2):65-76. doi:10.1016/S1383-5866(99)00072-6

126. Lee SY, Gagnon GA. Growth and structure of flocs following electrocoagulation. *Sep Purif Technol*. 2016;163:162-168. doi:10.1016/J.SEPPUR.2016.02.049

127. Jordan N, Marmier N, Lomenech C, Giffaut E, Ehrhardt JJ. Sorption of silicates on goethite, hematite, and magnetite: Experiments and modelling. *J Colloid Interface Sci*. 2007;312(2):224-229. doi:10.1016/j.jcis.2007.03.053

128. Rochelle M. Cornell US. *The Iron Oxides: Structure, Properties, Reactions, Occurrences and Uses - Rochelle M. Cornell, Udo Schwertmann*. 2nd ed. Wiley-VCH Verlag; 2006.

129. Lei Y, Hidayat I, Saakes M, Van Der Weijden R, Buisman CJN. Fate of calcium, magnesium and inorganic carbon in electrochemical phosphorus recovery from domestic wastewater. *Chem Eng J*. 2019;362:453-459. doi:10.1016/j.cej.2019.01.056

130. Wang H, Alfredsson V, Tropsch J, Ettl R, Nylander T. Formation of CaCO3 deposits on hard surfaces - Effect of bulk solution conditions and surface properties. *ACS Appl Mater Interfaces*. 2013;5(10):4035-4045. doi:10.1021/am401348v

131. Sahu O, Mazumdar B, Chaudhari PK. Treatment of wastewater by electrocoagulation: A review. *Environ Sci Pollut Res*. 2014;21(4):2397-2413. doi:10.1007/s11356-013-2208-6

132. McBeath ST, Nouri-Khorasani A, Mohseni M, Wilkinson DP. In-situ determination of current density distribution and fluid modeling of an electrocoagulation process and its effects on natural organic matter removal for drinking water treatment. *Water Res*. 2020;171:115404. doi:10.1016/j.watres.2019.115404

133. Van Genuchten CM, Bandaru SRS, Surorova E, Amrose SE, Gadgil AJ, Peña J. Formation of macroscopic surface layers on Fe(0) electrocoagulation electrodes during an extended field trial of arsenic treatment. *Chemosphere*. 2016;153:270-279. doi:10.1016/j.chemosphere.2016.03.027

134. Xu HY, Yang ZH, Luo YL. A novel approach to sustain Fe0-electrocoagulation for Cr(VI) removal by optimizing chloride ions. *Sep Purif Technol*. 2015;156:200-206. doi:10.1016/j.seppur.2015.09.074

135. Lakshmipathiraj P, Bhaskar Raju G, Raviatul Basariya M, Parvathy S, Prabhakar S. Removal of Cr (VI) by electrochemical reduction. *Sep Purif Technol*. 2008;60(1):96-102. doi:10.1016/j.seppur.2007.07.053

136. Refaey SAM. Inhibition of steel pitting corrosion in HCl by some inorganic anions. *Appl Surf Sci*. 2005;240(1-4):396-404. doi:10.1016/j.apsusc.2004.07.014

137. Arroyo MG, Pérez-Herranz V, Montañés MT, García-Antón J, Guiñón JL. Effect of pH and chloride concentration on the removal of hexavalent chromium in a batch electrocoagulation reactor. *J Hazard Mater*. 2009;169(1-3):1127-1133. doi:10.1016/j.jhazmat.2009.04.089

138. Dura A, Breslin CB. The removal of phosphates using electrocoagulation with Al−Mg anodes. *J Electroanal Chem*. 2019;846:113161. doi:10.1016/j.jelechem.2019.05.043

139. Trompette JL, Vergnes H. On the crucial influence of some supporting electrolytes during electrocoagulation in the presence of aluminum electrodes. *J Hazard Mater*. Published online 2009. doi:10.1016/j.jhazmat.2008.07.148

140. Gotsi M, Kalogerakis N, Psillakis E, Samaras P, Mantzavinos D. Electrochemical oxidation of olive oil mill wastewaters. *Water Res*. 2005;39(17):4177-4187. doi:10.1016/j.watres.2005.07.037

141. Kabdaşli I, Vardar B, Arslan-Alaton I, Tünay O. Effect of dye auxiliaries on color and COD removal from simulated reactive dyebath effluent by electrocoagulation. *Chem Eng J*. 2009;148(1):89-96. doi:10.1016/j.cej.2008.08.006

142. Khandegar V, Saroha AK. Electrocoagulation for the treatment of textile industry effluent - A review. *J Environ Manage*. 2013;128:949-963. doi:10.1016/j.jenvman.2013.06.043

143. He CC, Hu CY, Lo SL. Evaluation of sono-electrocoagulation for the removal of Reactive Blue 19 passive film removed by ultrasound. *Sep Purif Technol*. 2016;165:107-113. doi:10.1016/j.seppur.2016.03.047

144. Moradi M, Vasseghian Y, Arabzade H, Mousavi Khaneghah A. Various wastewaters treatment by sono-electrocoagulation process: A comprehensive review of operational parameters and future outlook. *Chemosphere*. 2021;263:128314. doi:10.1016/j.chemosphere.2020.128314

145. Kovatcheva VK, Parlapanski MD. Sono-electrocoagulation of iron hydroxides. In: *Colloids and Surfaces A: Physicochemical and Engineering Aspects*. Vol 149. Elsevier Science Publishers B.V.; 1999:603-608. doi:10.1016/S0927-7757(98)00414-2

146. Wang CT, Chou WL, Kuo YM. Removal of COD from laundry wastewater by electrocoagulation/electroflotation. *J Hazard Mater*. 2009;164(1):81-86. doi:10.1016/j.jhazmat.2008.07.122

147. He CC, Hu CY, Lo SL. Integrating chloride addition and ultrasonic processing with electrocoagulation to remove passivation layers and enhance phosphate removal. *Sep Purif Technol*. 2018;201:148-155. doi:10.1016/j.seppur.2018.03.011

148. Hashim K, Shaw A, AlKhaddar R, Pedrola M, Phipps D. Iron removal, energy consumption and operating cost of electrocoagulation of drinking water using a new flow column reactor. *j*. 2017;189. doi:10.1016/j.jenvman.2016.12.035

149. Raschitor A, Fernandez CM, Cretescu I, Rodrigo MA, Cañizares P. Sono-electrocoagulation of wastewater polluted with Rhodamine 6G. *Sep Purif Technol*. 2014;135:110-116. doi:10.1016/j.seppur.2014.08.003

150. Prajapati AK. Sono-assisted electrocoagulation treatment of rice grain based distillery biodigester effluent: Performance and cost analysis. *Process Saf Environ Prot*. 2021;150:314-322. doi:10.1016/j.psep.2021.04.030

151. Asaithambi P, Govindarajan R. Hybrid Sono-Electrocoagulation Process for the Treatment of Landfill Leachate Wastewater: Optimization through a Central Composite Design Approach. *Environ Process*. 2021;8(2):793-816. doi:10.1007/s40710-021-00509-z

152. Maha Lakshmi P, Sivashanmugam P. Treatment of oil tanning effluent by electrocoagulation: Influence of ultrasound and hybrid electrode on COD removal. *Sep Purif Technol*. 2013;116:378-384. doi:10.1016/j.seppur.2013.05.026

153. Mao X, Hong S, Zhu H, Lin H, Wei L, Gan F. Alternating pulse current in electrocoagulation for wastewater treatment to prevent the passivation of al electrode. *J Wuhan Univ Technol Mater Sci Ed*. 2008;23(2):239-241. doi:10.1007/s11595-006-2239-7

154. Vasudevan S, Kannan BS, Lakshmi J, Mohanraj S, Sozhan G. Effects of alternating and direct current in electrocoagulation process on the removal of fluoride from water. *J Chem Technol Biotechnol*. 2011;86(3):428-436. doi:10.1002/jctb.2534

155. Cerqueira AA, Souza PSA, Marques MRC. Effects of direct and alternating current on the treatment of oily water in an electroflocculation process. *Brazilian J Chem Eng*. 2014;31(3):693-701. doi:10.1590/0104-6632.20140313s00002363

156. Ghanizadeh G, Shariati neghab G, Salem M, Khalagi K. Taguchi experimental design for electrocoagulation process using alternating and direct current on fluoride removal from water. *Desalin Water Treat*. 2016;57(27):12675-12683. doi:10.1080/19443994.2015.1049562

157. Karamati-Niaragh E, Alavi Moghaddam MR, Emamjomeh MM, Nazlabadi E. Evaluation of direct and alternating current on nitrate removal using a continuous electrocoagulation process: Economical and environmental approaches through RSM. *J Environ Manage*.

2019;230:245-254. doi:10.1016/j.jenvman.2018.09.091

158. Vasudevan S, Lakshmi J. Effect of alternating and direct current in an electrocoagulation process on the removal of cadmium from water. *Water Sci Technol*. 2012;65(2):353-360. doi:10.2166/wst.2012.859

159. Hasani G, Maleki A, Daraei H. A comparative optimization and performance analysis of four different electrocoagulation-flotation processes for humic acid removal from aqueous solutions. *Process Saf Environ Prot*. 2019;121:103-117. doi:10.1016/j.psep.2018.10.025

160. Secula M, Cretescu I, Cagnon B, Manea L, Stan C, Breaban I. Fractional Factorial Design Study on the Performance of GAC-Enhanced Electrocoagulation Process Involved in Color Removal from Dye Solutions. *Materials (Basel)*. 2013;6(7):2723-2746. doi:10.3390/ma6072723

161. Asaithambi P, Sajjadi B, Abdul Aziz AR, Wan Daud WMA Bin. Performance evaluation of hybrid electrocoagulation process parameters for the treatment of distillery industrial effluent. *Process Saf Environ Prot*. 2016;104:406-412. doi:10.1016/j.psep.2016.09.023

162. Vasudevan S, Lakshmi J. Effects of alternating and direct current in electrocoagulation process on the removal of cadmium from water - A novel approach. *Sep Purif Technol*. 2011;80(3):643-651. doi:10.1016/j.seppur.2011.06.027

163. Ashraf SN, Rajapakse J, Dawes LA, Millar GJ. Electrocoagulation for the purification of highly concentrated brine produced from reverse osmosis desalination of coal seam gas associated water. *J Water Process Eng*. 2019;28:300-310. doi:10.1016/j.jwpe.2019.02.003

164. Ozyonar F, Karagozoglu B. Treatment of pretreated coke wastewater by electrocoagulation and electrochemical peroxidation processes. *Sep Purif Technol*. 2015;150:268-277. doi:10.1016/j.seppur.2015.07.011

165. Alkhatib AM, Hawari AH, Hafiz MA, Benamor A. A novel cylindrical electrode configuration for inducing dielectrophoretic forces during electrocoagulation. *J Water Process Eng*. 2020;35:101195. doi:10.1016/j.jwpe.2020.101195

166. Fekete É, Lengyel B, Cserfalvi T, Pajkossy T. Electrochemical dissolution of aluminium in electrocoagulation experiments. *J Solid State Electrochem*. 2016;20(11):3107-3114. doi:10.1007/s10008-016-3195-6

167. Grøterud O, Smoczyński L. Phosphorus removal from water by means of electrolysis. *Water Res*. 1986;20(5):667-669. doi:10.1016/0043-1354(86)90032-1

168. Eyvaz M. Treatment of brewery wastewater with electrocoagulation: Improving the process performance by using alternating pulse current. *Int J Electrochem Sci*. 2016;11(6):4988-5008. doi:10.20964/2016.06.11

169. Smoczyński L, Kalinowski S, Ratnaweera H, Kosobucka M, Trifescu M, Pieczulis-Smoczyńska K. Electrocoagulation of municipal wastewater – a pilot-scale test. *Desalin Water Treat*. 2017;72:162-168. doi:10.5004/dwt.2017.20645A

170. Betancor-Abreu A, Mena VF, González S, Delgado S, Souto RM, Santana JJ. Design and optimization of an electrocoagulation reactor for fluoride remediation in underground

water sources for human consumption. *J Water Process Eng*. 2019;31:100865. doi:10.1016/j.jwpe.2019.100865

171. Doran GF, Carini FH, Fruth DA, Drago JA, Leong LYC. Evaluation of Technologies to Treat Oil Field Produced Water to Drinking Water or Reuse Quality. Published online October 5, 1997. doi:10.2118/38830-MS

172. Zhang K, Pernitsky D, Jafari M, Lu Q. Effect of MgO Slaking on Silica Removal during Warm Lime Softening of SAGD Produced Water. *Ind Eng Chem Res*. 2021;60(4):1839-1849. doi:10.1021/ACS.IECR.0C05484

173. Zhang L, Mishra D, Zhang K, Perdicakis B, Pernitsky D, Lu Q. Impact of influent deviations on polymer coagulant dose in warm lime softening of synthetic SAGD produced water. *Water Res*. 2021;200:117202. doi:10.1016/J.WATRES.2021.117202

174. Bridle M. Treatment of SAGD Produced Waters Without Lime Softening. *SPE/PS-CIM/CHOA Int Therm Oper Heavy Oil Symp Proc*. 2005;2005. doi:10.2118/97686-MS

175. Heins W, Peterson D. Use of Evaporation for Heavy Oil Produced Water Treatment. *J Can Pet Technol*. 2005;44(01):26-30. doi:10.2118/05-01-01

176. Si M, Bai L, Du K. Fuel consumption analysis and cap and trade system evaluation for Canadian in situ oil sands extraction. *Renew Sustain Energy Rev*. 2021;146:111145. doi:10.1016/j.rser.2021.111145

177. Ingelsson M, Yasri N, Roberts EPL. Electrode passivation, faradaic efficiency, and performance enhancement strategies in electrocoagulation—a review. *Water Res*. 2020;187:116433. doi:10.1016/j.watres.2020.116433

178. Tamura H, Goto K, Yotsuyanagi T, Nagayama M. Spectrophotometric determination of iron(II) with 1,10-phenanthroline in the presence of large amounts of iron(III). *Talanta*. 1974;21(4):314-318. doi:10.1016/0039-9140(74)80012-3

179. Clesceri LS, Eaton AD. Clesceri: Standard Methods for the Examination of... - Google Scholar. *Am Public Heal Assoc* . Published online 1992. Accessed May 20, 2021. https://scholar.google.com/scholar_lookup?title=Standard Methods for the Examination of Water and Wastewater&publication_year=1992&author=A.E. Green Berg&author=L.S. Clesceri&author=A.D. Eaton

180. Cline J.D. Spectrophotometric Determination of hydrogen sulfide in natural waters. *Limnol Oceanogr*. 1969;14(3):454-458. doi:10.4319/lo.1969.14.3.0454

181. Atkins P, De Paula J. *Book Review* Physical chemistry for the life sciences. Vol 4.; 2005. Accessed May 20, 2021. http://omicron.ch.tuiasi.ro/EEMJ/

182. Ohfuji H, Rickard D. High resolution transmission electron microscopic study of synthetic nanocrystalline mackinawite. *Earth Planet Sci Lett*. 2006;241(1-2):227-233. doi:10.1016/j.epsl.2005.10.006

183. Wolthers M, Van Der Gaast SJ, Rickard D. The structure of disordered mackinawite. *Am Mineral*. 2003;88(11-12 PART 2):2007-2015. doi:10.2138/am-2003-11-1245

184. Jeong HY, Han YS, Park SW, Hayes KF. Aerobic oxidation of mackinawite (FeS) and its environmental implication for arsenic mobilization. *Geochim Cosmochim Acta*. 2010;74(11):3182-3198. doi:10.1016/j.gca.2010.03.012

185. Jeong HY, Lee JH, Hayes KF. Characterization of synthetic nanocrystalline mackinawite: Crystal structure, particle size, and specific surface area. *Geochim Cosmochim Acta*. 2008;72(2):493-505. doi:10.1016/j.gca.2007.11.008

186. Csákberényi-Malasics D, Rodriguez-Blanco JD, Kis VK, Rečnik A, Benning LG, Pósfai M. Structural properties and transformations of precipitated FeS. *Chem Geol*. 2012;294-295:249-258. doi:10.1016/j.chemgeo.2011.12.009

187. Bouroushian M. *Electrochemistry of Metal Chalcogenides* . Springer Science & Business Media; 2010. Accessed May 20, 2021. https://books.google.ca/books?hl=en&lr=&id=B8WgWHjN54oC&oi=fnd&pg=PR5&ots=qU2ZXrQeah&sig=sIKR5hVlAsQfPegInX15jxBIAFk&redir_esc=y#v=onepage&q&f=false

188. Pokrovski GS, Schott J, Farges F, Hazemann JL. Iron (III)-silica interactions in aqueous solution: Insights from X-ray absorption fine structure spectroscopy. *Geochim Cosmochim Acta*. 2003;67(19):3559-3573. doi:10.1016/S0016-7037(03)00160-1

189. Hiemstra T, Barnett MO, van Riemsdijk WH. Interaction of silicic acid with goethite. *J Colloid Interface Sci*. 2007;310(1):8-17. doi:10.1016/j.jcis.2007.01.065

190. Swedlund PJ, Webster JG. Adsorption and polymerisation of silicic acid on ferrihydrite, and its effect on arsenic adsorption. *Water Res*. 1999;33(16):3413-3422. doi:10.1016/S0043-1354(99)00055-X

191. Swedlund PJ, Hamid RD, Miskelly GM. Insights into H4SiO4 surface chemistry on ferrihydrite suspensions from ATR-IR, Diffuse Layer Modeling and the adsorption enhancing effects of carbonate. *J Colloid Interface Sci*. 2010;352(1):149-157. doi:10.1016/j.jcis.2010.08.011

192. Morse JW, Arvidson RS, Lüttge A. Calcium carbonate formation and dissolution. *Chem Rev*. 2007;107(2):342-381. doi:10.1021/cr050358j

193. Montes-Hernandez G, Findling N, Renard F, Auzende AL. Precipitation of ordered dolomite via simultaneous dissolution of calcite and magnesite: New experimental insights into an old precipitation enigma. *Cryst Growth Des*. 2014;14(2):671-677. doi:10.1021/cg401548a

194. Xu J, Yan C, Zhang F, Konishi H, Xu H, Teng HH. Testing the cation-hydration effect on the crystallization of Ca-Mg-CO 3 systems. *Proc Natl Acad Sci U S A*. 2013;110(44):17750-17755. doi:10.1073/pnas.1307612110

195. Hasson D, Sidorenko G, Semiat R. Calcium carbonate hardness removal by a novel electrochemical seeds system. *Desalination*. 2010;263(1-3):285-289. doi:10.1016/j.desal.2010.06.036

196. Zhi S, Zhang S. A novel combined electrochemical system for hardness removal. *Desalination*. 2014;349:68-72. doi:10.1016/j.desal.2014.06.023

197. Zeppenfeld K. Electrochemical removal of calcium and magnesium ions from aqueous solutions. *Desalination*. 2011;277(1-3):99-105. doi:10.1016/j.desal.2011.04.005

198. Chen X, Chen G. Electroflotation. In: *Electrochemistry for the Environment*. Springer New York; 2010:263-277. doi:10.1007/978-0-387-68318-8_11

199. Lei Y, Remmers JC, Saakes M, Van Der Weijden RD, Buisman CJN. Influence of Cell Configuration and Long-Term Operation on Electrochemical Phosphorus Recovery from Domestic Wastewater. *ACS Sustain Chem Eng*. 2019;7(7):7362-7368. doi:10.1021/acssuschemeng.9b00563

200. Fuladpanjeh-Hojaghan B, Elsutohy MM, Kabanov V, Heyne B, Trifkovic M, Roberts EPL. In-Operando Mapping of pH Distribution in Electrochemical Processes. *Angew Chemie Int Ed*. 2019;58(47):16815-16819. doi:10.1002/anie.201909238

201. Gobbi LCA, Nascimento IL, Muniz EP, Rocha SMS, Porto PSS. Electrocoagulation with polarity switch for fast oil removal from oil in water emulsions. *J Environ Manage*. 2018;213:119-125. doi:10.1016/j.jenvman.2018.01.069

202. Radjenovic J, Sedlak DL. Challenges and Opportunities for Electrochemical Processes as Next-Generation Technologies for the Treatment of Contaminated Water. *Environ Sci Technol*. 2015;49(19):11292-11302. doi:10.1021/acs.est.5b02414

203. Bandaru SRS, Van Genuchten CM, Kumar A, et al. Rapid and Efficient Arsenic Removal by Iron Electrocoagulation Enabled with in Situ Generation of Hydrogen Peroxide. *Environ Sci Technol*. 2020;54(10):6094-6103. doi:10.1021/acs.est.0c00012

204. Busenberg E, Plummer NL. Thermodynamics of magnesian calcite solid-solutions at 25°C and 1 atm total pressure. *Geochim Cosmochim Acta*. 1989;53(6):1189-1208. doi:10.1016/0016-7037(89)90056-2

205. De Leeuw NH, Parker SC. Surface Structure and Morphology of Calcium Carbonate Polymorphs Calcite, Aragonite, and Vaterite: An Atomistic Approach. *J Phys Chem B*. 1998;102(16):2914-2922. doi:10.1021/jp973210f

206. Chen M, Dollar O, Shafer-Peltier K, Randtke S, Waseem S, Peltier E. Boron removal by electrocoagulation: Removal mechanism, adsorption models and factors influencing removal. *Water Res*. 2020;170:115362. doi:10.1016/j.watres.2019.115362

207. Kobya M, Demirbas E, Ulu F. Evaluation of operating parameters with respect to charge loading on the removal efficiency of arsenic from potable water by electrocoagulation. *J Environ Chem Eng*. 2016;4(2). doi:10.1016/j.jece.2016.02.016

208. Mamelkina M, Tuunila R, Sillanpää M. Removal of sulfate from mining waters by electrocoagulation. *j*. 2017;182. doi:10.1016/j.seppur.2017.03.044

209. Génin J-MR, Ruby C, Géhin A, Refait P. Synthesis of green rusts by oxidation of Fe(OH)2, their products of oxidation and reduction of ferric oxyhydroxides; –pH Pourbaix diagrams. *Comptes Rendus Geosci*. 2006;338(6-7):433-446. doi:10.1016/j.crte.2006.04.004

210. Drissi SH, Refait P, Abdelmoula M, Génin JMR. The preparation and thermodynamic

properties of Fe(II)Fe(III) hydroxide-carbonate (green rust 1); Pourbaix diagram of iron in carbonate-containing aqueous media. *Corros Sci*. 1995;37(12):2025-2041. doi:10.1016/0010-938X(95)00096-3

211. Beverskog B, Puigdomenech I. Revised Pourbaix diagrams for iron at 25-300°C. *Corros Sci*. 1996;38(12):2121-2135. doi:10.1016/S0010-938X(96)00067-4

212. Keddam M. Anodic dissolution. In: *Corrosion Mechanisms in Theory and Practice: Third Edition*. CRC Press; 2011:149-216. doi:10.1201/b11020-7

213. Vázquez A, Rodríguez I, Lázaro I. Primary potential and current density distribution analysis: A first approach for designing electrocoagulation reactors. *Chem Eng J*. 2012;179:253-261. doi:10.1016/j.cej.2011.10.078

214. Comninellis C, Chen G. *Electrochemistry for the Environment*. Springer New York; 2010. doi:10.1007/978-0-387-68318-8

215. Cañizares P, Jiménez C, Martínez F, Rodrigo MA, Sáez C. The pH as a key parameter in the choice between coagulation and electrocoagulation for the treatment of wastewaters. *J Hazard Mater*. 2009;163(1):158-164. doi:10.1016/J.JHAZMAT.2008.06.073

216. Bian Y, Ge Z, Albano C, Lobo FL, Ren ZJ. Oily bilge water treatment using DC/AC powered electrocoagulation. *Environ Sci Water Res Technol*. Published online 2019. doi:10.1039/c9ew00497a

217. Gao S, Brown B, Young D, Singer M. Formation of iron oxide and iron sulfide at high temperature and their effects on corrosion. *Corros Sci*. 2018;135:167-176. doi:10.1016/j.corsci.2018.02.045

218. Gao S, Du M, Tian J. Effects of chloride ions on electro-coagulation-flotation process with aluminum electrodes for algae removal. *J Hazard Mater*. 2010;182(1-3):827-834. doi:10.1016/J.JHAZMAT.2010.06.114

219. Ben Grich N, Attour A, Le Page Mostefa M, Guesmi S, Tlili M, Lapicque F. Fluoride removal from water by electrocoagulation: Effect of the type of water and the experimental parameters. *Electrochim Acta*. 2019;316:257-265. doi:10.1016/J.ELECTACTA.2019.05.130

220. Gabrielli C, Maurin G, Francy-Chausson H, Thery P, Tran TTM, Tlili M. Electrochemical water softening: principle and application. *Desalination*. 2006;201(1-3):150-163. doi:10.1016/j.desal.2006.02.012

221. Malakootian M, Yousefi N. The efficiency of the electrocoagulation process using aluminum electrodes in the removal of hardness from water. *J Environ Heal Sci Eng*. 2009;6(2):131-136. Accessed August 4, 2021. https://ijehse.tums.ac.ir/index.php/jehse/article/view/203

222. Kim JH, An B min, Lim DH. Electricity production and phosphorous recovery as struvite from synthetic wastewater using magnesium-air fuel cell electrocoagulation. 2018;132:200-210. Accessed May 12, 2020. https://pubmed.ncbi.nlm.nih.gov/29331908/

223. Kruk DJ, Elektorowicz M, Oleszkiewicz JA. Struvite precipitation and phosphorus

removal using magnesium sacrificial anode. *Chemosphere*. 2014;101:28-33. doi:10.1016/J.chemosphere.2013.12.036

Appendix I: Statistics

t-Test: Two-Sample Assuming Equal Variances

The values highlighted in yellow should be below 0.05 for 95% confidence

tStat > tCritical to reject the null hypothesis (values in orange)

Red cells indicate that the p-value is not below 0.05 and tStat < tCritical. Therefore the null hypothesis cannot be rejected

NaCl Solution Fe-EC in the Flow-Through Experiments t = 6hr

DC	PR f = 2 min	PR f = 1 min	PR f = 0.5 min
1.099	0.994752792	0.878407437	0.789984966
0.949	0.924363852	0.813254037	0.787658059
1.03	0.908657229	0.845830737	0.82721548

DC to PR f = 2 min

	Variable 1	*Variable 2*
Mean	1.025972	0.942591
Variance	0.005685	0.002102
Observations	3	3
Pooled Variance	0.003894	
Hypothesized Mean Difference	0	
df	4	
t Stat	1.636531	
P(T<=t) two-tail	0.177069	
t Critical two-tail	2.776445	

DC to PR f = 1 min

	Variable 1	*Variable 2*
Mean	1.02597213	0.845830737
Variance	0.005685334	0.001061241
Observations	3	3
Pooled Variance	0.003373288	
Hypothesized Mean Difference	0	
df	4	
t Stat	3.798677666	
P(T<=t) two-tail	0.019125412	
t Critical two-tail	2.776445105	

DC to PR f = 0.5 min

	Variable 1	*Variable 2*
Mean	1.025972	0.80162
Variance	0.005685	0.000493
Observations	3	3
Pooled Variance	0.003089	
Hypothesized Mean Difference	0	
df	4	
t Stat	4.943858	
P(T<=t) two-tail	0.007795	
t Critical two-tail	2.776445	

PR f = 2 min to f = 1 min

	Variable 1	*Variable 2*
Mean	0.942591	0.845831
Variance	0.002102	0.001061
Observations	3	3
Pooled Variance	0.001582	
Hypothesized Mean Difference	0	
df	4	
t Stat	2.979702	
P(T<=t) two-tail	0.040751	
t Critical two-tail	2.776445	

PR f = 2 min to f = 0.5 min

	Variable 1	*Variable 2*
Mean	0.942591291	0.801619502
Variance	0.002102291	0.000492719
Observations	3	3
Pooled Variance	0.001297505	
Hypothesized Mean Difference	0	
df	4	
t Stat	4.793175073	
P(T<=t) two-tail	0.008691369	
t Critical two-tail	2.776445105	

PR f = 1 min to f = 0.5 min

	Variable 1	*Variable 2*
Mean	0.845831	0.80162
Variance	0.001061	0.000493
Observations	3	3
Pooled Variance	0.000777	
Hypothesized Mean Difference	0	
df	4	
t Stat	1.942555	
P(T<=t) two-tail	0.124013	
t Critical two-tail	2.776445	

Na2SO4 Solution Fe-EC in the Flow-Through Experiments t = 6hr

DC	PR f = 2 min	PR f = 1 min	PR f = 0.5 min
1.0646	0.839431742	0.5549673	0.399646297
1.0989	0.901094781	0.5828902	0.211981238
1.0803	0.869099808	0.5142465	0.156135468

DC to PR f = 2 min

	Variable 1	*Variable 2*
Mean	1.081236	0.869875
Variance	0.000295	0.000951
Observations	3	3
Pooled Variance	0.000623	
Hypothesized Mean Difference	0	
df	4	
t Stat	10.37014	
P(T<=t) two-tail	0.000488	
t Critical two-tail	2.776445	

DC to PR f = 1 min

	Variable 1	*Variable 2*
Mean	1.0812362	0.550701351
Variance	0.0002952	0.00119164
Observations	3	3
Pooled Variance	0.0007434	
Hypothesized Mean Difference	0	
df	4	
t Stat	23.830981	
P(T<=t) two-tail	1.839E-05	
t Critical two-tail	2.7764451	

DC to PR f = 0.5 min

	Variable 1	*Variable 2*
Mean	1.081236	0.255921
Variance	0.000295	0.016272
Observations	3	3
Pooled Variance	0.008284	
Hypothesized Mean Difference	0	
df	4	
t Stat	11.10582	
P(T<=t) two-tail	0.000374	
t Critical two-tail	2.776445	

PR f = 2 min to f = 1 min

	Variable 1	*Variable 2*
Mean	0.869875	0.550701
Variance	0.000951	0.001192
Observations	3	3
Pooled Variance	0.001071	
Hypothesized Mean Difference	0	
df	4	
t Stat	11.94291	
P(T<=t) two-tail	0.000282	
t Critical two-tail	2.776445	

PR f = 2 min to f = 0.5 min

	Variable 1	*Variable 2*
Mean	0.8698754	0.255921001
Variance	0.000951	0.016272408
Observations	3	3
Pooled Variance	0.0086117	
Hypothesized Mean Difference	0	
df	4	
t Stat	8.1028314	
P(T<=t) two-tail	0.0012611	
t Critical two-tail	2.7764451	

PR f = 1 min to f = 0.5 min

	Variable 1	*Variable 2*
Mean	0.550701	0.255921
Variance	0.001192	0.016272
Observations	3	3
Pooled Variance	0.008732	
Hypothesized Mean Difference	0	
df	4	
t Stat	3.863551	
P(T<=t) two-tail	0.018092	
t Critical two-tail	2.776445	

SGW Solution Fe-EC in the Flow-Through Experiments t = 6hr

DC	PR f = 2 min	PR f = 1 min	PR f = 0.5 min
1.00406	0.871426715	0.50261194	0.063524564
0.91622	0.734139195	0.50755661	0.103780057
1.027911	0.785331152	0.51540993	0.085862873

DC to PR f = 2 min

	Variable 1	*Variable 2*
Mean	0.98273	0.796966
Variance	0.00346	0.004813
Observations	3	3
Pooled Variance	0.004137	
Hypothesized Mean Difference	0	
df	4	
t Stat	3.537368	
P(T<=t) two-tail	0.02407	
t Critical two-tail	2.776445	

DC to PR f = 1 min

	Variable 1	*Variable 2*
Mean	0.98273044	0.50852616
Variance	0.00345998	4.16521E-05
Observations	3	3
Pooled Variance	0.00175081	
Hypothesized Mean Difference	0	
df	4	
t Stat	13.8800513	
P(T<=t) two-tail	0.00015621	
t Critical two-tail	2.77644511	

DC to PR f = 0.5 min

	Variable 1	*Variable 2*
Mean	0.98273	0.084389
Variance	0.00346	0.000407
Observations	3	3
Pooled Variance	0.001933	
Hypothesized Mean Difference	0	
df	4	
t Stat	25.02246	
P(T<=t) two-tail	1.51E-05	
t Critical two-tail	2.776445	

PR f = 2 min to f = 1 min

	Variable 1	*Variable 2*
Mean	0.796966	0.508526
Variance	0.004813	4.17E-05
Observations	3	3
Pooled Variance	0.002428	
Hypothesized Mean Difference	0	
df	4	
t Stat	7.169924	
P(T<=t) two-tail	0.002003	
t Critical two-tail	2.776445	

PR f = 2 min to f = 0.5 min

	Variable 1	*Variable 2*
Mean	0.79696569	0.084389165
Variance	0.00481349	0.000406755
Observations	3	3
Pooled Variance	0.00261012	
Hypothesized Mean Difference	0	
df	4	
t Stat	17.0823176	
P(T<=t) two-tail	6.8882E-05	
t Critical two-tail	2.77644511	

PR f = 1 min to f = 0.5 min

	Variable 1	*Variable 2*
Mean	0.508526	0.084389
Variance	4.17E-05	0.000407
Observations	3	3
Pooled Variance	0.000224	
Hypothesized Mean Difference	0	
df	4	
t Stat	34.69209	
P(T<=t) two-tail	4.12E-06	
t Critical two-tail	2.776445	

SPW Solution Fe-EC in the Flow-Through Experiments t = 6hr

DC	PR f = 2 min	PR f = 1 min	PR f = 0.5 min
0.9313	0.208141842	0.23623925	0.05799816
0.8464	0.148747537	0.14170864	0.034670916
0.8557	0.12012658	0.20814184	0.092203695

DC to PR f = 2 min

	Variable 1	*Variable 2*
Mean	0.877826	0.159005
Variance	0.00217	0.002016
Observations	3	3
Pooled Variance	0.002093	
Hypothesized Mean Difference	0	
df	4	
t Stat	19.24465	
P(T<=t) two-tail	4.3E-05	
t Critical two-tail	2.776445	

DC to PR f = 1 min

	Variable 1	*Variable 2*
Mean	0.87782571	0.195363243
Variance	0.00216986	0.002356478
Observations	3	3
Pooled Variance	0.00226317	
Hypothesized Mean Difference	0	
df	4	
t Stat	17.5697639	
P(T<=t) two-tail	6.1626E-05	
t Critical two-tail	2.77644511	

DC to PR f = 0.5 min

	Variable 1	*Variable 2*
Mean	0.877826	0.061624
Variance	0.00217	0.000837
Observations	3	3
Pooled Variance	0.001504	
Hypothesized Mean Difference	0	
df	4	
t Stat	25.77953	
P(T<=t) two-tail	1.34E-05	
t Critical two-tail	2.776445	

PR f = 2 min to f = 1 min

	Variable 1	*Variable 2*
Mean	0.159005	0.195363
Variance	0.002016	0.002356
Observations	3	3
Pooled Variance	0.002186	
Hypothesized Mean Difference	0	
df	4	
t Stat	-0.95239	
P(T<=t) two-tail	0.394829	
t Critical two-tail	2.776445	

PR f = 2 min to f = 0.5 min

	Variable 1	*Variable 2*
Mean	0.15900532	0.061624257
Variance	0.00201559	0.000837367
Observations	3	3
Pooled Variance	0.00142648	
Hypothesized Mean Difference	0	
df	4	
t Stat	3.15782237	
P(T<=t) two-tail	0.03425559	
t Critical two-tail	2.77644511	

PR f = 1 min to f = 0.5 min

	Variable 1	*Variable 2*
Mean	0.195363	0.061624
Variance	0.002356	0.000837
Observations	3	3
Pooled Variance	0.001597	
Hypothesized Mean Difference	0	
df	4	
t Stat	4.098847	
P(T<=t) two-tail	0.014867	
t Critical two-tail	2.776445	

NaCl Solution Al-EC in the Flow-Through Experiments t = 6hr

DC	PR f = 2 min	PR f = 1 min	PR f = 0.5 min
2.664064	4.746549633	4.78989712	3.670087083
2.284774	4.134266404	4.58219042	4.036734562
2.290192	4.771835666	4.48646472	3.386522284

DC to PR f = 2 min

	Variable 1	*Variable 2*
Mean	2.41301	4.550884
Variance	0.047278	0.130337
Observations	3	3
Pooled Variance	0.088808	
Hypothesized Mean Difference	0	
df	4	
t Stat	-8.78621	
P(T<=t) one-tail	0.000463	
t Critical one-tail	2.131847	
P(T<=t) two-tail	0.000925	
t Critical two-tail	2.776445	

DC to PR f = 1 min

	Variable 1	*Variable 2*
Mean	2.41301001	4.619517419
Variance	0.04727849	0.024062784
Observations	3	3
Pooled Variance	0.03567064	
Hypothesized Mean Difference	0	
df	4	
t Stat	-14.308548	
P(T<=t) one-tail	6.9299E-05	
t Critical one-tail	2.13184679	
P(T<=t) two-tail	0.0001386	
t Critical two-tail	2.77644511	

DC to PR f = 0.5 min

	Variable 1	*Variable 2*
Mean	2.41301	3.697781
Variance	0.047278	0.106269
Observations	3	3
Pooled Variance	0.076774	
Hypothesized Mean Difference	0	
df	4	
t Stat	-5.67891	
P(T<=t) one-tail	0.002373	
t Critical one-tail	2.131847	
P(T<=t) two-tail	0.004745	
t Critical two-tail	2.776445	

PR f = 2 min to f = 1 min

	Variable 1	*Variable 2*
Mean	4.550884	4.619517
Variance	0.130337	0.024063
Observations	3	3
Pooled Variance	0.0772	
Hypothesized Mean Difference	0	
df	4	
t Stat	-0.30253	
P(T<=t) one-tail	0.388663	
t Critical one-tail	2.131847	
P(T<=t) two-tail	0.777325	
t Critical two-tail	2.776445	

PR f = 2 min to f = 0.5 min

	Variable 1	*Variable 2*
Mean	4.5508839	3.69778131
Variance	0.13033745	0.106269229
Observations	3	3
Pooled Variance	0.11830334	
Hypothesized Mean Difference	0	
df	4	
t Stat	3.03772453	
P(T<=t) one-tail	0.01924397	
t Critical one-tail	2.13184679	
P(T<=t) two-tail	0.03848794	
t Critical two-tail	2.77644511	

PR f = 1 min to f = 0.5 min

	Variable 1	*Variable 2*
Mean	4.619517	3.697781
Variance	0.024063	0.106269
Observations	3	3
Pooled Variance	0.065166	
Hypothesized Mean Difference	0	
df	4	
t Stat	4.422234	
P(T<=t) one-tail	0.005745	
t Critical one-tail	2.131847	
P(T<=t) two-tail	0.011491	
t Critical two-tail	2.776445	

SGW Solution Al-EC in the Flow-Through Experiments t = 6hr

DC	PR f = 2 min	PR f = 1 min	PR f = 0.5 min
1.571346	1.457559191	1.44852846	1.40518098
1.909095	1.383507237	1.46839606	1.327516735
1.638174	1.717644102	1.73389941	1.394344108

DC to PR f = 2 min

	Variable 1	*Variable 2*
Mean	1.706205	1.51957
Variance	0.03199	0.030796
Observations	3	3
Pooled Variance	0.031393	
Hypothesized Mean Difference	0	
df	4	
t Stat	1.2901	
P(T<=t) one-tail	0.133273	
t Critical one-tail	2.131847	
P(T<=t) two-tail	0.266546	
t Critical two-tail	2.776445	

DC to PR f = 1 min

	Variable 1	*Variable 2*
Mean	1.70620518	1.550274645
Variance	0.03198983	0.025387221
Observations	3	3
Pooled Variance	0.02868853	
Hypothesized Mean Difference	0	
df	4	
t Stat	1.12751591	
P(T<=t) one-tail	0.16128951	
t Critical one-tail	2.13184679	
P(T<=t) two-tail	0.32257902	
t Critical two-tail	2.77644511	

DC to PR f = 0.5 min

	Variable 1	*Variable 2*
Mean	1.706205	1.375681
Variance	0.03199	0.001769
Observations	3	3
Pooled Variance	0.01688	
Hypothesized Mean Difference	0	
df	4	
t Stat	3.1158	
P(T<=t) one-tail	0.017836	
t Critical one-tail	2.131847	
P(T<=t) two-tail	0.035671	
t Critical two-tail	2.776445	

PR f = 2 min to f = 1 min

	Variable 1	*Variable 2*
Mean	1.51957	1.550275
Variance	0.030796	0.025387
Observations	3	3
Pooled Variance	0.028092	
Hypothesized Mean Difference	0	
df	4	
t Stat	-0.22437	
P(T<=t) one-tail	0.416733	
t Critical one-tail	2.131847	
P(T<=t) two-tail	0.833466	
t Critical two-tail	2.776445	

PR f = 2 min to f = 0.5 min

	Variable 1	*Variable 2*
Mean	1.51957018	1.375680608
Variance	0.03079588	0.001769178
Observations	3	3
Pooled Variance	0.01628253	
Hypothesized Mean Difference	0	
df	4	
t Stat	1.38106459	
P(T<=t) one-tail	0.11969986	
t Critical one-tail	2.13184679	
P(T<=t) two-tail	0.23939971	
t Critical two-tail	2.77644511	

PR f = 1 min to f = 0.5 min

	Variable 1	*Variable 2*
Mean	1.550275	1.375681
Variance	0.025387	0.001769
Observations	3	3
Pooled Variance	0.013578	
Hypothesized Mean Difference	0	
df	4	
t Stat	1.835076	
P(T<=t) one-tail	0.070199	
t Critical one-tail	2.131847	
P(T<=t) two-tail	0.140398	
t Critical two-tail	2.776445	

SPW Solution Al-EC in the Flow-Through Experiments t = 6hr

DC	PR f = 2 min	PR f = 1 min	PR f = 0.5 min
1.585796	0.777184287	0.881760095	0.611560771
1.520774	0.834077862	1.291393831	0.678388144
1.659847	0.853764845	1.022278193	0.63070591

DC to PR f = 2 min

	Variable 1	*Variable 2*
Mean	1.588806	0.821676
Variance	0.004842	0.001582
Observations	3	3
Pooled Variance	0.003212	
Hypothesized Mean Difference	0	
df	4	
t Stat	16.57826	
P(T<=t) one-tail	3.88E-05	
t Critical one-tail	2.131847	
P(T<=t) two-tail	7.75E-05	
t Critical two-tail	2.776445	

DC to PR f = 1 min

	Variable 1	*Variable 2*
Mean	1.588805743	1.06514404
Variance	0.004842134	0.04332806
Observations	3	3
Pooled Variance	0.024085097	
Hypothesized Mean Difference	0	
df	4	
t Stat	4.132589291	
P(T<=t) one-tail	0.007231699	
t Critical one-tail	2.131846786	
P(T<=t) two-tail	0.014463399	
t Critical two-tail	2.776445105	

DC to PR f = 0.5 min

	Variable 1	*Variable 2*
Mean	1.588806	0.640218
Variance	0.004842	0.001184
Observations	3	3
Pooled Variance	0.003013	
Hypothesized Mean Difference	0	
df	4	
t Stat	21.16442	
P(T<=t) one-tail	1.47E-05	
t Critical one-tail	2.131847	
P(T<=t) two-tail	2.95E-05	
t Critical two-tail	2.776445	

PR f = 2 min to f = 1 min

	Variable 1	*Variable 2*
Mean	0.821676	1.065144
Variance	0.001582	0.043328
Observations	3	3
Pooled Variance	0.022455	
Hypothesized Mean Difference	0	
df	4	
t Stat	-1.98991	
P(T<=t) one-tail	0.058731	
t Critical one-tail	2.131847	
P(T<=t) two-tail	0.117463	
t Critical two-tail	2.776445	

PR f = 2 min to f = 0.5 min

	Variable 1	*Variable 2*
Mean	0.821675664	0.640218275
Variance	0.001581506	0.001184338
Observations	3	3
Pooled Variance	0.001382922	
Hypothesized Mean Difference	0	
df	4	
t Stat	5.976148779	
P(T<=t) one-tail	0.001969807	
t Critical one-tail	2.131846786	
P(T<=t) two-tail	0.003939615	
t Critical two-tail	2.776445105	

PR f = 1 min to f = 0.5 min

	Variable 1	*Variable 2*
Mean	1.065144	0.640218
Variance	0.043328	0.001184
Observations	3	3
Pooled Variance	0.022256	
Hypothesized Mean Difference	0	
df	4	
t Stat	3.488456	
P(T<=t) one-tail	0.012579	
t Critical one-tail	2.131847	
P(T<=t) two-tail	0.025158	
t Critical two-tail	2.776445	

Coagulant production q= 300 C/L Al-EC in SPW

DC	PR f = 10 min	PR f = 0.5 min
1.806576786	1.541955483	0.838921049
1.776538692	1.655671124	0.708040783
1.559120108	1.538379519	0.836775471

DC to PR f = 10 min

	Variable 1	*Variable 2*
Mean	1.714079	1.578669
Variance	0.018235	0.00445
Observations	3	3
Pooled Variance	0.011342	
Hypothesized Mean Difference	0	
df	4	
t Stat	1.557193	
P(T<=t) one-tail	0.097209	
t Critical one-tail	2.131847	
P(T<=t) two-tail	0.194417	
t Critical two-tail	2.776445	

DC to PR f = 0.5 min

	Variable 1	*Variable 2*
Mean	1.714078529	0.794579101
Variance	0.018234656	0.005617811
Observations	3	3
Pooled Variance	0.011926234	
Hypothesized Mean Difference	0	
df	4	
t Stat	10.31206016	
P(T<=t) one-tail	0.000249455	
t Critical one-tail	2.131846786	
P(T<=t) two-tail	0.000498909	
t Critical two-tail	2.776445105	

PR f= 10 min to f = 0.5 min

	Variable 1	*Variable 2*
Mean	1.578669	0.794579
Variance	0.00445	0.005618
Observati	3	3
Pooled Va	0.005034	
Hypothesi	0	
df	4	
t Stat	13.53486	
P(T<=t) on	8.62E-05	
t Critical o	2.131847	
P(T<=t) tw	0.000172	
t Critical t	2.776445	

Silica Removal q= 300 C/L Al-EC in SPW

DC	PR f = 10 min	PR f = 0.5 min
6.614	7.998	36.72
6.206	9.894	38.66
9.454	10	36.82

DC to PR f = 10 min

	Variable 1	*Variable 2*
Mean	7.424667	9.297333
Variance	3.130261	1.269009
Observations	3	3
Pooled Variance	2.199635	
Hypothesized Mean Difference	0	
df	4	
t Stat	-1.54643	
P(T<=t) one-tail	0.098451	
t Critical one-tail	2.131847	
P(T<=t) two-tail	0.196902	
t Critical two-tail	2.776445	

DC to PR f = 0.5 min

	Variable 1	*Variable 2*
Mean	7.424666667	37.4
Variance	3.130261333	1.1932
Observations	3	3
Pooled Variance	2.161730667	
Hypothesized Mean Difference	0	
df	4	
t Stat	-24.96944326	
P(T<=t) one-tail	7.63583E-06	
t Critical one-tail	2.131846786	
P(T<=t) two-tail	1.52717E-05	
t Critical two-tail	2.776445105	

PR f= 10 min to f = 0.5 min

	Variable 1	*Variable 2*
Mean	9.297333	37.4
Variance	1.269009	1.1932
Observations	3	3
Pooled Variance	1.231105	
Hypothesized Mean Difference	0	
df	4	
t Stat	-31.0203	
P(T<=t) one-tail	3.22E-06	
t Critical one-tail	2.131847	
P(T<=t) two-tail	6.44E-06	
t Critical two-tail	2.776445	

Calcium Removal q= 300 C/L Al-EC in SPW

DC	PR f = 10 min	PR f = 0.5 min
36.42	38.52	44.02
34.16	38.36	44.2
37.02	38.08	45.58

DC to PR f = 10 min

	Variable 1	*Variable 2*
Mean	35.86667	38.32
Variance	2.274533	0.0496
Observations	3	3
Pooled Variance	1.162067	
Hypothesized Mean Difference	0	
df	4	
t Stat	-2.78732	
P(T<=t) one-tail	0.024724	
t Critical one-tail	2.131847	
P(T<=t) two-tail	0.049447	
t Critical two-tail	2.776445	

DC to PR f = 0.5 min

	Variable 1	*Variable 2*
Mean	35.86666667	44.6
Variance	2.274533333	0.7284
Observations	3	3
Pooled Variance	1.501466667	
Hypothesized Mean Difference	0	
df	4	
t Stat	-8.729066832	
P(T<=t) one-tail	0.000474435	
t Critical one-tail	2.131846786	
P(T<=t) two-tail	0.000948869	
t Critical two-tail	2.776445105	

PR f= 10 min to f = 0.5 min

	Variable 1	*Variable 2*
Mean	38.32	44.6
Variance	0.0496	0.7284
Observati	3	3
Pooled Va	0.389	
Hypothesi	0	
df	4	
t Stat	-12.3319	
P(T<=t) on	0.000124	
t Critical o	2.131847	
P(T<=t) tw	0.000248	
t Critical t	2.776445	

Magnesium Removal q= 300 C/L Al-EC in SPW

DC	PR f = 10 min	PR f = 0.5 min
15.38	15.88	15.2
14	15.36	16.36
14.94	15.3	16.38

DC to PR f = 10 min

	Variable 1	*Variable 2*
Mean	14.77333	15.51333
Variance	0.496933	0.101733
Observations	3	3
Pooled Variance	0.299333	
Hypothesized Mean Difference	0	
df	4	
t Stat	-1.65653	
P(T<=t) one-tail	0.086478	
t Critical one-tail	2.131847	
P(T<=t) two-tail	0.172955	
t Critical two-tail	2.776445	

DC to PR f = 0.5 min

	Variable 1	*Variable 2*
Mean	14.77333333	15.98
Variance	0.496933333	0.4564
Observations	3	3
Pooled Variance	0.476666667	
Hypothesized Mean Difference	0	
df	4	
t Stat	-2.140550873	
P(T<=t) one-tail	0.049513259	
t Critical one-tail	2.131846786	
P(T<=t) two-tail	0.099026518	
t Critical two-tail	2.776445105	

PR f= 10 min to f = 0.5 min

	Variable 1	*Variable 2*
Mean	15.51333	15.98
Variance	0.101733	0.4564
Observations	3	3
Pooled Variance	0.279067	
Hypothesized Mean Difference	0	
df	4	
t Stat	-1.08193	
P(T<=t) one-tail	0.170075	
t Critical one-tail	2.131847	
P(T<=t) two-tail	0.340151	
t Critical two-tail	2.776445	